3.4 Cooperative Phenomena in Complex Macroscopic Systems

Development of new tensor-network-based methods and study of critical phenomena in quantum/classical magnets

Naoki KAWASHIMA

Institute for Solid State Physics,

The University of Tokyo, Kashiwa-no-ha, Kashiwa, Chiba 277-8581

Tensor-network is now widely recognized as a new framework/language for developing numerical methods for otherwise intractable many-body problems and describing the structure of the problem from the information-scientific viewpoint. In SY2022, we developed a few new numerical methods for studying quantum spin system in two spatial dimensions and classical statistical-mechanical models based on tensor-network representation. We then applied them to some typical examples.

In [1], we studied the square-lattice S=2 Heisenberg model with cubic anisotropy. The magnetic anisotropy is quite ubiquitous --- it can be found in virtually every magnet though in many cases its effect is very weak. However, the true nature of critical phenomena can be dramatically altered by such a weak symmetry breaking field. In spite of the universal nature of the anisotropy, it is hard to incorporate in the numerical calculation in an accurate way. We studied the simplest lattice spin model for the two-dimensional quantum ferromagnet with cubic anisotropy by means of mean-field analysis and tensor network calculation. It turned out that while the mean-field approximation produces a qualitatively correct phase diagram, the 2D iPEPS calculation yielded a quantitatively accurate one. We also observed that iPEPS calculation became slower in pinning down the direction of the magnetic easy axes as one approaches the phase boundary --- an indication of the ``easy-axis softening". In fact, the low-energy effective theory in the reduced Hilbert space restricted in the lower atomic levels indicate the asymptotic U(1) symmetry on the phase boundary, which is consistent with the above-mentioned softening phenomena. From these results together with renormalization group considerations, we concluded that the emergence of the continuous symmetry becomes exact on the phase boundary. Therefore, this criticality belongs to the same universality class as the 3D classical XY model. The iPEPS calculation of the correlation functions and other quantities support this interpretation. Thus, our iPEPS calculation provided the first systematic and correct analysis, beyond the mean-field approximation, of the phase boundary and the critical phenomena of this simple quantum spin system.

In [2], we studied the phase transitions of the two-dimensional q-state Potts model. While the universality class of the model is well established, the scaling function of the Binder parameter had not been accurately obtained before. In particular, we focused on the non-monotonic behavior of the Binder parameter. We discovered that for q=3 its non-monotonic behavior as a function of the temperature is not the non-universal properties. Instead it reflects a bump in the scaling function. Therefore, the non-monotonicity is the universal property of the Potts model.

In [3], we developed an open source software called TeNeS. It is a program package for obtaining ground states of two-dimensional quantum lattice problems. It is based on the corner transfer matrix renormalization group (CTMRG) method. In principle, it is designed for an arbitrary two-body Hamiltonian and an arbitrary two-dimensional lattice can be dealt with by deforming it to a non-uniform square lattice, though the numerical efficiency of such a treatment strongly depends on the original problem.

References

[1] Wei-Lin Tu, Xinliang Lyu, S. R. Ghazanfari, Huan-Kuang Wu, Hyun-Yong Lee, Naoki Kawashima: arXiv:2204.01197.

[2] Hiroshi Watanabe, Yuichi Motoyama, Satoshi Morita, and Naoki Kawashima, Progress of theoretical and experimental physics 2023, 033A02 (1-19) (2023).

[3] Yuichi Motoyama, Tsuyoshi Okubo, Kazuyoshi Yoshimi, Satoshi Morita, Takeo Kato, Naoki Kawashima: Computational Physics Communications 279 108437 (1-15) (2022).

Large-scale Molecular Simulation of Soft Materials using All-Atom and Coarse-Grained Models

Wataru SHINODA

Research Institute for Interdisciplinary Science,

Okayama University, 3-1-1 Tsushima-naka, Okayama 700-8530

We illustrate here a simulation study on action of antimicrobial peptide (AMP), melittin, on lipid membranes as an example of our research works using massive parallel computer simulations. In this study, we conducted a series of coarse-grained molecular dynamics (CG-MD) simulations to investigate the complicated actions of melittin in lipid membrane systems. In a membrane system with a lower peptide/lipid (P/L) ratio than the threshold value for melittin pore formation, no pores were found during the simulation, although the peptides formed dimers on the membrane. At a higher P/L ratio than the threshold value, we successfully observed pore formation caused by the insertion of melittin peptides through their N-terminals. During the pore formation, it was found that membrane curvature was locally induced in the vicinity of the peptide aggregate. These findings were consistent with experimental observations and suggested melittin action. Additionally, we performed CG-MD simulations for large-scale membrane systems at high peptide concentrations twice. Interestingly, two different membrane pore formation processes were observed in the systems with the same number of peptides in different initial configurations. One system showed lipid extraction and pore formation by melittin peptides without inducing membrane curvature, while another showed large pores in a significantly curved membrane. (Figure 1) This result indicated that, depending on the melittin arrangements on the membrane at high melittin concentration, pores were formed either by relaxation of bending energy due to large curvature or by the peptide insertion into the thinned membrane due to lipid extraction.

Through this study, we have gained some insight into the behavior of melittin, an AMP, on lipid membranes. The membrane pore formation process of antimicrobial activity cannot be induced by a single melittin peptide, even at P/L ratios above the concentration required for pore formation. This was energetically evidenced by the free energy profile of a single melittin insertion into the membrane. These results were also supported by 5 μs CG-MD simulations. Pore formation is always induced by cooperative actions such as induction of melittin membrane curvature and extraction of lipids from the membrane. These two events are the key factors

that trigger pore formation. Cooperative action occurs when aggregates of melittin composed of at least four or more peptides are formed on the membrane. Although aggregation of cationic peptides appears to be disadvantageous, the screening effects of electrostatic interactions indicate that aggregation may occur on the membrane, as in the CG-MD simulations. However, spontaneous assembly of melittin peptides does not necessarily result in the formation of pores because the free energy barrier required for pore formation is small. The findings of this study will contribute to the development of antimicrobial agents that mimic AMP against viral and bacterial infection. We hope that the CG force field (pSPICA) developed in this research will help us to better understand the activities of AMP.

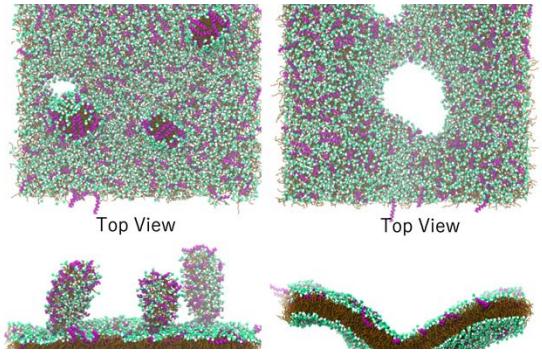

Figure 1: Observed membrane pore formation processes in a large membrane patch at P/L=5/128.

References

[1] Y. Miyazaki and W. Shinoda, Biochim. Biophys. Acta - Biomembranes, **1864**, 183955 (2022).

Crossover of fluctuating surfactant adsorbed interface

Shunta Kikuchi and Hiroshi WATANABE
Department of Applied Physics and Physico-Informatics, Keio University
Yokohama, Kanagawa 223-8522, Japan

We investigated the mechanical properties of a surfactant adsorbed at the interface between two liquids. The restoring force of the membrane is largely due to interfacial tension and elasticity. These are explained by the elastic energy model by Helfrich with the following equation [1].

$$|h(q)|^2 = \frac{k_B T}{\gamma q^2 + \kappa q^4},$$

where q is the wavenumber, $h(q)$ is the Fourier component of the fluctuation of the membrane, γ is the surface tension, and κ is the bending rigidity. The biomembrane is composed of a phospholipid bilayer, and its restoring force is thought to be either interfacial tension or elasticity, but the observed fluctuations are dominated by elasticity, with no effect of interfacial tension. We therefore investigated fluctuations in monolayer membranes to determine how the effects of interfacial tension and elasticity contribute to the resilience of the membranes.

We represented two kinds of liquids by preparing two kinds of atoms. The same type of atoms interacted with the Lennard-Jones potential, and the different type of atoms interacted with the WCA potential to reproduce a system in which the two liquids are phase-separated. We modeled the surfactant as a diatomic molecule and prepared an initial state in which the surfactant is adsorbed at the interface. Then, molecular dynamics was used for time evolution to observe the fluctuations at the surfactant-adsorbed interface. LAMMPS was used for time evolution.

Our investigation revealed a significant dependence of the interfacial tension within the system on the surfactant's natural length. Modifying the natural length could alter the interfacial tension from finite to nearly zero while maintaining the system's temperature constant. The findings demonstrate that the influence of q^2 is discernible in the film fluctuations when large values characterize interfacial tension. Conversely, a transition from q^2 to q^4 becomes evident in the Fourier spectrum when interfacial tension approaches near-zero values [2]. This crossover implies that when surfactant molecules are sufficiently adsorbed at the interface, and the interfacial tension is nearly zero, the bending stiffness dominates in the restoring force. In contrast, it plays the dominant role when the interfacial tension possesses finite values.

References

[1] W. Helfrich, Z. Natuforsch **C28**, 693 (1973).

[2] K. Shunta and H. Watanabe, J. Chem. Phys. **158**, 124901 (2023).

Correlation between the structure of charged phospholipid bilayer membrane and ion distribution

Yuji HIGUCHI
Research Institute for Information Technology, Kyushu University
Motooka Nishi-ku, Fukuoka 819-0395

We have studied soft matter by molecular simulations and revealed the self-assembly processes of amphiphilic molecules [1], water dynamics on lipid bulayer [2], and fracture processes of semicrystalline polymers [3]. This year, we studied the ion distribution on a charged surface as a model of biomembranes by coarse-grained molecular dynamics simulation using GROMACS [4] on systems B and C.

The electrostatics in soft matter systems is relevant to its self-assembly structures and dynamics, and therefore, essential to be understood. In particular, ion distributions on a charged surface as a model of biomembranes containing charged phospholipids have been extensively studied. Although theoretical studies have revealed the ion distributions perpendicular to the homogeneous charged surface, the ion distributions parallel to the heterogeneous charged surface and their dynamics are still unclear. Our coarse-grained molecular dynamics simulations show the dynamical changes of ion distribution profiles on the lipid membrane during phase separation. Figure 1 shows a typical snapshot of phase separation of neutral and negatively charged lipids with a NaCl concentration of 100 mM, and the cation distribution near the lipid membrane at 2.0 μs. The cations following negatively charged lipids in microsecond order indicate rapid redistribution of cations parallel to the membrane. We compare the simulation results with the modified Poisson–Boltzmann theory and reveal the importance of the ion-ion interactions in an aqueous solution. These results will contribute to the future development of the theory.

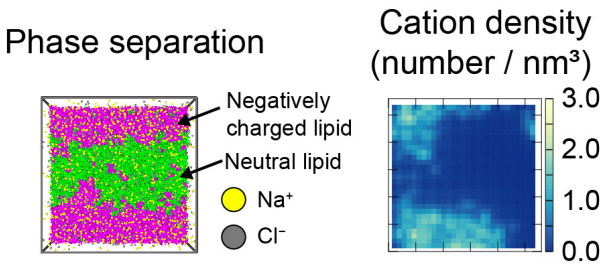

Figure 1: Phase separation and cation distribution of the charged and neutral lipids mixture at 2.0 μs with a NaCl concentration of 100 mM. The snapshot of the top view of the membrane and cation density (number/nm^3) near the surface.

References

[1] R. Wakabayashi, R. Imatani, M. Katsuya, Y. Higuchi, H. Noguchi, N. Kamiya, and M. Goto: Chem. Commun. **58** (2022) 585.

[2] Y. Higuchi, Y. Asano, T. Kuwahara, and M. Hishida: Langmuir **37** (2021) 5329.

[3] Y. Higuchi: Phys. Rev. E **103** (2021) 042502.

[4] M. J. Abraham, T. Murtola, R. Schulz, S. Páll, J. C. Smith, B. Hess, and E. Lindahl, SoftwareX **1-2** (2015) 19.

Constructing a Dataset of Thermal and Dielectric Properties of Polymers Using Molecular Dynamics Simulations

Yuta YOSHIMOTO

Department of Mechanical Engineering,

The University of Tokyo, 7-3-1 Hongo, Bunkyo-ku, Tokyo 113-8656

We have constructed a dataset of thermal and frequency-dependent dielectric properties of polymers using high-throughput molecular dynamics (MD) simulations. More than 500 polymers are constructed from the repeating units of previously synthesized polymers [1,2] and virtual polymers in the PI1M database [3] using RadonPy [4], an open-source Python library. As shown in Fig. 1(a), the MD-calculated values of coefficients of linear thermal expansion (CLTEs) show reasonable agreement with the available experimental values. Additionally, as shown in Fig. 1(b) and (c), the MD-calculated dielectric constants also exhibit reasonable agreement with the experimental counterparts at 10 MHz and 1 GHz, validating our MD simulation protocol. Currently, virtual polymers in the PI1M database have been screened using machine learning-aided prediction models of CLTEs and dielectric constants to further extend the dataset.

References

[1] L. Chen et al.: npj Comput. Mater. **6** (2020) 61.

[2] S. Otsuka et al.: Int. Conf. on Emerging Intelligent Data and Web Technologies (2011) 22.

[3] R. Ma and T. Luo: J. Chem. Inf. Model. **60** (2020) 4684.

[4] Y. Hayashi et al.: npj Comput. Mater. **8** (2022) 222.

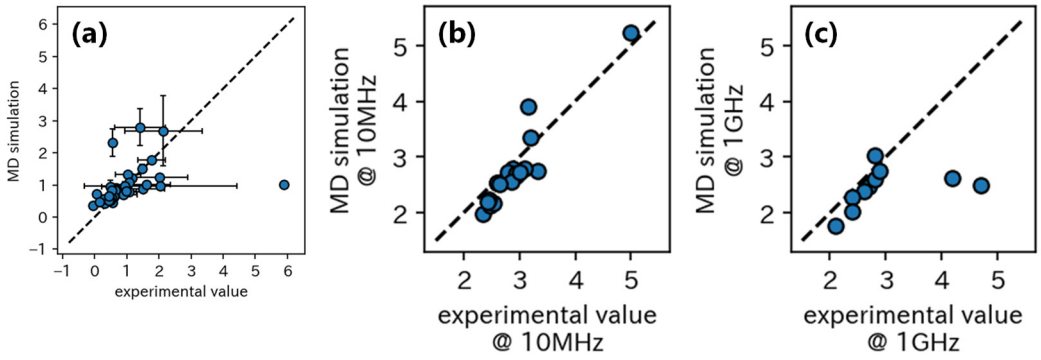

Fig. 1: Comparison of the MD-calculated values of coefficients of linear thermal expansion (a), dielectric constants at 10 MHz (b) and 1 GHz (c) with the experimental counterparts [1,2].

Critical Phenomena of Active Brownian Particles with Uniaxial Self-propulsion

Hiroyoshi Nakano
Institute for Solid State Physics, University of Tokyo
Kashiwa-no-ha, Kashiwa, Chiba 277-8581

Active matter is a distinct class of nonequilibrium many-body systems that show unique collective phenomena such as flocking, motility-induced phase separation, giant number fluctuations and active turbulence. Many experimental realizations have been reported, ranging from swimming bacteria to synthetic colloidal particles, which motivate extensive investigations of properties of active matter.

Active Brownian particles (ABPs) are one of the minimal model modeled on biologial motions [1]. The motion of the particles basically consists of three steps: (i) translational random walk, (ii) random rotation of the particle's orientation, and (iii) propelling movement along the particle's orientation. The ABPs undergo a phase separation even when the particles interact with each other via only excluded volume interactions. Its origin is sought for the self-propulsion. This type of phase separation is called motility-induced phase separation (MIPS) [2]. The speciality of the origin of the MIPS motivates the studies of whether the macroscopic behaviors of the MIPS are different from those of the phase separation induced by the intrinsic attractive force, such as the equilibrium liquid-gas transition.

Related to this problem, we focused on the ABPs with uniaxial self-propulsion [3]. This model is the ABPs that are refined so that the particles prefer to be oriented along a certain axis. We particularly examined the properties of critical phenomena by using the finite-size scaling method.

The result is summarized in Fig. 1. Figure 1 (a) presents typical snapshot of the phase-separated state, and Fig. 1 (b) presents the phase diagram. The phase-separated state appears at the large self-propulsion force F_0. The critical point is located at the triangle point in Fig. 1 (b). The binder ratios U for four system sizes are plotted in Fig. 1 (c), which shows that the binder ratios U cross at the unique point. It implies that this model undergoes the second-order phase transition. The critical exponent is estimated as

$$\beta = 0.35(4)\ ,\ \nu_x = 0.65(6). \tag{1}$$

Surprisingly, this result is quite close to the critical exponent of the three-dimensional Ising model even though this model is in two-dimensions.

Our sophisticated simulations demonstrated that this result can be understood from the similarities between the ABPs with uniaxial self-propulsion and randomly driven lattice gas (RDLG). For the RDLG, the particles are subjected to the random driving forces along one axis. It is well known that the universality class of the RDLG is the same as that of the two-dimensional Ising model with the dipolar long-range interaction, which is close to that of the three-dimensional Ising model. Our simulations showed that the ABPs with uniaxial self-propulsion exhibits the same macroscopic behaviors as the RDLG in the homogeneous state and the phase-separated state. Based on this result, we consider that the critical point

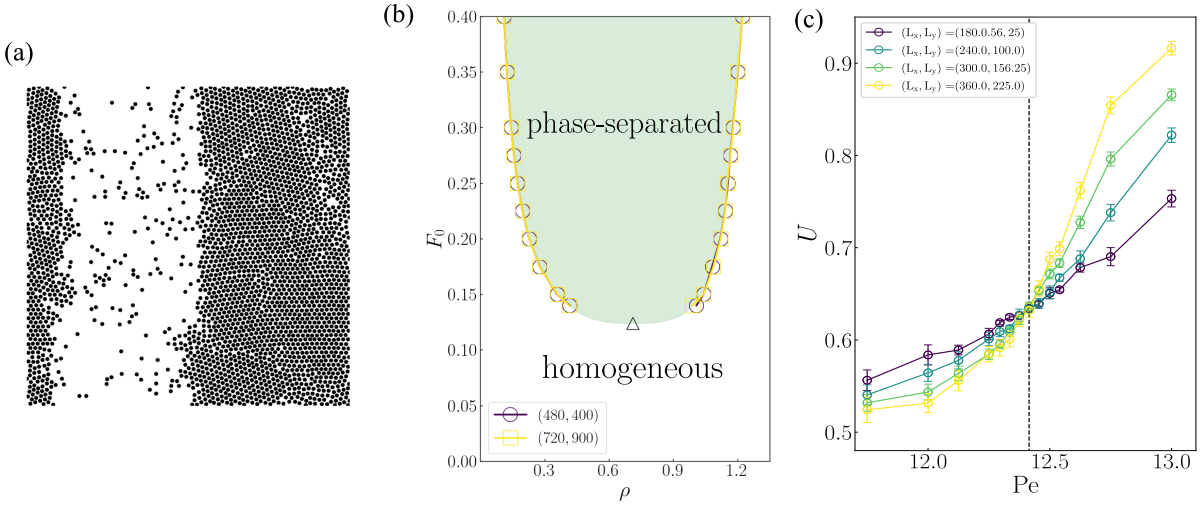

Figure 1: (a) Typical snapshot of phase-separated state. (b) Phase diagram of the ABPs with uniaxial self-propulsion. (c) Binder ratios for four system sizes.

of the ABPs with uniaxial self-propulsion belongs to the same universality class as that of the RDLG [4].

In summary, we performed the simulations of the two-dimensional ABPs with uniaxial self-propulsion. We showed that this model undergoes the MIPS and that the critical behaviors is quite close to the three-dimensional Ising model. Our result suggested that the critical points presumably belongs to the same universality class as that of the RDLG.

References

[1] Y. Fily and M. C. Marchetti: Phys. Rev. Let. **108**, 235702 (2012).

[2] M. E. Cates and J. Tailleur: Annu. Rev. Condens. Matter Phys. **6**, 219-244 (2015).

[3] H. Nakano, and K. Adach: in preparation.

[4] K. Adachi, K. Takasan, and K. Kawaguchi: Phys. Rev. Research **4** 013194 (2022).

Numerical Study on Novel Spin Nematic Phase

Tôru SAKAI[1,2], Hiroki NAKANO[1], Rito FURUCHI[1],
and Tokuro SHIMOKAWA[3]
[1]*Graduate School of Science, University of Hyogo,*
Kouto, Kamigori, Hyogo 678-1297, Japan
[2]*National Institute for Quantum Science and Technology,*
SPring-8, Kouto, Sayo, Hyogo 679-5148, Japan
[3]*Theory of Quantum Matter Unit,*
Okinawa Institute of Science and Technology Graduate University,
Onna-son, Okinawa 904-0495, Japan

1 Field-induced spin nematic Tomonaga-Luttinger liquid of the S=1/2 spin ladder system with anisotropic ferromagnetic rung interaction

The $S = 1/2$ quantum spin ladder system with the anisotropic ferromagnetic exchange interaction on the rung under magnetic field is investigated using the numerical diagonalization and the density matrix renormalization group (DMRG) analyses[1]. It is found that the nematic-spin-correlation-dominant Tomonaga-Luttinger liquid appears in some high magnetic field. It is included in the Tomonaga-Luttinger liquid phase where the two-magnon bound state is realized. For some suitable parameters, after the field-induced phase transition from this two-magnon Tomonaga-Luttinger liquid phase to the single-magnon Tomonaga-Luttinger liquid one, the re-entrant transition to the two-magnon phase would possibly occur, as the magnetization curves by DMRG indicate. Several phase diagrams with respect to the coupling anisotropy, the magnetization and the magnetic field are presented. The present result is a proposal of the candidate system which exhibits the spin nematic phase without the biquadratic interaction or the frustration. This mechanism also had been prposed for $S = 1$ antiferromagnetic chain with the single-ion anisotropy[2].

2 Spin Nematic Liquid of the S=1/2 Distorted Diamond Spin Chain in Magnetic Field

The spin nematic order has attracted a lot of interest in the field of magnetism. It is a kind of multipole order of spins. The previous theoretical and numerical studies[3] predicted that the spin nematic order would be induced by the frustration of the ferromagnetic and antiferromagnetic exchange interactions, or the biquadratic interaction. The spin nematic order is characterized by the long-range four spin correlation and the two-magnon bound state. The previous numerical diagonalization and the finite-size scaling study had indicated that a two-magnon bound state can occur in the S=1 antiferromagnetic chain with the single-ion anisotropy under magnetic field[4].The recent analysis of the critical exponents of the spin correlation functions[5] suggested that this two-magnon bound state includes the spin nematic liquid phase, as well as the spin density wave (SDW) liquid one. The phase di-

agrams with respect to the anisotropy and the magnetization were obtained by the numerical diagonalization of finite size clusters. In the present study[6], the S=1/2 distorted diamond spin chain is investigated using the numerical diagonalization of finite-size clusters. This system is a typical frustrated system. The recently discovered candidate material of this system, $K_3Cu_3AlO_2(SO_4)_4$ called alumoklyuchevskite[7], includes the ferromagnetic interactions. Thus we investigated the distorted diamond chain with the ferromagnetic interactions, as well as the coupling anisotropy. As a result we found that a two-magnon bound state appears in the magnetization process. We also discus about the spin nematic liquid behaviors.

References

[1] T. Sakai, R. Nakanishi, T. Yamada, R. Furuchi, H. Nakano, H. Kaneyasu, K. Okamoto and T. Tonegawa, Phys. Rev. B 106 (2022) 064433.

[2] T. Sakai, H. Nakano, R. Furuchi and K. Okamoto, J. Phys.: Conf. Ser. 2164 (2022) 012030.

[3] T. Hikihara et al., Phys. Rev. B 78 (2008) 144404.

[4] T. Sakai, Phys. Rev. B 58 (1998) 6268.

[5] T. Sakai, H. Nakano, K. Okamoto and R. Furuchi, J. Phys.: Conf. Ser. 2164 (2022) 012030.

[6] T. Sakai, H. Nakano, R. Fruchi and K. Okamoto, AIP Advances 13 (2023) 015313.

[7] M. Fujihara et al., Sci. Rep. 7 (2017) 16785.

Magnetization Plateau with Spontaneous Symmetry Breaking

Tôru SAKAI[1,2], Hiroki NAKANO[1], Rito FURUCHI[1],
and Tokuro SHIMOKAWA[3]
[1]*Graduate School of Science, University of Hyogo,*
Kouto, Kamigori, Hyogo 678-1297, Japan
[2]*National Institute for Quantum Science and Technology,*
SPring-8, Kouto, Sayo, Hyogo 679-5148, Japan
[3]*Theory of Quantum Matter Unit,*
Okinawa Institute of Science and Technology Graduate University,
Onna-son, Okinawa 904-0495, Japan

1 Translational Symmetry Broken Magnetization Plateau of the S=2 Antiferromagnetic Chain with Anisotropies

The magnetization plateau of the S=2 antiferromagnetic chain with interaction and single-ion anisotropies is investigated using the numerical diagonalization of finite-size clusters and some size scaling analyses[1]. The previous level spectroscopy analysis indicated that two different magnetization plateau phases appear at half of the saturation magnetization. One is due to the large-D mechanism and the other is due to the Haldane one. In the present study the phase diagram is extended to wider region of the anisotropies. As a result we find another half magnetization plateau phase, where the translational symmetry is spontaneously broken .

2 S=2 Quantum Spin Chain with the Biquadratic Exchange Interaction

The $S = 2$ quantum spin chain with the single-ion anisotropy D and the biquadratic exchange interaction is investigated using the numerical diagonalization of finite-size clusters and the level spectroscopy analysis. It is found that the intermediate-D phase corresponding to the symmetry protected topological (SPT) phase appears in a wide region of the ground state phase diagram. We also obtain the phase diagram at the half of the saturation magnetization which includes the SPT plateau phase[2].

References

[1] T. Yamada, R. Nakanishi, R. Furuchi, H. Nakano, H. Kaneyasu, K. Okamoto, T. Tonegawa and T. Sakai, arXiv:2208.10983; to appear in JPS Conf. Proc.

[2] T. Sakai, T. Yamada, R. Nakanishi, R. Furuchi, H. Nakano, H. Kaneyasu, K. Okamoto and T. Tonegawa, J. Phys. Soc. Jpn. 91 (2022) 074702.

Simulation of Quantum Many-Body Systems by Tensor Network and Sampling

Synge TODO
Department of Physics, University of Tokyo, Tokyo, 113-0033
Institute for Solid State Physics, University of Tokyo, Kashiwa, 277-8581

We developed novel numerical methods by combining quantum Monte Carlo, tensor network algorithms, and other optimization techniques. We investigated topological quantum phase transitions in strongly correlated many-body systems and optimization of quantum operations in quantum computing.

Tensor Renormalization Group and Markov Chain Monte Carlo Methods

The real-space renormalization group method using tensor networks has recently been widely used as a numerical method for many-body spin systems. The tensor renormalization group method can efficiently compute physical quantities for large classical/quantum systems. By extending the tensor network to a form in which tensors are placed not only on vertices but also on lines connecting vertices, we have increased the accuracy of the real-space renormalization method by about 100 times compared to existing numerical methods that require a similar amount of computation time. This method applies to general tensor networks. We are also working on a new sampling method that combines tensor network representation and Markov chain Monte Carlo methods.

Tensor Renormalization Group for Lattice Fermion Systems

Quantum many-body systems involving lattice fermions appear in various fields of physics. For example, lattice quantum chromodynamics is typical in particle physics, a many-body system describing the interaction between quarks via gluons. Strongly correlated electron systems in condensed matter physics are another example of a many-body system consisting of lattice fermions. We develop a method to calculate path integrals of lattice fermion systems. We represent the path integral of a lattice fermion system by a tensor network and perform approximate network contraction using the tensor renormalization group to compute the path integral in the infinite volume limit. We extended the bond-weighted tensor renormalization group (BTRG) to handle fermionic systems and performed empirical calculations using 2-dimensional Wilson fermions [1].

Worm Algorithm with Geometric Assignment Method

In Monte Carlo methods, there are cases where there are constraints on the "states" to be summed, and it is difficult to sample while satisfying the constraints (e.g., satisfiability problems). The worm algorithm is a method for efficient sampling by expanding the state space in such situations. A worm is a kink (point) that breaks a constraint, and the idea of the worm algorithm is that the constraint is violated once and then reconciled later. This Monte Carlo method introduces a constraint-breaking worm (kink), and sampling is performed by stochastically moving the worm. The conventional worm algorithm moves the worm almost wholly at random. We proposed a guideline for moving the worm for efficient computation—moving the

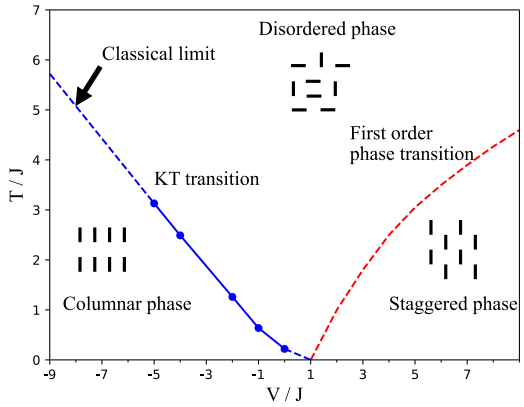

Figure 1: Finite-temperature phase diagram of square-lattice quantum dimer model.

worm straight ahead as much as possible—and confirmed a 25-fold improvement in computational efficiency compared to the conventional worm algorithm [2].

Finite-Temperature Phase Transition of the Quantum Dimer Model

The quantum dimer model was proposed by Rokhsar and Kivelson in 1988 as a low-energy effective model for frustrated magnetic materials. Although the Hamiltonian of the quantum dimer model has no negative sign problem, Monte Carlo simulations have been complicated because of the strong geometric restriction on the dimer configuration. We developed an efficient quantum Monte Carlo method that combines a cluster update method based on the stochastic series expansion (SSE) with a fast operator search method using priority queues. By choosing the appropriate order parameter and finite scaling, we obtained a finite-temperature phase diagram of the quantitative phase diagram of the quantum dimer model. The critical exponent at the critical point is consistent with the Kosterlitz-Thouless transition of the classical dimer model. The slope in the classical limit is also compatible with the critical temperature of the classical model. The slope of the phase boundary decreases as the quantum fluctuations increase, suggesting that the critical temperature becomes zero at the Rohksar-Kivelson (RK) point, i.e., the columnar dimer phase at absolute zero extends to the RK point without intermediate phases.

Continuous-Space Path-Integral Monte Carlo

The continuous-space path-integral Monte Carlo method is the only method that can numerically calculate physical quantities such as the superfluid density and condensation rate of interacting Bose particle systems. The worm algorithm allows for simulations in the grand canonical ensemble of superfluid helium in systems of several hundred particles. However, implementing the algorithm is complex, involving seven different update procedures. We developed more efficient and simpler update methods in the canonical ensemble. Advanced Markov-chain Monte Carlo methods, such as Hamiltonian Monte Carlo and event chain Monte Carlo, have been used to reduce the autocorrelation time of the simulation further. In addition, the Wang-Landau algorithm allows the hyperparameters to be automatically adjusted during the simulation, whereas the conventional worm algorithm has many hyperparameters that significantly affect the performance of the algorithm.

References

[1] Shinichiro Akiyama, Bond-weighting method for the Grassmann tensor renormalization group, J. High Energy Phys. **11**, 030 (2022).

[2] Hidemaro Suwa, Lifted directed-worm algorithm, Phys. Rev. E **106**, 055306 (2022).

Novel phenomena in frustrated magnets

Tsuyoshi OKUBO
Institute for Physics of Intelligence, The University of Tokyo
7-3-1 Hongo, Bunkyo-ku, Tokyo 133-0033

Frustrated interactions often induce novel phenomena in spin systems. One striking effect when we consider the quantum fluctuation may be the stabilization of quantum spin liquid without having long-range magnetic order [1, 2]. The ground state of the Kitaev model on the honeycomb lattice is one of the fundamental quantum spin liquids in the two-dimension[3, 4]. In the Kitaev model, the interactions are Ising type, $S_i^\gamma S_j^\gamma$, and the spin component $\gamma = x, y, z$ is determined from the direction to the neighboring site. Another example is the Kagome lattice Heisenberg model [1, 2]. It has been widely discussed on the possibility of the gapped Z_2 spin liquid or the gapless $U(1)$ spin liquid in the Kagome lattice Heisenberg antiferromagnets, e.g., see Ref. [5] and references therein.

In this year's project, we investigated finite temperature properties of frustrated spin models in the two-dimension, particularly concerning the thermal Hall conductivity. We mainly considered the Kagome lattice Heisenberg model with Dzyaloshinskii-Moriya (DM) interaction and compared its thermal Hall conductivity with the Kitaev model. To numerically calculate the thermal Hall conductivities at a finite temperature, we consider several finite-size clusters with open edges and represent their density matrix as a matrix product operator (MPO).

We calculate the MPO representing a density matrix at a given temperature by the exponential tensor renormalization grope (XTRG) algorithm [6]. In XTRG, we calculate the density matrix at an inverse temperature β, $\rho(\beta)$, through the relationship $\rho(\beta) = \rho(\beta/2)\rho(\beta/2)$ starting from the initial condition $\rho(\beta_0) = \exp(-\beta_0\mathcal{H}) \simeq 1-\beta_0\mathcal{H}$ for the sufficiently small β_0, where $\mathcal{H}$ is the Hamiltonian of the system. Once we have an MPO representation of a density matrix at $\beta/2$, we can approximate $\rho(\beta)$ through a standard tensor network compression algorithm to multiply two MPOs. When the bond dimension of the MPO is D, both the computation cost and the memory consumption of the XTRG algorithm scale $O(D^4)$. Although they are higher than the costs for the ground state, which scale $O(D^3)$, we can still calculate finite temperature properties by XTRG.

By the XTRG algorithm, we successfully calculated the temperature dependence of the energy current localized at the edge of the cylindrical system for the Kagome lattice Heisenberg model with the DM interaction under a magnetic field. We can calculate the thermal Hall conductivity by taking the temperature derivative of the energy current. In this system, the direction of the thermal Hall current depends on the sign of the DM interaction. Interestingly, in the XTRG calculation, its sign is opposite to the one calculated by Schwinger Boson mean-field theory [7]. We also found that similar sign inversion in the thermal Hall current is also observed in the case of the Kitaev model at high temperature: the sign is opposite to the expectation from the linear spin wave theory, although the sign at the low-temperature value is consistent with the expectation from the analysis of the Kitaev spin liquid. It will be a future problem to un-

derstand the origin of the difference in signs in high-temperature regions.

References

[1] L. Savary and L. Balents, Rep. Prog.Phys. **80** (2017) 016502.

[2] Y. Zhou, K. Kanoda, and T.K. Ng, Rev. Mod. Phys. **89** (2017) 025003.

[3] A. Kitaev, Ann. Phys. **321** (2006) 2.

[4] Y. Motome and J. Nasu, J. Phys. Soc.Jpn. **89** (2020) 012002.

[5] Y.C. He, M. P. Zaletel, M. Oshikawa, and F. Pollman, Phys. Rev. X, **7** (2017) 031020.

[6] H. Li, D.-W. Qu, H.-K. Zhang, *et al.* Phys. Rev. Research **2** (2020) 043015.

[7] H. Doki, M. Akazawa, H.-Y. Lee, J. H. Han, K. Sugii, M. Shimozawa, N. Kawashima, M. Oda, H. Yoshida, and M. Yamashita, Phys. Rev. Lett. **121** (2018) 097203.

Theoretical design of novel proteins for medical and industrial applications

Nao SATO[1], Hirotaro SHIMAMURA[2], Rina AOYAMA[1], Mizuki TERANISHI[1], Koji OOKA[3], Runjing LIU[1], Kaho KOTANI[1], Masataka YOSHIMURA[1], Yuuki HAYASHI[1,4], Shunji SUETAKA[1], and Munehito ARAI[1,2]

[1]Department of Life Sciences, Graduate School of Arts and Sciences, [2]Department of Physics, Graduate School of Science, [3]College of Arts and Sciences, and [4]Environmental Science Center, The University of Tokyo, Komaba, Meguro, Tokyo 153-8902

Proteins are widely used in medicine and industry as therapeutic agents for various diseases and as enzymes for industrial production. However, these proteins have been developed through extensive experiments, which require much time and cost. Therefore, there is an urgent need to develop efficient and theoretical methods for designing novel proteins. Here, we theoretically designed a variety of novel proteins using the Rosetta software suite [1] and experimentally verified the validity of our theoretical designs. In addition, we constructed a theory that can predict the folding mechanism of proteins, to elucidate the principles of protein design.

The KIX domain of CREB-binding protein is associated with leukemia, cancer and various viral diseases and has attracted considerable attention in drug discovery. We rationally designed a KIX inhibitor by performing theoretical saturation mutagenesis to search for the peptides expected to bind KIX more tightly than the original partner proteins. Among the 12 designed peptides, we experimentally found that a mutant of the MLL TAD peptide had the highest binding affinity for KIX among all previously reported inhibitors targeting the MLL site of KIX [2]. Thus, our approach may be useful for the rational design of helical peptides that inhibit protein-protein interactions involved in various diseases.

The programmed death-1 (PD-1) protein on the surface of T cells inhibits excessive inflammatory activity of T cells by binding to programmed death ligand-1 (PD-L1) expressed on antigen-presenting cells. However, reduced PD-1 function can cause abnormally activated T cells to damage normal cells, leading to autoimmune diseases. To prevent the T-cell activation by turning on the immune checkpoint, we theoretically designed PD-1 agonists that tightly bind the PD-L1 binding site of PD-1. Using Rosetta, we performed in silico saturation mutagenesis on the fragment of human PD-L1 and selected the mutants that are predicted to have high affinity for PD-1.

Experimental verification showed that we have successfully designed the PD-1 binders with higher affinity than the wild-type PD-L1, which may be useful as inhibitors of autoimmune diseases.

The novel coronavirus (SARS-CoV-2) infects human cells when its receptor-binding domain (RBD) binds to human ACE2. Antibodies that inhibit this binding have been used as antiviral drugs. However, existing drugs may become less effective as new variants of SARS-CoV-2 with mutations in the RBD emerge. Here, we theoretically modified existing antibody drugs to bind tightly to the RBD mutant of SARS-CoV-2 and experimentally showed that the modified antibodies were able to bind tightly to the RBD mutant. This approach is expected to be useful in the future as new viral variants emerge.

Formation of a ternary complex by interleukin 33, its receptor ST2, and IL-1 receptor accessory protein (IL-1RAcP) induces allergic diseases. To inhibit the complex formation, we have theoretically designed small proteins that tightly bind ST2 but inhibit the binding of IL-1RAcP. Experiments to verify the designs are ongoing.

Enzymes are widely used in the industrial production of useful substances. Therefore, it is necessary to develop efficient methods to improve enzymes. Using the Rosetta software, we are developing a universal method that can generally improve the activity of various enzymes. We have applied this method to enzymes such as dihydrofolate reductase and aldehyde deformylating oxygenase. Verification of this method is underway.

Elucidating the mechanisms by which proteins fold into specific three-dimensional structures is necessary to understand the design principles of proteins. To solve this problem, we are developing a statistical mechanics theory that can draw the folding free-energy landscapes of any proteins [3]. The program is written in C++ and Python. We have successfully calculated the free energy landscapes of folding reactions for all-α and all-β proteins in agreement with experiments. Our method can be used to draw the free energy landscapes of proteins associated with folding, binding, and catalysis, and to develop new protein design methods based on the prediction of protein dynamics.

References

[1] J. K. Leman, et al.: Nature Methods, **17**, 665 (2020).

[2] N. Sato, S. Suetaka, Y. Hayashi, and M. Arai: Scientific Reports, **13**, 6330 (2023).

[3] K. Ooka, R. Liu, and M. Arai: Molecules, **27**, 4460 (2022).

Multiscale Flow Simulations on Complex Fluids Undergoing Phase Transition

Yohei MORII and Toshihiro KAWAKATSU

Department of Physics, Tohoku University, Sendai, Miyagi 980-8578

The knowledge on the properties of complex flows, such as a viscoelastic polymer flow, around an obstacle plays a crucial role in designing flow channels in machines. In the present study, we analyze a flow of a dilute polymer solution passing through a moving wing using the multiscale simulation platform named MSSP, where smoothed particle hydrodynamics (SPH) method is coupled with microscopic particle simulations or phenomenological constitutive relations.

We modelled the wing using Joukowski wing as shown in Fig.1, and the polymer chains are modelled either by a Maxwellian constitutive relation (infinitely extensible) or FENE dumbbells (finite extensible). Simulations were performed at Ohtaka, where 2,560,000 SPH particles with 5,000,000,000 dumbbell particles embedded in these SPH particles were used. From the simulation data, we evaluated the rift coefficient C_{L} which is defined as the magnitude of the force exerted on the wing in the perpendicular direction to the inflow velocity divided by the inflow speed.

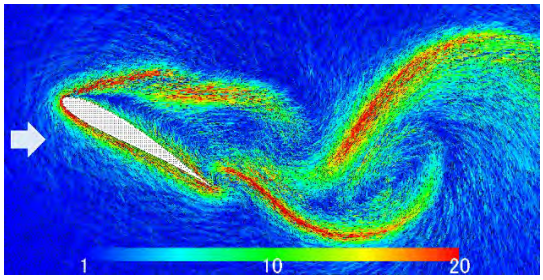

Fig.1 Flow pattern of a polymer solution around a Joukowski wing. Shown are the direction (bars) and the extension (colors) of polymers chains.

Figure 1 shows a snapshot of the molecular orientations and the bond stretching of the FENE dumbbells around a fixed Joukowski wing. When the wing starts to rotate slowly changing its angle to the inflow direction as $0° \rightarrow 45° \rightarrow 0°$, the value of C_{L} changes as shown in Fig.2, where the data are shown for Newtonian (red), Maxwellian(green) and FENE dumbbell(blue) models, respectively. We can confirm that the oscillation in C_{L} is suppressed by adding stretchable polymers(Maxwellian) while such a suppression is less obvious for FENE dumbbells.

References

[1] Y.Morii and T.Kawakatsu, Phys. Fluids, **33**, 093106 (2021).

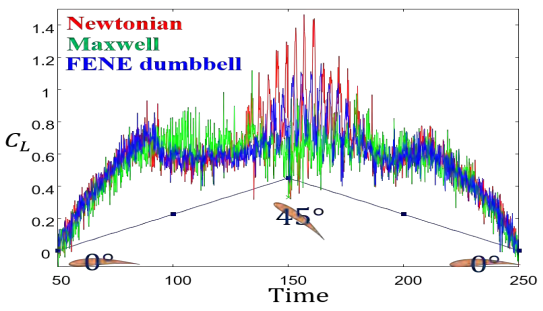

Fig.2 C_{L} as a function of the angle of the wing.

Simulations of quantum-classical-hybrid algorithms for sensor materials with considering noise

Wataru Mizukami

Center for Quantum Information and Quantum Biology, Osaka University, Osaka 560-0043, Japan

In the fiscal year, a domestically produced quantum computer was made publicly available in the cloud, and IBM announced a quantum computer with 443 quantum bits. Quantum computers with thousands of quantum bits are expected to appear in the near future, indicating significant progress in the development of quantum computing. A promising application for quantum computers is the simulation of quantum many-body systems. In the field of materials development, it is expected that simulations will become more accurate than current methods. Research into such simulation techniques is gaining momentum.

Our aim is to apply quantum computing to the development of materials for use in sensors. However, performing practical computations on realistic quantum chemistry problems with a large number of degrees of freedom using only quantum computers with limit number of qubits is not feasible. In addition, current quantum computers have short coherence times, making it difficult to perform useful computations using only quantum computers. As a result, the development of quantum-classical hybrid algorithms that utilise both quantum and classical computers has become crucial. In this study, we have performed the development and validation of quantum-classical hybrid algorithms using the ISSP's supercomputer and a quantum circuit simulator rather than an actual quantum computer.

This year, following up on last year's work, we focused on accelerating the simulation of the variational quantum eigensolver (VQE), a representative quantum-classical hybrid algorithm. We worked on speeding up VQE computations using GPUs and implemented VQE with multi-GPU support.

Moreover, we have been developing a method that combines the auxiliary-field quantum Monte Carlo (AFQMC) technique with VQE to compensate for degrees of freedom that cannot be handled by VQE alone. While a combination of AFQMC and quantum computation was proposed by Google in 2021, we have designed and implemented an algorithm that results in a more practical quantum circuit than their implementation. We tested this algorithm on simple systems, such as the OH molecule, and confirmed its satisfactory performance.

Tensor renormalization-group study of random spin systems

Koji HUKUSHIMA
Department of Basic Science, University of Tokyo
3-8-1 Komaba, Meguro-ku, Tokyo 153-8902

Statistical mechanical studies of spin glasses with both randomness and frustration have been conducted for a long time. It is an important issue whether the picture of phase transitions established in the mean-filed spin-glass model can be applied to finite-dimensional spin-glass models. It is quite difficult to study the finite-dimensional spin glass models using analytical methods. Therefore, the main results for these models have been obtained mainly by numerical studies, such as Markov-chain Monte Carlo (MCMC) methods. However, the long relaxation times of the MCMC methods for spin-glass systems are a serious barrier to studying large sizes. Recently, the tensor renormalization group (TRG) method, numerical calculation methods using tensor networks have attracted much attention.

In this project, we employ the higher-order tensor renormalization group (HOTRG) method, one of the TRG-type methods, to study the two-dimensional Ising spin-glass model. Previous studies have suggested that the spin-glass phase transition does not occur at finite temperatures in this system when the distribution of interactions is close to symmetric and highly disordered[1]. We investigate the phase transition of the system near the Nishimori line. Then, the stiffness of the system is calculated for sizes up to the linear dimension $L = 256$ using the HOTRG method, which calculates the free energy under different boundary conditions. In the calculations at higher temperatures than the Nishimori line, both boundary conditions lead to the same transition point and values close to the critical exponent of the pure Ising universality class, the latter of which is consistent with the picture dominated by the pure Ising fixed point there, as pointed out in many previous studies.

In contrast to the phase transitions above and on the Nishimori line, the transition points analyzed here have different values for the twist and replica boundary conditions. In other words, the paramagnetic/ferromagnetic and paramagnetic/non-paramagnetic transition points are different from each other, suggesting the existence of some non-paramagnetic phase between the paramagnetic and ferromagnetic phases at finite temperatures in the two-dimensional EA Ising model. This may correspond to the spin-glass phase or the previously proposed random antiphase state. The value of this transition point at low temperature is roughly consistent with the Nishimori fixed point, suggesting that the boundary between the paramagnetic and "spin-glass" phases descends almost vertically from the Nishimori fixed point toward lower temperatures. Meanwhile, the "spin-glass"/ferromagnetic phase boundary shows a re-entrant transition.

We also studied the critical phenomena of the J_1-J_2 Ising model by varying the parameter g using HOTRG[2]. This system involves a competition between the ferromagnetic interaction J_1 and antiferromagnetic interaction J_2. Furthermore, weak first-order and second-order transitions are observed near the ratio $g = J_2/|J_1| = 1/2$. Our results, based on HOTRG calculations for significantly larger sizes, indicate that the region of the first-order transition is marginally narrower than that in previous studies. Moreover, the universality class of the second-order transition connected to the transition line is not necessarily fully consistent with the Ashkin–Teller class considered earlier.

[1] K. Yoshiyama, K. Hukushima: in preparation.

[2] K. Yoshiyama, K. Hukushima: arXiv:2303.07733

Molecular dynamics study of phase separation induced by binding molecules

Koji HUKUSHIMA
Department of Basic Science, University of Tokyo
3-8-1 Komaba, Meguro-ku, Tokyo 153-8902

Chromatin is highly folded into a hierarchical structure in the nucleus while interacting with nuclear molecules. In addition, regions of active and repressed gene expression are formed on chromatin. These epigenetic regions are established and maintained by writer molecules that write and reader molecules that recognize chemical modifications on chromatin. The relationship between the one-dimensional epigenetic pattern on chromatin and the three-dimensional chromatin structure is an interesting question that has not yet been elusidated.

The SBS (Strings and Binders Switch) model[1] is a coarse-grained polymer model that takes into account the phase separation between chromatin and nuclear molecules that bind to chromatin, and to some extent recapitulates the experimental results such as HiC and FISH. In this model, chromatin forms clusters due to the effective attraction between chromatin segments via molecules that bind multivalently to chromatin[1,2].

In this project, we consider two types of binding molecules in the SBS model that promote or repress transcription as playing the roles of reader and writer of epigenetic modifications. When polymer segments are bound to these binding molecules, the state stochastically changes depending on the type of the binding molecule. The binding molecules switch between two states, one in which they can bind chromatin and one in which they cannot, at a constant rate, as in the previous study[3]. In this model, a one-dimensional pattern of epigenetic modification appears on the polymer, accompanied by a three-dimensional structure.

In this study, we performed coarse-grained molecular dynamics simulations on the SBS model with two types of biding molecules. From the time-series data of the coordination dynamics obtained by the molecular dynamics simulations, we devised a method to extract the time evolution of cluster formation, fission, coalescence, and annihilation. With the help of the method, it is revealed that the clusters move dynamically along the polymer, repeating coalescence and fission, and that there are no independent clusters. The evaluation of the lifetime of the clusters also suggested the existence of a phase that goes to infinity below a certain nonzero switching rate, despite a finite switching rate. This can be regarded as a dynamical percolation transition.

Our simulations also showed that the sequence of clusters of alternating types and the hierarchical structure of these clusters on the chromatin polymer emerge with the two types of binding molecules. When the binding molecules do not switch states, the polymer takes on a sausage-like shape with hierarchical structure, and as the switching rate increases, the structure becomes more dynamic and the clusters become more independent of each other. This provides insight into the mechanisms underlying the dynamics and stability of one-dimensional epigenetic patterns and three-dimensional cluster structures on chromatin in the SBS model.

The present work has been done in collaboration with Ryo Nakanishi.

[1] Mariano Barbieri et al., PNAS, 2012 109 (40) 16173-16178.
[2] Andrea M. Chiariello et al., Sci. Rep., 2016 29775(6).
[3] Chris A. Brackley et al., Biophys. J., 2017 112(6) 1085-1093.

Numerical simulations combined with machine learning to search for magnetic skyrmion in frustrated magnets

Satoru Hayami
Graduate School of Science, Hokkaido University, Sapporo 060-0810, Japan

A magnetic skyrmion, which is characterized by a topologically-nontrivial swirling spin texture, has attracted considerable attention, since it leads to unconventional transport phenomena, such as the topological Hall effect. In order to realize new electronic and spintronic devices based on the skyrmion, it is highly desired to understand when and how such topological spin textures are stabilized from the microscopic viewpoint. In the project with number 2022-Ca-0002, we have numerically investigated the possibility of magnetic skyrmions by focusing on magnetic frustration mechanisms in localized and itinerant systems. We have presented the main results this year below.

(i) Skyrmion crystals in trilayer systems: We have theoretically investigated a new stabilization mechanism of the skyrmion crystals in a trilayer system [1]. By focusing on the role of the layer-dependent Dzyaloshinskii-Moriya interaction and performing the simulated annealing for the spin model, we obtained various types of skyrmion crystal phases with different skyrmion number in a low-temperature phase diagram. We found the skyrmion crystal phases characteristics of the layered system: the twisted surface skyrmion crystal, anti-skyrmion crystal, and high-topological-number skyrmion crystal phases.

(ii) Rectangular and square skyrmion crystals in centrosymmetric tetragonal magnets: We considered the instability toward the rectangular skyrmion crystal without fourfold rotational symmetry on a centrosymmetric square lattice with magnetic anisotropy [2]. The model includes the effect of frustrated exchange interactions and the easy-axis single-ion anisotropy. We have shown that a competition of the interactions in momentum space triggers the formation of both rectangular and square skyrmion crystals. We have also shown that a phase transition between them occurs while varying the amplitude of the magnetic field.

(iii) Skyrmion crystals in a nonsymmorphic lattice structure: We have numerically investigated the stabilization mechanism of the skyrmion crystals in a nonsymmorphic lattice system with screw symmetry [3]. By performing unbiased numerical simulations based on the simulated annealing for a layered spin model to be characterized as a nonsymmorphic system with a threefold screw axis, we revealed that the skyrmion crystal is stabilized in both zero and nonzero magnetic fields by the interplay between the ferromagnetic interlayer exchange interaction and the layer- and momentum-dependent anisotropic exchange interactions. We also found two new types of skyrmion crystals characteristics of a threefold-screw system. Our result indicated a possibility to realize the skyrmion crystal in nonsymmorphic systems without a solely rotational symmetry within the same plane, which leads to extending the scope of the skyrmion crystal-hosting materials.

(iv) Skyrmion crystals in a ferromagnetic/antiferromagnetic bilayer: We proposed

a new stabilization mechanism of the skyrmion crystal in a bilayer system, which is composed of ferromagnetic and antiferromagnetic layers but free from the Dzyaloshinskii-Moriya interaction [4]. By performing the variational calculation and Monte Carlo simulation for the frustrated spin model, we found that the skyrmion crystal is robustly stabilized from zero to finite temperatures for the strong interlayer coupling. The results provided a new scenario to realize the skyrmion crystal in multi-layer systems including the domain structure and heterostructure by making use of the layer degree of freedom.

(v) Skyrmion crystal in the Hubbard model: We investigated a realization of the skyrmion crystal in the centrosymmetric triangular-lattice Hubbard model without localized spins [5]. On a basis of the self-consistent mean-field calculations, we found two types of skyrmion crystals with spatially nonuniform charge modulations in the ground state at a zero magnetic field. We have also shown that an unconventional triple-Q vortex phase without the net spin scalar chirality emerges. Furthermore, we found that the magnetic field induces the topological phase transition from the $3Q$ vortex phase to another skyrmion crystal phase. We clarified that the microscopic origin of these phases is the site-dependent moment reduction due to the kinetic motion of electrons in the Hubbard model, which is qualitatively different from the situation in the Kondo lattice model and other spin models.

(vi) Various topological spin textures in an itinerant honeycomb magnet: We have theoretically revealed new types of topological spin textures consisting of the magnetic skyrmion by focusing on the sublattice degree of freedom in the lattice structure [6]. We found five types of skyrmion crystals with different topological properties from the conventional one in an itinerant honeycomb magnet based on the simulated annealing. We have shown that the sublattice degree of freedom in the itinerant magnet enables us to realize the unobserved skyrmion crystals, such as the antiferro-type skyrmion crystal and ferri-type skyrmion crystal.

(vii) Magnetic field–temperature phase diagrams for centrosymmetric tetragonal magnets: We systematically constructed the magnetic field–temperature phase diagrams of the effective spin model for the itinerant electron model on a square lattice on the basis of an efficient steepest descent method with a small computational cost [7]. We found two distinct mechanisms to stabilize the square-type skyrmion crystal from zero to finite temperatures: One is the positive biquadratic interaction and the other is the high-harmonic wave-vector interaction. By showing the phase diagrams for different sets of model parameters, we discussed the stability tendency of the skyrmion crystal and other multiple-Q states.

References

[1] S. Hayami, Phys. Rev. B **105**, 184426 (2022)

[2] S. Hayami, Phys. Rev. B **105**, 174437 (2022).

[3] S. Hayami, Phys. Rev. B **105**, 224411 (2022).

[4] K. Okigami, R. Yambe, and S. Hayami, J. Phys. Soc. Jpn. **91**, 103701 (2022).

[5] K. Kobayashi and S. Hayami, Phys. Rev. B **106**, L140406 (2022).

[6] R. Yambe and S. Hayami, Phys. Rev. B **107**, 014417 (2023).

[7] S. Hayami and Y. Kato, J. Magn. Magn. Mater. **571**, 170547 (2023).

Universality classes of 3D $\pm J$ Ising model

Y. Ozeki and Y. Terasawa

Graduate School of Informatics and Engineering, The University of Electro-Communications

We investigate the universality classes of the $\pm J$ Ising model in three dimensions. Together with the ferromagnetic (FM) classes obtained previously [1], the spin glass (SG) transition is analyzed by the use of dynamical scaling analysis for nonequilibrium relaxation (NER) process [2]. the p-dependence of SG transition temperature $T_{\mathrm{SG(p)}}$ and critical exponents γ, ν, z are obtained.

To estimate the dynamical exponent z precisely, an extrapolation scheme is introduced for the asymptotic value of logarithmic derivative of the dynamical Binder parameter at the transition point. To do this, we performed Monte-Carlo simulation for multi-replica systems. Each replica system has the same bonds J_{ij}, while the initial configuration of relaxation is distinct. The replica overlap $q^{AB}(t)$ between two replicas A and B at time t, is defined by:

$$q^{AB}(t) = \frac{1}{N}\sum_i S_i^{(A)}(t) S_i^{(B)}(t), \qquad (1)$$

where $S_i^{(A)}$ is the i-th spin variable in replica A at time t. Te SG Binder parameter is obtained by

$$g_{\mathrm{SG}}(t,T) = \frac{1}{2}\left(3 - \frac{q^{(4)}(t)}{\{q^{(2)}(t)\}^2}\right), \qquad (2)$$

where

$$q^{(k)}(t) = \frac{2}{n(n-1)}\left[\sum_{A>B}\{q^{AB}(t)\}^k\right]_J. \qquad (3)$$

When $T = T_{\mathrm{SG}}$, this function is expected to diverge as

$$N \times g_{\mathrm{SG}}(t,T) \sim t^{d/z} \qquad (4)$$

where d is the spacial dimension. This relation allows us to estimate z independently.

The SG region in $0.5 \le p \le p_{\mathrm{mc}}$ is analyzed. To estimate T_{SG} and $z\nu$, we perform the dynamical scaling analysis for SG susceptibility $\chi_{\mathrm{SG}}(t)$ with the linear size $L = 61$, 512 independent samples and 64 replicas are used for averaging. To estimate z, we calculate $g_{\mathrm{SG}}(t)$ with the linear size $L = 31$, 460800 independent samples and 64 replicas are used for averaging.

In Figs. 1, the resulting p-dependence of SG critical exponent ν on the PM-SG boundary are shown

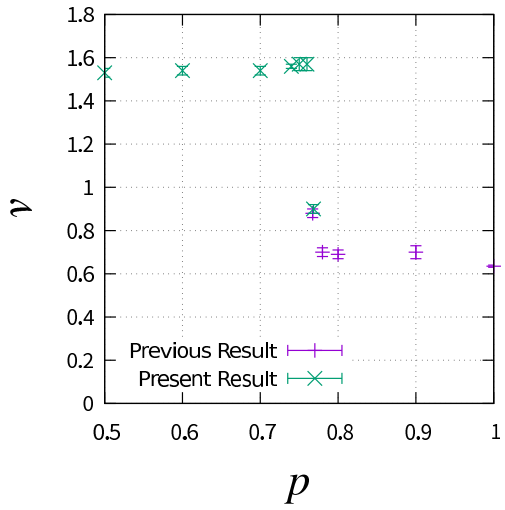

Figure 1: Result of estimated ν.

together with the previously obtained FM exponents on the PM-FM boundary [1]. Since both the FM and SG transitions occur at the multi-critical point (MCP), and FM and SG exponents become identical with each other [3], one may survey an exponent in whole region including SG and FM phases. As for the exponent ν, there exist three FM universality classes associated with the non-random FM fixed point ($p = 1$), the random fixed point ($p_{\mathrm{mc}} < p < 1$), and the MCP ($p = p_{\mathrm{mc}}$) [1]. On the other hand, the present result indicates a single universality class for PM-SG transition in $0.5 \le p < p_{\mathrm{mc}}$, and ν takes a value ~ 1.55.

References

[1] Y. Ozeki and N. Ito, *J. Phys.: Math. Theor.* **40** R149 (2007).

[2] Y. Echinaka and Y. Ozeki, *Phys. Rev.* E**94** 043312 (2016).

[3] Y. Ozeki and N. Ito, *J. Phys.A: Math. Gen.* **31** 5451 (1998).

Localization-delocalization transition in non-Hermitian random system

TOMI OHTSUKI[1]
TOHRU KAWARABAYASHI[2]
KEITH SLEVIN[3]
1) Dept. Phys., Sophia University, Chiyoda-ku, Tokyo 102-8554, Japan
2) Dept. Phys., Toho University, Miyama 2-2-1, Funabashi 274-8510, Japan
3) Dept. Phys., Osaka University, Toyonaka, Osaka 560-0043, Japan

Random quantum systems lack translational/rotational symmetries but can exhibit time reversal, spin rotation, chiral, and particle-hole symmetries. These symmetries classify random quantum systems into 10 distinct symmetry classes. The Wigner-Dyson classes discovered in the 1950s and 1960s have undergone significant research. Recent experimental findings regarding topological insulators and Weyl semimetals have inspired researchers to explore random systems outside of the Wigner-Dyson classes. These newly discovered 7 classes [3 chiral classes (Gade-Wegner classes) and 4 Bogoliubov-de Gennes classes] exhibit discrete chiral or particle-hole symmetries.

We have studied a series of Hamiltonians that pertain to the newly discovered quantum classes. We then introduced non-Hermiticity to the Hamiltonian, and we were able to extend the classification of systems to encompass 38 distinct classes. Through our research, we demonstrated that the inclusion of non-Hermitian elements alters the universality class [1] and that the widely utilized transfer matrix method employed in Anderson transitions also applies to non-Hermitian systems [2]. Additionally, our investigations revealed that the critical behaviors of the 38 non-Hermitian classes can be mapped to universality classes for the 10 Hermitian symmetry classes [3] (see Fig. 1).

Condensed matter physics has seen a significant increase in the utilization of machine learning techniques. Our research involves using convolutional neural networks (CNN) to analyze wave functions and study various quantum phase transitions. Specifically, we employ this method to classify wave functions in quasi-periodic systems[4]. Moreover, we utilize the neural network to interpret the quantum fingerprints in mesoscopic systems [5].

References

1. X. Luo, T. Ohtsuki, R. Shindou, Physical Review Letters **126**, 090402 (2021).
2. X. Luo, T. Ohtsuki, and R. Shindou, Physical Review B **104**, 104203 (2021).
3. X. Luo, Z. Xiao, K. Kawabata, T. Ohtsuki, and R. Shindou, Physical Review Research **4**, L022035 (2022).
4. X. Luo, T. Ohtsuki, Physical Review B **106**, 104205 (2022).
5. S. Daimon, K. Tsunekawa, S. Kawakami, T. Kikkawa, R. Ramos, K. Oyanagi, T. Ohtsuki, E. Saitoh, Nature Communications **13**, 3160 (2022).

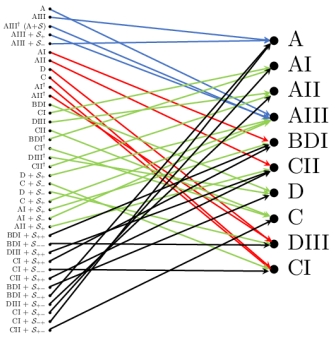

Figure 1: Correspondence of the Anderson transitions in non-Hermitian and Hermitian systems.

Slow spin dynamics near phase boundary between different ordered phases

Hidemaro SUWA
Department of Physics, University of Tokyo, Tokyo 113-0033

The metastable state is ubiquitous in our daily lives and in condensed matter physics. A typical example of the metastable state is diamond, a solid form of carbon. Graphite is the most stable phase at room temperature, but diamond is also stable as a metastable state, indicating that the time scale of relaxation is much longer than that of experiments. The metastable state is essential to not only statistical mechanics but also several functional materials. For example, the use of the metastable state enables higher-density storage and broader applications in phase-change memory. Recently, a skyrmion-lattice phase of MnSi has been stabilized by rapid cooling as a metastable state in a wider region of the phase diagram.

What is the condition for a metastable state to stay for a long time, or in what situation do the relaxation dynamics become significantly slow? We can find some answers in glass systems. Slow dynamics typically emerge near a eutectic point, a triple point between a liquid, a crystal, and another crystal phase. In the dynamics of particle systems, the particle number is usually conserved in time evolution. On the other hand, the dynamics of spin systems are typically non-conserved: magnetization is not conserved in time evolution. The question we answer through this project is where slow dynamics appear in the Ising model, a prototype model of statistical mechanics.

In analogy to the eutectic point, we derived one of the simplest Ising models showing a "Y-shape" first-order phase boundary (Fig. 1): the J_1-J_2-J_3 Ising model with a four-spin interaction. The four-spin interaction could be induced by integrating out other degrees of freedom, mimicking an effect of interactions with charge, phonons, etc. We studied the quench dynamics of the Ising model using the Monte Carlo method on ISSP System B in the class C project (ID: 2022-Ca-0100). The initial state is a random spin configuration, and the time evolution is simulated by Glauber dynamics. The relaxation time becomes significantly longer near the phase boundary. We also studied snapshot configurations and the structure factor as a function of time. Near the phase boundary, clusters of the metastable state remain for a quite long time and prevent vortices from recombining and annihilating. Our simulation is consistent with experimentally observed slow dynamics in vanadium oxides. The result of this project sheds new light on the stability of the metastable state and slow dynamics emerging near a phase boundary.

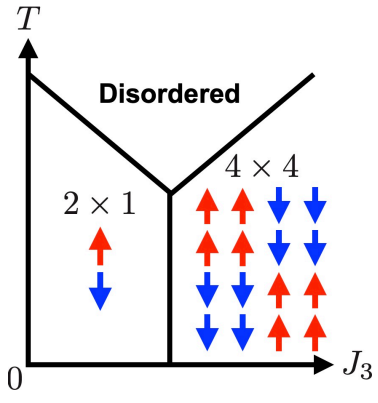

Figure 1: Schematic Y-shape phase diagram of the Ising model. The phase boundaries are of the first order.

Polymer Dynamics under Elongational Flow

Takahiro MURASHIMA

Department of Physics, Tohoku University,

Aramaki-aza-Aoba, Aoba-ku, Sendai, Miyagi 980-8578

Fundamental studies of polymer dynamics under elongational flows are important for a better understanding of complex flow in the molding process. We have developed a uniform elongational flow method [1] that can handle very large deformations under arbitrary (uniaxial, planar, and biaxial) elongational flows. This code works on LAMMPS [2], which brings the benefits of massive parallel computation at ISSP. Our previous work [3] was the first to discover the stress overshoot phenomena of ring/linear blends under biaxial elongational flow using this method. In this project, we investigated multicyclic/linear blend systems under biaxial elongational flows. We found sharper overshoot phenomena of multicyclic/linear blend than those of monocyclic/linear blend in our previous work [3]. The origin of overshoot in multicyclic/linear blend was the open-to-closed topological transition. This work [4] was selected as a supplementary journal cover of Macromolecules as shown in Fig. 1.

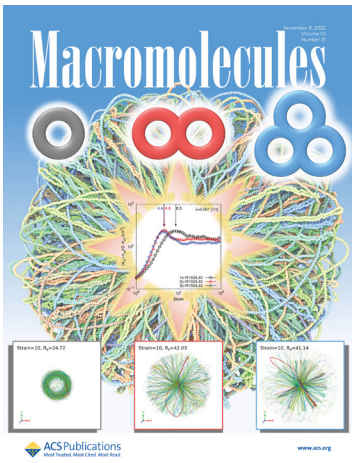

Fig. 1: Supplementary Journal Cover of Macromolecules, Volume 55, Issue 21 [4].

References

[1] T. Murashima, K. Hagita, T. Kawakatsu, Nihon Reoroji Gakkaishi, **46**, 207 (2018); https://github.com/t-murash/LAMMPS-UEFEX

[2] S. Plimpton, J. Comp. Phys. **117**, 1 (1995); A. P. Thompson et al., Comp. Phys. Comm., 271, 10817 (2022); https://www.lammps.org

[3] T. Murashima, K. Hagita, T. Kawakatsu, Macromolecules, **54**, 7210 (2021).

[4] T. Murashima, K. Hagita, T. Kawakatsu, Macromolecules, **55**, 9358 (2022).

Stability of quantum spin liquids in frustrated spin systems

Kota IDO

Institute for Solid State Physics,

The University of Tokyo, Kashiwa-no-ha, Kashiwa, Chiba 277-8581

The Kitaev spin liquid has attracted attention in order to realize topological quantum computing by Majorana fermions [1, 2]. However, because Kitaev candidate materials have additional magnetic interactions such as the Heisenberg term, the ground state becomes a magnetic ordered state. Applying a magnetic field is a promising way to suppress the magnetic order. In fact, it is reported that the half-integer quantization of the thermal Hall conductivity has been measured in a Kitaev candidate material under a magnetic field, which signals the realization of the Kitaev spin liquid by applying the magnetic field [3]. Therefore, it is desirable to accurately solve the extended Kitaev model under a magnetic field.

The variational Monte Carlo (VMC) method is a numerical method applicable to analysis of two-dimensional systems [4, 5]. Recently, by introducing the Jastrow-BCS wavefunction constructed from the Jordan-Wigner fermions, we succeeded in analyzing the magnetization process of the Kitaev honeycomb model with high accuracy [6]. However, the application of this approach is limited to only the Kitaev model with the magnetic field along z-direction. Thus, it is still challenging problem to solve the Kitaev model with other perturbative terms under the magnetic field along arbitrary direction.

In this project, we analyze the magnetization process of the Kitaev-Heisenberg model under the magnetic field along [001] or [111] direction by using the generalized spinon pair-product wavefunction, which has been already used for analysis of quantum spin liquids in strongly correlated systems [4]. We find that the VMC results by using this trial wavefunction can well reproduce the exact diagonalization results even when we impose a sublattice structure on the trial wavefunction. Applications to large size systems will be reported elsewhere.

References

[1] A. Kitaev, Ann. Phys. **321**, 2 (2006).

[2] H. Takagi et al., Nat. Rev. Phys. **1**, 264 (2019).

[3] Y. Kasahara et al., Nature **559**, 227 (2018).

[4] M. Kurita, Y. Yamaji, S. Morita, and M. Imada, Phys. Rev. B **92**, 035122 (2015).

[5] T. Misawa et al., Comput. Phys. Commun. **235**, 447 (2019).

[6] K. Ido and T. Misawa, Phys. Rev. B **101**, 045121 (2020).

Efficient Sampling Simulation of the Soft Modes Significantly Contribute to Protein Properties

D. P. TRAN, K. TAKEMURA, T.N. WIJAYA, R. OSAWA, M. YOSHIOKA, H. NAKAYA, S. IKIZAWA, T.Y. CHU, H. T. NGUYEN and A. KITAO

School of Life Science and Technology, Tokyo Institute of Technology

Ookayama, Meguro, Tokyo 152-8550

In this project, we employed Parallel Cascade Selection Moelcular Dynamics simulation (PaCS-MD) [1] as the enhanced sampling method to conduct efficient molecular simulation. Recently, we used the conmbination of the PaCS-MD together with Markov State Modeling (MSM) to unveil the energetic and kinetics of the interfacial activation of *Candida antarctica* Lipase B (CALB) [2].

We first constructed the well-relaxed structures of the CALB/W in water and the interface of water and tricaprylin (CALB/I). After that, we performed the PaCS-MD/MSM from open-to-close and close-to-open for both CALB/W and CALB/I with 30 replicas. Each trajectory length is 0.1ns. We monitored the the α5 helix (residues 142–146) and half of the α10 helix (residues 278–287) in all PaCS-MD simulations.

Then we constructed the free energy landscape (FEL) of both systems by using Markov State Modeling from the inter-Cα distances between Arg309 and Leu144 (Dist1) and Ala146 and Val286 (Dist2) and plot in Figure 1. We found that the FEL of CALB/W spans larger conformational space than that of the CALB/I, because of the flexibility of the lid region in water. The minima i1 and i2 in CALB/I FEL are stiffer comparing to that of w1-3 in CALB/W FEL. The free energy level of the closed conformation is much lower than that of the open conformation in water.

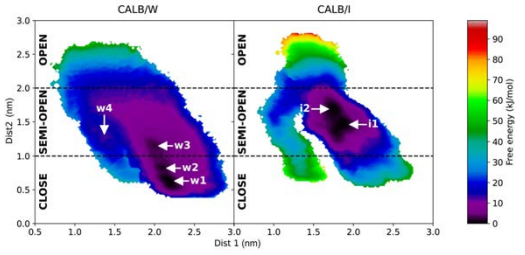

Figure 1. Free energy landscape (FEL) of CALB/W and /I obtained by PaCS-MD/MSM

After that, we performed the PCCA++ [3] to explore macroscopic view of the open-close transition of CALB. We employed the coarse graining the microstates into 6 microstates for both

cases. The CALB/W conformation can be split into three states: closed states (WC1, WC2, and WC3), one semi-open state (WS), and two open states (WO1 and WO2). In CALB/W, we found that the transition from semi-open state to the closed state is one-order of magnitude faster than that to the open state. In contrast, the CALB/I exhibits the timescale of semi-open to open states in nanosecond order. CALB prefers the transition to the closed state in water but moves to the open state in the interface.

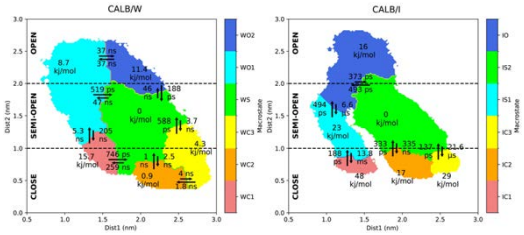

Figure 2. Microstates assignment using PCCA++ for both CALB/W and /I. PCCA++ results and MFPT between macrostates for CALB/W (left) and CALB/I (right). Transition time and free energy difference are also indicated.

Via analysis of PaCS/MSM, we found that the closed state is the most stable in the water system but the stable conformation in the interface system shifts to the semi-open state. In the interface system, the transition probability to the open state is higher than in the water system. We also suggest double mechanisms of substrate binding as followed: i) small and hydrophilic substrates bind without interfacial activation, ii) large and bulky substrates bind via interfacial activation. These findings could help expand CALB applications towards a wide variety of substrates.

References

[1] R. Harada and A. Kitao. J Chem Phys 139, 035103 (2013).

[2] T. N. Wijaya, A. Kitao (2023), ChemRxiv. doi: 10.26434/chemrxiv-2023-17v42

[3] S. Roeblitz, M. Weber, Adv Data Anal Classif 7, 147 (2013)

Thermal effects on quantum frustrated magnetisms

Tokuro Shimokawa

Theory of Quantum Matter Unit, Okinawa Institute of Science and Technology Graduate University, Onna 904-0495, Japan

Investigating the effects of thermal fluctuations in quantum frustrated magnets is crucial for developing our understanding of quantum spin liquids. $Ca_{10}Cr_7O_{28}$ (CCO) [1] is a quantum spin liquid candidate that can be described by the S=1/2 bilayer breathing kagome (BBK) Heisenberg model. Here, we examine the importance of thermal fluctuations by focusing on the J_1-J_2 classical honeycomb-lattice Heisenberg model corresponding to the classical system of this S=1/2 BBK model.

To do this, we employ classical Monte Carlo simulations, utilizing a hybrid parallelization approach combining the heat-bath method, over-relaxation method, and replica exchange method. We investigate the ordering behavior of the honeycomb lattice model in a finite-temperature magnetic field with a focus on the several J_2/J_1 parameter values. Physical quantities, including specific heat, magnetic susceptibility, equal-time structure factor, and chirality, are examined to identify the presence of a Skyrmion lattice state with sublattice structure and other additional multiple-q states [2].

We also report on the investigation of the static and dynamic properties of the S=1/2 J_A-J_B-J_C honeycomb-lattice Heisenberg model, which is believed to be important for understanding the quantum spin liquid behavior in different honeycomb-lattice material $Cu_2(pymca)_3(ClO_4)$ [3]. The investigations were carried out using quantum Monte Carlo simulations based on ALPS application [4] and exact diagonalization. Our results demonstrate the realization of a quantum paramagnetic state in this material, and suggest that focusing on dynamic properties is crucial for experimentally identifying this state [5].

References

[1] C. Balz, *et al.* Nat. Phys. **12** 942 (2016).

[2] T. S., *et al*, in preparation

[3] Z. Honda, *et al*, J. Phys. Soc. Jpn. **84**, 034601 (2015).

[4] A. Albuquerque, *et al*, J. Magn. Magn. Mater. **310**, 1187 (2007).

[5] T. S., Ken'ichi Takano, Zentaro Honda, Akira Okutani, and Masayuki Hagiwara, Phys. Rev. B **106**, 134410 (2022).

Matrix Product Renormalization Group

Masahiko G. YAMADA[AB]
Masahiro O. TAKAHASHI[B]
Takumi SANNO[B]
Yutaka AKAGI[C]
Hidemaro SUWA[C]
Satoshi FUJIMOTO[BD]
Masafumi UDAGAWA[A]
[A] *Department of Physics, Gakushuin University, Mejiro, Tokyo, 171-8588, Japan*
[B] *Department of Materials Engineering Science, Osaka University, Toyonaka 560-8531, Japan*
[C] *Department of Physics, The University of Tokyo, Hongo, Tokyo, 113-0033, Japan*
[D] *Center for Quantum Information and Quantum Biology, Osaka University, Toyonaka 560-8531, Japan*

In order to support and endorse the results found in [1], we have reproduced the matrix product renormalization group (MPRG) calculation done in [1] using the ISSP supercomputer. We newly find that by using the ISSP supercomputer the calculation with a larger bond dimension χ is possible. Indeed, the calculations with $\chi = 128$ are possible for both transverse-field Ising model and the spin-1/2 antiferromagnetic Heisenberg model.

The results agree well with an exact solution or a quantum Monte Carlo simulation. This means that MPRG has a potential to realize a large scale simulation up to $\chi = 128$ and a good scalability. The advantage over other methods will be discussed in the future, but it is likely that MPRG is superior to other conventional tensor network methods.

Currently, the algorithm of MPRG is not suitable for parallel computing, while it may be straightforward to support a graphics processing unit (GPU). We will persue this direction in the future study.

References

[1] M. G. Yamada, T. Sanno, M. O. Takahashi, Y. Akagi, H. Suwa, S. Fujimoto, M. Udagawa: arXiv:2212.13267 (2022).

Magnetism and superconductivity in ternary chromium chalcogenides

Harald JESCHKE
Research Institute for Interdisciplinary Science, Okayama University
3-1-1 Tsushima-naka, Kita-ku, Okayama 700-8530

We study $CrGeTe_3$ which is a van-der-Waals bound layered ferromagnet. Materials like $CrGeTe_3$ or CrI_3 have been intensely investigated in recent years because detached monolayers still order ferromagnetically and are discussed for various nanotechnological applications.

Recently, pressure experiments for $CrGeTe_3$ reported an interesting temperature-pressure phase diagram; importantly, at high pressures, an insulator to metal transition roughly coincides with increases of Curie-Weiss and magnetic ordering temperatures. Our aim is to understand the phase diagram and to investigate the nature of the strongly correlated metal at high pressures.

We perform calculations using density functional theory (DFT) in combination with dynamical mean field theory (DFMT), as implemented in DCore. Based on experimental crystal structures, we prepare tight binding representations of the DFT bands for pressures up to $P = 10\,\mathrm{GPa}$. Figure 1 shows the spectral function of a ferromagnetic insulating solution at ambient pressure [1]. The difficulty in this material is the fact that Te $6p$ bands are very important at the Fermi level. The insulator to metal transition involves pressure induced widening of Te $6p$ bands which then establish a Fermi surface at around 5 GPa. By analyzing the renormalization factor Z where $Z^{-1} = 1 - \partial \mathrm{Im}\Sigma(i\omega)/\partial\omega|_{\omega\to 0^+}$, we find that correlations of some Cr $3d$ orbitals are enhanced by increasing pressure.

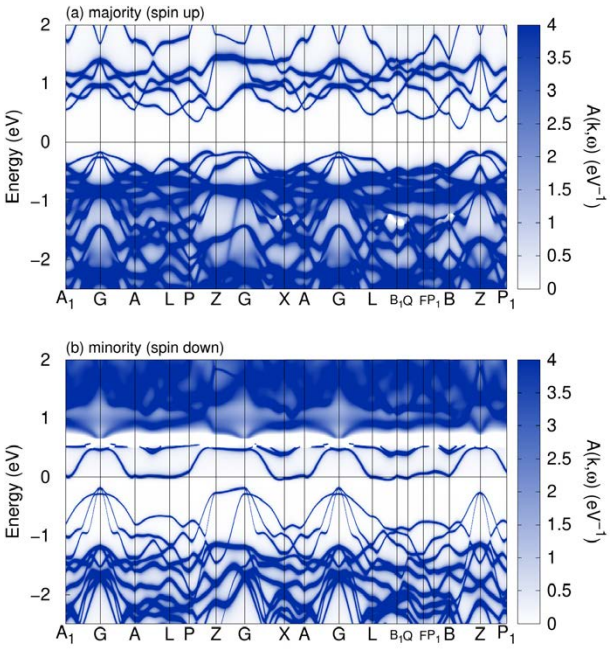

Figure 1: Spectral function for the ferromagnetic state of $CrGeTe_3$ at $P = 0\,\mathrm{GPa}$ and $T = 100\,\mathrm{K}$. Chromium magnetic moments are close to $3\,\mu_\mathrm{B}$.

References

[1] H.-X. Xu, M. Shimizu, J. Otsuki, H. O. Jeschke, in preparation.

Fluctuation exchange approximation calculations for the superconducting transition temperatures and pairing symmetries of organic charge transfer salts

Harald JESCHKE
Research Institute for Interdisciplinary Science, Okayama University
3-1-1 Tsushima-naka, Kita-ku, Okayama 700-8530

BEDT-TTF (bisethylene-dithio-tetrathiafulvalene) is a famous nearly flat molecule that forms hundreds of charge transfer (CT) salts, among them a number of famous superconductors. We study eight of the known ambient pressure superconductors in the κ phase where dimers of BEDT-TTF molecules form a triangular lattice which is doped with one hole per dimer. Our aim is to improve on earlier studies based on random phase approximation and two-particle selfconsistent approximation to predict the material dependence of superconducting transition temperature and order parameter. Our newly developed multi-orbital, multi-site fluctuation exchange approximation (flex) code was parallelized with OpenMP and MPI methods.

Figure 1 shows the leading solutions of the Eliashberg equation for one of the materials, together with the trend of the leading eigenvalues [1]. T_c trends are captured well by the dominant eigenvalue of the Eliashberg equation for five high-T_c materials. However, for three low-T_c materials, the present approach overestimates the strength of the s-wave solution. A possible reason for this discrepancy is the intra-dimer, inter-site interaction V that has been neglected so far and that is expected to play an important role in the κ-type CT salts.

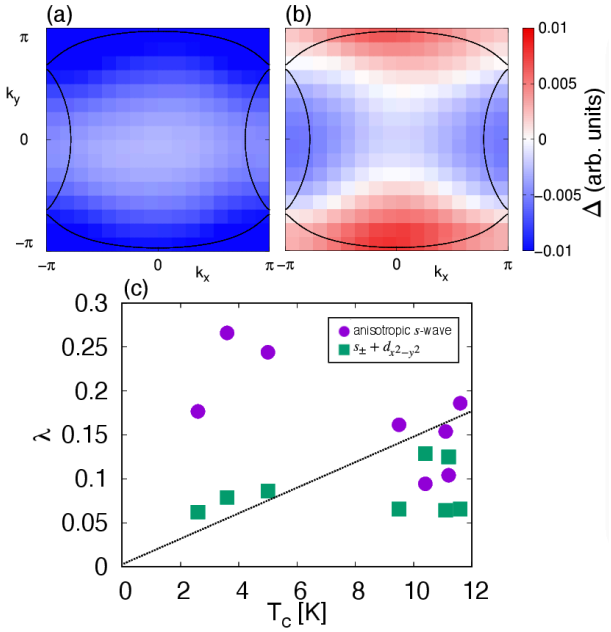

Figure 1: (a), (b) Imaginary part of an inter-dimer element of the anomalous self-energy for the two leading solutions for κ-$(ET)_2Cu[N(CN)_2]Br$. (c) Eigenvalues λ for anisotropic s-wave and for $s_\pm + d_{x^2-y^2}$-wave.

References

[1] M. Shimizu, D. Guterding, J. Otsuki, H. O. Jeschke, in preparation.

Numerical studies for science of bulk-edge correspondence and topological phases

Yasuhiro HATSUGAI

Department of Physics, University of Tsukuba

Tennodai 1-1-1, Tsukuba, Ibaraki 305-8571

The topological phases are independent of the symmetry breaking. It implies that there is no fundamental order parameter to characterize it. Most of them are gapped, and low-energy gapless excitation is absent. It implies that the bulk is hidden. However, with edges or boundaries, there exist low-energy gapless excitations that are localized only near the system boundaries and characterize the phase. This is the bulk-edge correspondence.

A topological pump (adiabatic pump) is another kind of topological phenomenon where the bulk-edge correspondence again governs the phenomena. Here the bulk-edge correspondence is special, that is, the edge states are hidden since the gapless nature of the edge states implies that the edge state cannot be observed by an experimental finite speed pump. Experimental observables for the topological pump are the center of mass (polarization) of the bulk, which is described by the Chern number integrated over the torus spanned by the time and gauge twist. In Fig. 1, we have shown numerical evaluation of the Chern numbers for the topological pump of SU(Q) interacting fermions [2]. The relation between the edge states spectrum and the Chern numbers are consistently discussed by using numerical studies.

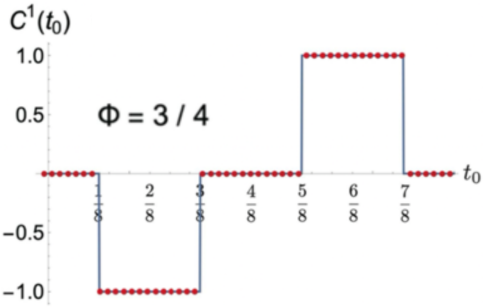

Fig. 1 Numerical results of the Chern number of SU(Q) topological pump (from ref. [2]).

References

[1] Y. Hatsugai, Phys. Rev. Lett. 71, 3697 (1993).).

[2] Y. Hatsugai, and Y. Kuno, arXiv:2210.11646

Effects of flux structures on Majorna excitations in Kitaev spin liquids

Akihisa Koga
Department of Physics, Tokyo Institute of Technology, Meguro, Tokyo 152-8551

Quantum spin liquids in the Kitaev model have been studied intensively in recent years. It is known that in the Kitaev model, spin degrees of freedom are split into itinerant Majorana fermions and localized fluxes due to the spin fractionalization. The ground state belongs to the flux-free state and low energy properties are described by itinerant Majorana fermions. In fact, the Majorana edge current has been observed in the half-quantized plateau in the thermal quantum Hall effect. Furthermore, the Majorana-mediated spin transport has been theoretically suggested, which should stimulate further investigation to realize quantum devices using Majorana fermions.

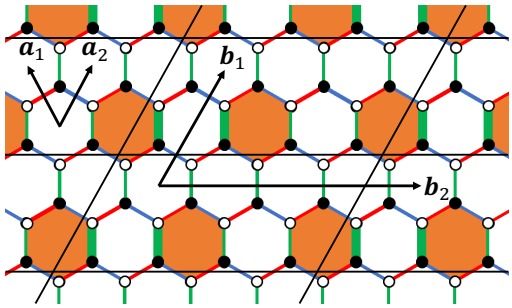

Figure 1: Flux configuration ($q = 2$) of the Kitaev model.

In our previous study [1], we have found that the gapped quantum spin liquid is realized in a certain flux configuration. This indicates that the flux configuration is a key role in controlling Majorana excitation. On the other hand, it is known that the large anisotropy in the exchange couplings stabilizes the gapped quantum spin liquid, which should be described by the toric code. Then a question arises. Are the above gapful states with distinct origins are adiabatically connected to each other? To answer this question, we consider several flux configurations to investigate how the anisotropy in the exchange couplings affects the Majorana excitations.

Motivated by this, we deal with the anisotropic Kitaev model with flux configurations. In particular, we focus on the triangular flux configurations, where the fluxes are periodically arranged in the honeycomb sheet, as shown in Fig. 1. Systematic numerical calculations demonstrate how the anisotropy of the exchange couplings and flux configuration induce the excitation gap. The induced gapped quantum spin liquid states are distinct from the gapped one realized in the large anisotropic limit. We then clarify the nature of gapped states in the Kitaev model, regarding the flux configuration as the superlattice potential for the flux-free state [2, 3].

References

[1] A. Koga, Y. Murakami, and J. Nasu, Phys. Rev. B **103**, 214421 (2021).

[2] A. Hashimoto, Y. Murakami, and A. Koga, J. Phys.: Conf. Ser. 2164, 012028 (2022).

[3] A. Hashimoto, Y. Murakami, and A. Koga, arXiv:2303.04295.

Molecular dynamics simulation of disease-related biomolecules

Hisashi Okumura

Exploratory Research Center on Life and Living Systems, Institute for Molecular Science, Okazaki, Aichi 444-8585

Proteins maintain their functions with correctly folded structures. However, when their concentration increases due to, for example, aging, they aggregate to form oligomers, spherical aggregates, and amyloid fibrils, needle-like aggregates. These protein aggregates are associated with about 40 human neurodegenerative diseases. For instance, the amyloid-β (Aβ) peptide is related to Alzheimer's disease. We have performed several molecular dynamics (MD) simulations of Aβ aggregates. In this fiscal year, we performed MD simulations of the dimerization process of Aβ peptides and specified the key residue for aggregation of Aβ peptides.

Aβ has two isoforms: Aβ40 and Aβ42. Although the difference between Aβ40 and Aβ42 is only two residues in the C-terminus, Aβ42 aggregates much faster than Aβ40. It is not clear why the C-terminal two residues accelerate the aggregation. To investigate the dimerization process, we performed Hamiltonian replica-permutation molecular dynamics simulations of two Aβ40 peptides and those of two Aβ42 peptides using the supercomputer at the Supercomputer Center, the Institute for Solid State Physics, the University of Tokyo [1]. The replica-permutation method is an improved version of the replica-exchange method, in which the transition ratio of replicas in the temperature or parameter space is improved.

As a result, we identified the key residue, Arg5, for the Aβ42 dimerization. The two C-terminal residues in Aβ42 tend to form contact with Arg5 because of the electrostatic attraction between them, stabilizing the β-hairpin. This β-hairpin promotes dimerization through the intermolecular β-sheets.

Thus, we asked experimental collaborators to examine the effects of amino-acid substitutions of Arg5 to verify our theoretical prediction. We found that the mutations remarkably suppressed the aggregation of Aβ42. In this way, our prediction was approved by the experiments.

References

[1] S. G. Itoh, M. Yagi-Utsumi, K. Kato, and H. Okumura, ACS Chem. Neurosci. **13,** 3139 (2022).

Nontrivial properties of interface and finite size effects of free energies

Naoko NAKAGAWA
Department of Physics, Ibaraki University
2-1-1 Bunkyo, Mito, Ibaraki 310-8512

We investigate liquid-gas coexistence associated with first-order transitions via molecular dynamics simulations using LAMMPS. We managed two kinds of systems, one is a simple fluid of Lennard-Jones particles and the other is the two components fluid of argon and krypton.

In the former systems, we notice the configuration of the coexistence states and examine the thermodynamic quantities. Despite the finiteness of the system size, we find a sharp interface separating the two phases, whereas both the shape and the position of the interfaces largely fluctuate.

We set temperature and mean mass density as almost particles are in liquid, while a small number of particles be in gas. When the aspect ratio of the box confining the particles is close to unity, we observe typically a bubble with a round-shaped interface. Changing the aspect ratio, the shape of the interface transitioned into a flat shape, where the gas occupies a stripe region that may situate adjacent to the boundary. To characterize the transition, we calculate the virial pressure corresponding to the mean pressure over the system, which may provide the global thermodynamic properties in phase coexistence. With the transition for the shape of the interface, we find a significant change in the value of the virial pressure. It drops even to a negative value when the size of the bubble is too small. This indicates that the system behaves attractively, although the liquid or gas without coexistence,

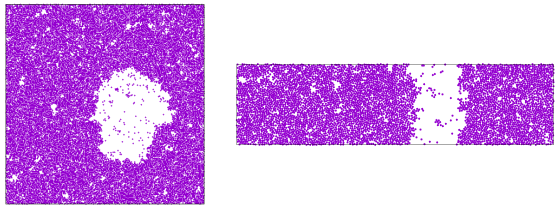

Figure 1: Phase coexistence of liquid and gas in the aspect ratio 1 and 4.

or the coexistence with a flat interface, shows positive pressure as is usual. Such anomaly of the virial pressure suggests that the system is not explained by thermodynamics in equilibrium, and may possess meta-stable or unstable characteristics. We will proceed calculations to characterize the local states for identifying the mechanism to maintain the metastability.

We also investigated the liquid-gas coexistence for the two components fluid of argon and krypton using the mixing free energy. The mixing free energy is numerically determined by applying the formula derived in [1]. We find that the finite size effects lead to the violation of the convexity in the free energy. To examine the stability of the coexistence states showing the violation of the convexity, we carefully examine the possibility of hysteresis. Up to now, we confirm that rather smaller systems do not show hysteresis in our setup. While we need further investigations with various system sizes, the result indicates that the finiteness of the system size may induce the violation of the

convexity in free energy in a different context from the metastability.

We have used the L4 CPU of System B with 4 nodes in 512 parallel computation using MPI for the calculation of 2×10^4 particles, the L16 CPU of System B with 16 nodes in 2048 parallel computation using MPI for the calculation of 8×10^4 particles, the L32 CPU of System B with 24 nodes in 3072 parallel computation using MPI for the calculations of 5×10^5 and 1×10^6 particles.

References

[1] A. Yoshida and N. Nakagawa: *Phys. Rev. Res.* **4**, 023119 (2022)

Nonequilibrium relaxation temperature scaling: Applications to quantum systems

Yoshihiko NONOMURA
MANA, National Institute for Materials Science
Namiki 1-1, Tsukuba, Ibaraki 305-0044

We numerically revealed that the critical nonequilibrium relaxation behaviors in cluster algorithms are described by the stretched-exponential simulation-time dependence of physical quantities in various classical spin systems [1, 2, 3] and in a quantum phase transition [4], and derived such a relaxation formula phenomenologically [5]. The nonequilibrium-to-equilibrium (NE-EQ) scaling used in these studies [1, 3, 4] were generalized to off-critical behaviors, and such a scaling was called as the "temperature scaling" [6].

Here we show that the temperature scaling also holds in quantum phase transitions. As an example, we consider the Néel-dimer quantum phase transition in the columnar-dimerized $S = 1/2$ antiferromagnetic Heisenberg model on a square lattice [4]. When the ratio of the strength of dimerized bonds to other bonds are taken as $(1 + \delta) : 1$, the staggered susceptibility in equilibrium diverges in the vicinity of the critical point δ_c as $\chi_{st}(t = \infty, \delta) \sim (\delta - \delta_c)^{-\gamma}$ with $\delta_c = 0.90947(6)$ [4]. Combining this formula with the initial-time stretched-exponential critical relaxation form $\chi_{st}(t; \delta_c) \sim \exp(ct^\sigma)$, we have $\chi_{st}(t, \delta)(\delta - \delta_c)^\gamma \sim \exp[ct^\sigma + \ln(\delta - \delta_c)^\gamma]$, or

$$\chi_{st}(t, \delta)(\delta - \delta_c)^\gamma \sim f_{sc}[ct^\sigma + \ln(\delta - \delta_c)^\gamma]. \quad (1)$$

Scaling results for the $L \times L$ periodic-boundary system with $L = 160$ and inverse temperature $\beta = L$ in the loop algorithm from dimer configurations are given in Figure 1. Using the estimate $\gamma = 1.400(3)$ obtained from this figure and the estimate $\gamma/\nu = 1.973(4)$ based on the NE-EQ scaling up to $L = 160$ [4], we have $\nu = 0.710(2)$ only with a diagonal quantity χ_{st}.

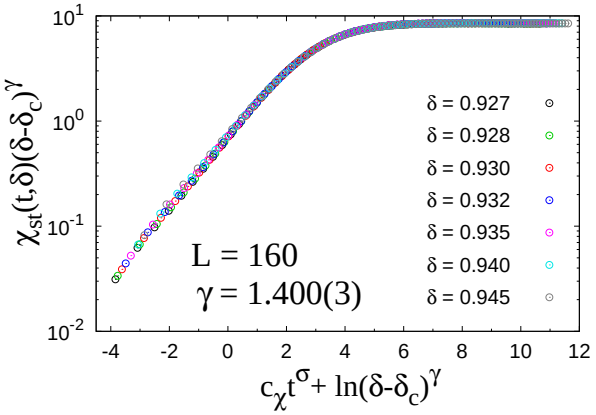

Figure 1: Temperature scaling of the staggered susceptibility in the 2D columnar-dimerized $S = 1/2$ antiferromagnetic Heisenberg model.

References

[1] Y. Nonomura, J. Phys. Soc. Jpn. **83**, 113001 (2014).

[2] Y. Nonomura and Y. Tomita, Phys. Rev. E **92**, 062121 (2015).

[3] Y. Nonomura and Y. Tomita, Phys. Rev. E **93**, 012101 (2016).

[4] Y. Nonomura and Y. Tomita, Phys. Rev. E **101**, 032105 (2020).

[5] Y. Tomita and Y. Nonomura, Phys. Rev. E **98**, 052110 (2018).

[6] Y. Nonomura and Y. Tomita, Phys. Rev. E **102**, 052118 (2020).

HPC-based fusion of quantum simulation, experiment analysis and data-driven science

Takeo Hoshi[1,2]

[1] *Department of Mechanical and Physical Engineering, Tottori University, 4-101 Koyama-Minami, Tottori 680-8550, Japan.*

[2]*Slow Positron Facility, Institute of Materials Structure Science, High Energy Accelerator Research Organization (KEK), Oho 1-1, Tsukuba, Ibaraki, 305-0801, Japan.*

We developed several new features on 2DMAT [1-6], an open-source data-analysis software for advanced experimental measurement techniques. 2DMAT was developed by the PASUMS project at FY2020, 2021[1]. A major achievement in the present project is the automated optimization of the massively parallel computation of the population annealing Monte Carlo (PAMC) method [7]. As results, we found an almost ideal parallel efficiency not only on the ISSP supercomputer (ohtaka) but also on the Fugaku supercomputer with upto 10^4 nodes [8] . As an application study, we used 2DMAT for the data analysis of total-reflection high-energy positron diffraction (TRHEPD)[9]. TRHEPD is an innovative measurement technology for the surface structure analysis and was realized at Slow Positron Facility, KEK [9]. The experimental setup of TRHEPD is similar to that of reflection high-energy electron diffraction (RHEED) but TRHEPD reveals the surface sensitivity and was used for the determination of surface structure. 2DMAT was applied to the analysis of Ge(001)-c4x2 surface structure as a test of the Bayesian inference by PAMC. [8] We analyzed the experiment diffraction data in the one-beam condition, in which only the z-coordinate of atom positions are measured. The Bayesian posterior probability distribution $P(X|D)$ was calculated for the data set of the atom positions X with the given experimental diffraction data set D and reproduced the correct atomic position of the $N_{\mathrm{a}} = 6$ atoms of the top-most and several subsurface layers. Moreover, the correct number of the atoms ($N_{\mathrm{a}} = 6$) was also reproduced from the calculated model evidence $P(D)$. In conclusion, the PAMC analysis, as a global search, determined the correct surface structure without any initial guess. Other application studies are ongoing.

References

[1] https://www.pasums.issp.utokyo.ac.jp/2DMAT

[2] K. Tanaka, *et al*. (T. Hoshi), Acta. Phys. Pol. A 137, 188 (2020).

[3] T. Hoshi, *et al*. (T. Hoshi), Comp. Phys. Commun. 271, 108186 (2022).

[4] T. Hanada, *et al*., Comp. Phys. Commun. 277 108371 (2022).

[5] Y. Motoyama, *et al*. (T. Hoshi), Comp. Phys. Commun. 280, 108465 (2022).

[6] K. Tanaka, *et al*. (T. Hoshi), JJAP Conf. Series 9, 011301 (2023).

[7] K. Hukushima, Y. Iba, AIP Conf. Proc. 690, 1604 (2003).

[8] N. Kinoshita, *et al*. (T. Hoshi), in JPS meeting, 22-25, Mar. 2023.

[9] https://www2.kek.jp/imss/spf/eng/

Chaotic dynamics in quantum many-body systems

Masaki TEZUKA

Department of Physics, Kyoto University, Kitashirakawa, Sakyo-ku, Kyoto 606-8502

The Sachdev-Ye-Kitaev (SYK) model is a model of fermions with independently random all-to-all four-point interactions obeying the Gaussian distribution. The model, both for Majorana and complex fermions, has an analytic solution in the limit of large number of fermions. The Lyapunov exponent, defined by the out-of-time ordered correlator, realizes the universal upper bound at low temperatures.

Previously, we studied the effect of a random hopping term, two-fermion interactions, added to the model [1]. The chaos bound behavior is lost and the eigenenergy spectrum becomes uncorrelated. The localization transition can be understood as a Fock-space localization, a type of many-body localization. We have obtained physical quantities related to this transition, such as the location of the transition point as well as the moments of the eigenstate wavefunctions and bipartite entanglement entropy close to the transition analytically and confirmed numerically [2].

A “sparse” version of the SYK model, in which the number of randomly chosen non-zero interaction terms is only on the order of the number of fermions, have been proposed a few years ago, and for Gaussian random couplings, the sparse model reproduces essential features of the original SYK model [3]. Using the ISSP Supercomputer, we analyzed the spectral statistics of a further simplification of the sparse SYK model, in which the magnitude of the nonzero couplings between Majorana fermions are set to be a constant [4]. In fact, this simplification is an improvement, as the spectral correlation is stronger and thus closer to the random-matrix universality for the same number of non-zero couplings, compared to the Gaussian random case.

We also studied the quantum error correction (QEC) capabilities of the unitary time evolution according to the SYK type Hamiltonians by the Hayden-Preskill protocol. This is a process in which one tries to decode an unknown quantum state thrown into a quantum many-body system with the knowledge of the initial state of the system and the time evolution, by accessing only a part of the system after the evolution. The error estimate for random unitary evolutions obeying the circular unitary (Haar) ensemble has been known. For the sparse SYK model, the QEC error estimate approaches the Haar value after a short time if the spectral statistics is random-matrix like. In the presence of two-fermion interactions, departure from the Haar value is observed before the Fock space localization [5].

References

[1] A. M. Garcia-Garcia, B. Loureiro, A. Romero-Bermudez, and M. Tezuka, Phys. Rev. Lett. **120** (2018), 241603.

[2] F. Monteiro, T. Micklitz, M. Tezuka, and A. Altland, Phys. Rev. Research **3** (2021), 013023; F. Monteiro, M. Tezuka, D. A. Huse, and T. Micklitz, Phys. Rev. Lett. **127** (2021), 030601.

[3] S. Su *et al.*, arXiv:2008.02303; A. M. Garcia-Garcia *et al.*, Phys. Rev. D **103**, 106002 (2021).

[4] M. Tezuka, O. Oktay, E. Rinaldi, M. Hanada, and F. Nori, Phys. Rev. B **107**, L081103 (2023).

[5] Y. Nakata and M. Tezuka, arXiv: 2303.02010.

Molecular Dynamics Simulation of Dissolution of Stretched PEG Crystal in Aqueous Solution

Koichi Mayumi, Kosuke Aomura, Haru Shinohara

The Institute for Solid State Physics,

The University of Tokyo, Kashiwa-no-ha, Kashiwa, Chiba 277-8581

Hydrogel is a material in which water is confined in a polymer network. Hydrogel has high biocompatibility and is expected to be applied to biomaterials, but its mechanical strength has been a problem. In our laboratory, we have developed a hydrogel with both toughness and resilience by using the self-reinforcing effect [1]. In this self-reinforcing gel, polyethylene glycol (PEG) is used as the main chain of the polymer network and water as the solvent. When the strain is removed, the PEG chains form hydration with the solvent water, and the crystals are quickly melted. Such solvation and dissolution processes are thought to play an important role in the strain-induced crystals that are reversible against elongation. In this study, we performed all-atom molecular dynamics simulations to understand extended PEG crystal dissolves in aqueous solution.

Based on the structures reported from X-ray diffraction results [2, 3], all-atom models of zigzag PEG chain crystals consisting of 24 PEG chains with 42 repeat units were created (Fig. 1). After energy minimization calculations, 4200 water molecules are added to the box so that the polymer fraction was 38 wt%. A stretching force was applied to both ends of each polymer chain for 400 ns. The applied force f was set at 6 points: 0, 10, 30, 70, 100, and 210 kJ/(mol nm). GROMACS 2016.5 was used as computational software. Simulations were performed on Ohtaka, ISSP supercomputer system B. The number of atoms in the

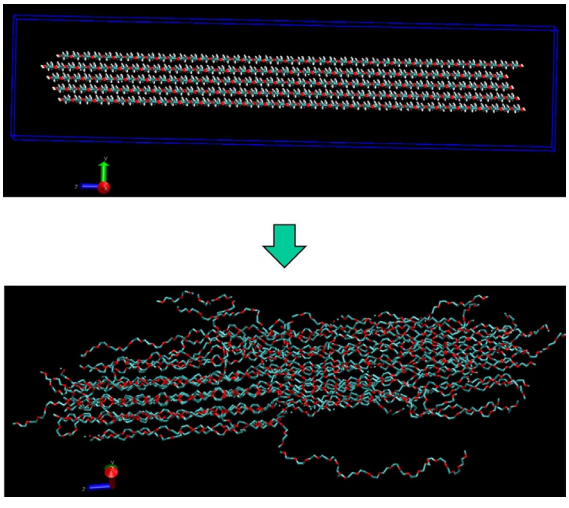

Fig. 1 Snap-shots of PEG zig-zag crystals stretched under f = 10 kJ/(mol nm) at time t = 0 and t = 400 ns.

simulation box was about 24,000, and the computation speed was about 200 ns/day with a parallel number of 512.

For f = 0 kJ/(mol nm), the zigzag chain crystals are dissolved within 200 ns, which is consistent with the rapid dissolution of stretched induced PEG crystals just after the applied stretching force is unloaded in our experiments. When f is 10 kJ/(mol nm), the zigzag chain crystal is dissolved and then the a helical PEG crystal is formed..

References

[1] C. Liu, N. Morimoto, L. Jiang, S. Kawahara, T. Noritomi, H. Yokoyama, K. Mayumi, K. Ito, *Science*, **372,** 1078-1081(2021).
[2] Takahashi, Y., Tadokoro, H. *Macromolecules,* **6**, 672-675 (1973).
[3] Takahashi, Y., Sumita, I., Tadokoro, H. *J. Polym. Sci., B, Polym. Phys.*, **11**, 2113-2122 (1973).

Molecular dynamics simulation for chemical reactions in multicomponent systems of thermosetting resins

Yutaka Oya

Department of Materials Science and Technology,

Tokyo University of Science, Niijuku, Katsushika-ku, Tokyo 125-8585

In this year, we have studied following two topics. The first is to establish the methodology for reproducing the crosslinked reactions of thermosetting polymers based on full-atomistic molecular dynamics simulation. We focused on multicomponent system including base resin with epoxy groups, curing agent with amine groups and lignin with hydroxyl groups, which is one of promising candidates for matrix of bio-based composites. The chemical reactions among these components were successfully realized for systems of several hundred thousand atoms by LAMMPS software. In the future study, we systematically investigate the thermal and mechanical characteristics, such as Young's modulus, strength, glass-transition temperature, for the crosslinked structures formed by these molecules.

The second is to investigate the stacking structure of organic photovoltaic materials. It is well known that electron transfer occurs through the π-π stacking structure of the donor and acceptor molecules. Such photoexcited reactions of conjugated polymers are expected to be applied to nondestructive inspection of mechanical damages of a composite. In this study, full atomic molecular dynamics simulations were performed for reproducing the equilibrium structure of the system including IT-4F (donor molecule) and PDTB (accepter molecule) as shown in Figure 1. Further, frequency distributions for each type of stacking structure in the system were analyzed. As a result, it was found that J-aggregation between IT4F and PDTB molecules is dominant in the system. In the future study,

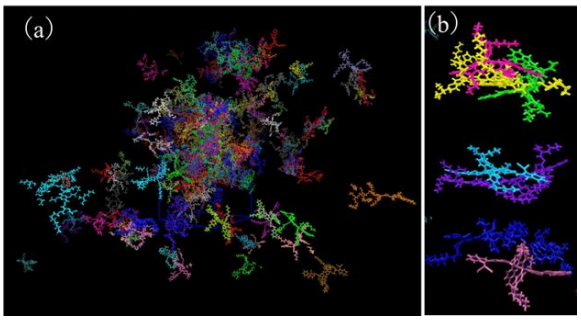

Figure 1. (a) Equilibrium structure of IT4F and PDTB molecules. (b) Snapshots of typical stacking structures obtained by molecular dynamics simulations.

Numerical study on low-energy states of quantum spin systems

Hiroki NAKANO
Graduate School of Science, University of Hyogo
Kouto, Kamigori, Hyogo 678-1297, Japan

Since researchers are often faced with many-body problems in the condensed matter physics, it is difficult to estimate physical quantities precisely. One of the typical issues is a quantum spin system. To study a quantum spin system, numerical approaches have widely and effectively been employed. Computational studies that were carried out have provided us with useful information of the target systems.

Within the field of quantum spin systems, three methods have been effectively used. The first and traditional one is the numerical diagonalization method. The second method is the quantum Monte Carlo (QMC) simulation. The third one is the density matrix renormalization group (DMRG) method. Each of these methods has advantages; however, it has also disadvantages at the same time. The QMC simulations can treat significantly large systems irrespective of the spatial dimensions of the systems; on the other hand, the negative sign problem with this approach prevents us with a difficulty in precise evaluation of physical quantities in frustrated systems. When the spatial dimension of a target system is one, however, the DMRG method is very useful irrespective of whether or not the target system includes frustration. Unfortunately, this method is still under development for the cases when the spatial dimension is larger than one. We can apply the numerical diagonalization method to various systems irrespective of the presence of frustrations and the spatial dimension. This method, on the other hand, has a severe weak point that it can treat only systems with very small sizes. To overcome this disadvantage of the numerical diagonalization method, we developed a hybrid-type parallelized code of Lanczos diagonalization[1]. This code enables us to treat various large systems that have not been treated yet within this method. We, therefore, study various quantum spin systems by this method as a primary approach in this project.

In the project in 2022, we tackled the $S = 1$ Heisenberg antiferromagnet in one dimension[2]. We successfully carried out Lanczos diagonalizations of this system up to 30 sites under the twisted boundary condition. The 30-site system was treated within Lanczos-diagonalization studies for the first time to the best of our knowledge. Note here that the largest treated matrix dimension is 18,252,025,766,941. Our results were analyzed via a convergence-acceleration technique; we finaly concluded

$$\Delta/J = 0.410479239 \pm 0.000000041$$

as the Haldane gap, namely, the spin excitation above the nondegenerate ground state. We confirmed that this result agrees with the result from the DMRG method[3]. We also studied the $S = 1/2$ Heisenberg antiferromagnet on the floret-pentagonal lattice[4]. Our calculations successfully clarified the behavior around the five-ninth of the saturation magnetization in its magnetization process. Our studies contribute much to our deeper understandings of

the quantum magnetism. Further investigations would clarify nontrivial quantum effects in these systems.

References

[1] H. Nakano and A. Terai: J. Phys. Soc. Jpn. **78**, 014003 (2009).

[2] H. Nakano, H. Tadano, N. Todoroki and T. Sakai: J. Phys. Soc. Jpn. **91**, 074701 (2022).

[3] H. Ueda and K. Kusakabe: Phys. Rev. B **84**, 054446 (2011).

[4] . R. Furuchi, H. Nakano, and T. Sakai: arXiv:2209.13887 to be published in JPS Conf. Proc.

Study of ground states and dynamics in frustrated quantum magnets using MPS-based simulations

Matthias GOHLKE
Theory of Quantum Matter Unit, Okinawa Institute of Science and Technology
1919-1 Tancha, Onna-son, Okinawa 904-0495

Competing interactions—or frustration—between the constituents of a many-body system have proven to be an origin of exotic phases of matter. A famous example in this context are quantum spin liquids (QSL), that do not exhibit conventional magnetic order of spin-dipolar moments, but rather are defined by emergent gauge fields, fractionalized excitations, and topological order. A topical example in this context are Kitaev-like frustrated magnets, that exhibit a bond-dependent spin-exchange resulting in exchange frustration and, for certain choices of parameters, can result in a QSL ground state. Part of the computational resources provided by ISSP has been used to study the related anisotropic Kitaev-Γ model [see (II)].

On the other hand, ordering of higher moments like spin-quadrupoles may occur as well. Unlike spin-dipolar order, spin-quadrupolar order is defined by a director—an arrow without a head—in close analogy to the rods of nematic order and liquid crystals. Thus, spin-quadrupolar order is also named quantum spin nematic (QSN). Part of the resources have been used to study the QSN phase stabilizing in a frustrated ferromagnet with external magnetic field [see (I)].

(I) QSN in a Spin-$\frac{1}{2}$ Frustrated Ferromagnet. Here, we focus on a quantum magnet with spin-$\frac{1}{2}$ degrees of freedom. Such magnets can only exhibit a QSN states if two spin-$\frac{1}{2}$ are combined into an effective spin-1 [1]. In fact, such QSN states on bonds has theoretically been observed in frustrated ferromagnets with ring-exchange on the square lattice [2].

Experimentally, the nature of such a ground state is intrinsically difficult to verify, due to the lack of probes that couple directly to the spin-quadrupole moments. Instead, it is necessary to examine the dynamics of a QSN: A continuous symmetry for the director of a spin-quadrupole remains, that give rise to a gapless Goldstone mode [3, 4].

Here, we study the square-lattice frustrated J_1-K model [1], with dominant ferromagnetic Heisenberg exchange J_1 between nearest neighbor spins, cyclic ring-exchange K around squares, and h_z the Zeeman coupling to a magnetic field along the z-axis. Using iDMRG and the matrix product states (MPS) framework as well as a recently developed exact diagonalization (ED) method near saturation [5], we confirm the existence of the QSN phase in an extended range of $K/|J_1|$. Overall we find a good agreement between high-field ED on symmetric clusters and iDMRG on cylindrical geometries with a circumference of $L_{\mathrm{circ}} = 6$ sites. The QSN phase is sandwiched between high-field polarized and 4-sublattice AF phase. Additional phases (Neél, vector-chiral) occur for large K.

Given the ground state as an MPS, we can then obtain dynamical properties via a time-evolution unitary $U(dt)$ represented as a matrix product operator. We confirm the condensation of two-magnon bound state at the corresponding wave vector of the QSN

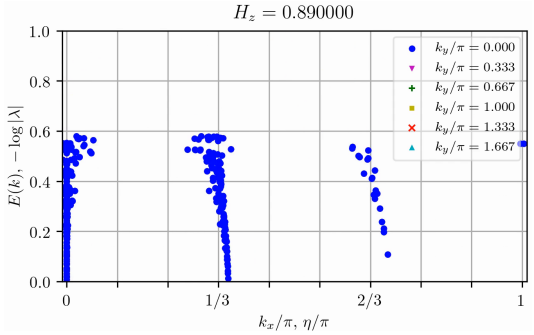

Figure 1: TM spectrum illustrating dominant correlations at $k_x = 0$ as well as incommensurate correlations near $k_x \approx 0.35\pi$.

state. Within the QSN phase, we observe (1) the magnon-like excitation that remains fully gapped, and (2) a gapless mode with its spectral weight in the dipolar structure factor vanishes as $\boldsymbol{q} \to 0$ & $\omega \to 0$ as predicted by prior mean-field studies. We do, however, observe relevant qualitative differences: an additional mode with a gapless node at an incommensurate, field-strength dependent wave vector occurs. Within this term, we have focused on identifying the incommensurate mode by means of the MPS transfer matrix (TM). The TM spectrum contains all the information on correlations. Momentum information is contained through the complex phase of the TM eigenvalues, and momentum along the circumference being a well defined quantum number as long as translation symmetry remains intact. Thus, the position in momentum space of the gapless modes can be extracted from the MPS, cf. Fig. 1.. Indeed, we find perfect agreement between the gapless mode in the dynamics and the TM, which will help us in further elucidating the nature of the incommensurate gapless mode accompanying the QSN phase.

All MPS-related simulations have been carried out using TenPy [8]. TenPy makes use of Cython and calls heavily optimized Lapack and Blas routines matrix operations, e.g. singular value decomposition.

(II) Extended QSL in an Anisotropic Kitaev-Γ Model. The characterization of quantum spin liquid phases in Kitaev materials has been a subject of intensive studies over the recent years. Most theoretical studies have focused on isotropic coupling strength in an attempt to simplify the problem. We, instead, have focused on an extended spin-1/2 Kitaev-Γ model on a honeycomb lattice with an additional tuning parameter that controls the coupling strength on one of the bonds [6], allowing us to connect the limit of isolated Kitaev-Γ chains, which is known to exhibit an emergent $SU(2)_1$ Tomonaga-Luttinger liquid (TLL) [7], to the two-dimensional model. We find that the critical properties of the TLL persist for finite inter-chain coupling, and a QSL develops in analogy to *sliding Luttinger liquids* that differs from the Kitaev spin liquid.

We have employed the TenPy package [8] to obtain the ground state in MPS form, study its scaling behavior via the MPS transfer matrix spectrum, and obtain dynamical properties.

References

[1] A. Andreev and I. Grishchuk, Sov. Phys. JETP **60** (1984) 267.

[2] N. Shannon, T. Momoi, and P. Sindzingre, Phys. Rev. Lett. **96** (2006) 027213.

[3] R. Shindou, S. Yunoki, and T. Momoi, Phys. Rev. B **87**, (2013) 054429.

[4] A. Smerald, H. T. Ueda, and N. Shannon, Phys. Rev. B **91** (2015) 174402.

[5] H. Ueda, S. Yunoki, and T. Shimokawa, Comp. Phys. Comm. **277** (2022) 108369.

[6] M. Gohlke, J. C. Pelayo, T. Suzuki, arXiv:2212.11000 (2022). *See also report by T. Suzuki.*

[7] Yang et al. Phys. Rev. Lett. **124**, 147205 (2020).

[8] J. Hauschild, and F. Pollmann, SciPost Phys. Lect. Notes 5 (2018).

Dynamical properties of the extended Kitaev-Γ model on a honeycomb lattice

Takafumi SUZUKI

Graduate School of Engineering,

University of Hyogo, Shosha, Himeji, Hyogo 670-2280

We have used ISSP supercomputer resources for the following two topics: (1) dynamical properties of the extended honeycomb-lattice Kitaev-Γ model and (2) supersolid states in two-dimensional hard-core bosonic Hubbard model with dipole interactions.

(1) Dynamical properties of the extended honeycomb-lattice Kitaev-Γ model

In this project, we have investigated ground states and dynamical properties of the S=1/2 Kitaev-Γ model [1] on a honeycomb lattice by the numerical exact diagonalization and density-matrix-renormalization-group approaches. The S=1/2 Kitaev-Γ model on a honeycomb lattice was proposed as the effective model of the honeycomb-lattice magnet, α-$RuCl_3$. So far, the ground-state phase diagram of this model with the isotropic coupling strength has been studied intensively. In recent experiments on the related compounds, RuX_3 (X=Br, I) [3], it has been reported that applying pressure can control the anisotropy of the coupling strength. The ground-state phase diagram of the S=1/2 Kitaev-Γ model with anisotropic interactions has not been fully understood yet. Note that the anisotropy means that by tuning the anisotropy, the model changes from the Kitaev-Γ spin chains to the isolated dimer model via the isotropically interacting model.

In the previous study, we focused on the ground phase diagram and the low-lying excitation in the case where the Kitaev interaction (K) and the Γ interaction (Γ) are negative and positive, respectively [4]. We clarified that the Tomonaga-Luttinger liquid (TLL) appearing in the spin chain limit (d=0) [5] persist for the finite interchain interactions and it becomes a proximate Tomonaga-Luttinger liquid (pTTL), which is analogous to sliding TLL [6]. In the pTTL phase, the dispersion curves for the low-lying excitation show a linear behavior around gapless wave-number points, which is similar to the characteristics observed in the S=1/2 antiferromagnetic Heisenberg chain. In this project, we have investigated the remaining part; the ground state and the excitations for $K \leqq 0$ and $\Gamma \geqq 0$. We have found that in the spin chain limit, an incommensurate phases exists between the TLL phase and D_4-symmetry-breaking phase [5]. In addition, we have found that the presence of the extended Kitaev spin liquid [5] is still controversial [7]. This implies that the extended Kitaev spin liquid phase is replaced by a different state from the D_3 ordered state [5]. These states we newly found in the chain limit changes two-dimensional long-range orders when the interchain interaction becomes finite [7].

(2) Supersolid states in two-dimensional hard-core bosonic Hubbard model with dipole interactions

In this project, we have studied the phase diagram of two-dimensional hard-core bosonic Hubbard model with dipole interactions. Many efforts have been made to realize supersolid states so far and ultracold-atomic gases trapped in optical lattices are candidate stages to study the supersolid states. In lattice Bose-Hubbard models, frustrated interactions play a key role to stabilize the supersolid states. In ref. [8], authors investigated the phase diagram of the two-dimensional bosonic hardcore Hubbard model with the dipole interactions by the mean-filed approach and the infinite entangled-pair-state. It was found that several supersolid states appear in between solid phases with different commensurate fillings by tilting the angle of the dipole axis from the direction perpendicular to the lattice plane. However, the range of the dipole interactions is restricted within a short

range in ref. [8]. Thus, when the farther neighbor interactions are included, whether those supersolid phases are stable or not is unclear.

We have investigated the phase diagram of the two-dimensional bosonic hardcore Hubbard model with the dipole interactions by quantum Monte Carlo computations and have applied two methods to discuss the details of each phase; finite-size-scaling analysis and machine-learning assisted approach. First, we have studied the phase diagram of the same model considered in ref. [8]. We have obtained consistent results with those by the iPEPS calculations. Next, we have investigated the phase diagram by changing the cut-off range of the dipole interactions. It has been found that two quarter solid states (ρ=1/4 and 3/4, where r is filling.) becomes unstable and diagonal-stripe solid states (ρ=1/3 and 2/3) becomes stable. The supersolid state related with the quarter solid disappears.

References

[1] J. G. Rau, E. Lee, and H. -Y. Kee, Phys. Rev. Lett. 112, 077204 (2014).
[2] T. Yamada, T. Suzuki, and S. Suga, Phys. Rev. B **102**, 024415 (2020).
[3] Y. Imai, et al., Phys. Rev. B **105**, L041112 (2022) and Y. Choi, et al., Phys. Rev. B **106**, 174430 (2022).
[4] M. Gohlke, J. C. Pelayo, and T. Suzuki, arXiv:2212.11000.
[5] W. Yang, et al., Phys. Rev. Lett. 124, 147205 (2020) and W. Yang, A. Nocera, and I. Affleck, Phys. Rev. Research 2, 033268 (2020).
[6] R. Mukhopadhyay, C. L. Kane, and T. C. Lubensky, Phys. Rev. B **64**. 045120 (2001).
[7] M. Gohlke, J. C. Pelayo, and T. Suzuki, in preparation.
[8] H.-K. Wu and W.-L. Tu, Phys. Rev. A **102**, 053306 (2020).

Systematic Searches for Grain Boundary Structures and Structure-based Prediction of Multiple Properties

Susumu FUJII
Division of Materials and Manufacturing Science, Osaka University
Yamadaoka, Suita, Osaka, 565-0871
Nanostructures Research Laboratory, Japan Fine Ceramics Center
Mutsuno, Atsuta, Nagoya 456-8587

Grain boundaries (GBs) are ubiquitus in inorganic solid materials except for glasses. At GBs, electronic and atomic structures that are different from its corresponding crystal structure are formed, providing unique properties that often determine macroscopic physical responces of materials. The GB structures vary significantly depending on the orientation between adjoined crystal grains, resulting in a variety of GB properties. Revealing GB structure-property relationship is important to improve the performance of structural and functional materials based on material microstructures.

To correlate GB structures with material properties, there are two technological difficulties. One is that a large-scale data for GB structures and their properties, with an accuracy comparable to first principles calculations, is necessary to provide a general and systematic understanding that is applicable to experimental design of microstructures. Another is that the computational and machine learning method to quantify GB structures and correlate them with properties is not well established. Regarding the latter, the authors reported that the use of structure descriptor and hierarchical clustering can clasify the local atomic environments composing GB structures, and multiple linear regression with the classified data provide an accurate prediction of GB thermal conductivities for MgO with physical interpretations [1].

The main drawback of our previous work is that we use an emprical potential to derive MgO GB structures and their thermal conductivities. In this study, we applied an accurate machine learing potential for silicon, distributed in MACHINE LEARNING POTENTIAL REPOSITORY [2], to our GB structure searches and property evaluations, to give more precise GB structure-property relationship [3]. Silicon is known as a typical semiconductor, and considered as a promising candidate for thermoelectric material. To reduce its high thermal conductivity, nanocrystalline silicon with high GB population has been extensively synthesized, leading to very low thermal conductivity less than 5 W/mK [4]. Revealing the impact of Si GBs on thermal conduction as well as electronic conduction is necessary for further improvement of its thermoelectric conversion efficiency.

We mainly performed GB structure searches with the methods of rigid body translations (RBTs) and structure optimization, and thermal conductivity calculations using perturbed molecular dynamics (MD). The necessary codes for RBTs and perturbed molecular dynamics were developed by the author, and the latter was implemented to the Large-scale Atomic/Molecular Massively Parallel Simula-

tor (LAMMPS) [5].

Using the code for RBTs and LAMMPS for structure optimization, we derived 45 silicon GB structures. Then, perturbed MD simulations were performed for calculating thermal conductivity of each GB structure. The perturbed MD simulations are highly computationally demanding, requiring large computational cells containing from three to thirteen thousands of atoms and with the time steps of more than one million. Repeating this simulation five times with different magnitude of perturbations for each GB yielded a set of statistically accurate thermal conductivities. As 230 separate perturbed MD simulations were necessary, all of them were performed in a single node rather than multiple nodes.

Compiling the GB structure data and thermal conductivity shows that bond angle strains at GBs significantly decreases their thermal conductivities. In addition, structural voids, formed at a few GBs, largely decreases GB thermal conductivities. These trends results from the features of covalent silicon, where one atom bonds strongly with four atoms to form a tetrahedron, and the strong directionality of the bonds tends to create voids at GBs.

In contrast to our results, a revious report using an empirical force field claims that GB energy is the dominant factor for determining GB thermal conductivity of silicon, rather than structural features of GBs [6]. A large scale calculations using supercomputers and the accurate machine learning potential indicate the importance of precisely estimating GB structures and their properties to reveal a robust GB structure-property relationship.

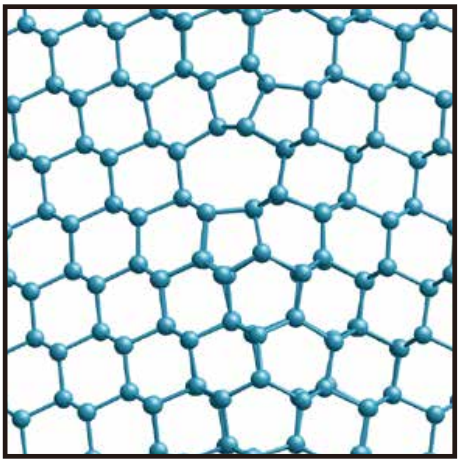

Figure 1: An example of silicon grain boundary structure derived using a machine learning potential.

References

[1] S. Fujii et al., Nature Commun. **11** (2020) 1854.

[2] A. Seko, arXiv:2007.14206.

[3] B. Jugdersuren et al., Phys. Rev. B. **96** (2017) 014206.

[4] S. Fujii and A. Seko, Comput. Mater. Sci. **204** (2022) 111137.

[5] S. Plimpton, J. Comput. Phys. **117** (1995) 1.

[6] J. Hickman and Y. Mishin, Phys. Rev. Mater. **4** (2020) 033405.

Kinetics of phase transition and polyamorphism

Kazuhiro Fuchizaki, Katsumi Nakamura, and Hiroki Naruta
Department of Physics, Ehime University, Matsuyama 790-8577

In FY2022, we continued to undertake the two tasks dealt with in FY2021: One was addressing the validity of the two-phase thermodynamic (2PT) model put forth by Goddard *et al.* [1], and the other was a new trial application of machine learning (ML) to judge the order of a phase transition.

One of our major issues is to explain a sign of the Clapeyron slope of a liquid-liquid transition (LLT) boundary. Liquid phosphorus [2] and sulfur [3] are known to undergo an LLT. However, the former (latter) LLT boundary has a negative (positive) slope, although both liquids are believed to be brought to high-density liquids via polymerization. Because a specific volume must be reduced upon an LLT, the entropy difference between high- and low-density liquids can determine the slope's sign. Therefore, a method to precisely evaluate a liquid entropy is required. The 2PT model has been widely used for this purpose. However, because the model was based on many assumptions, we must examine the validity before applying the model.

The second task is a brand-new research project that has not been tried thus far. We could finish the project in FY2022, and the submitted paper is now under review. Most of the computation time was exhausted in preparing the learning data.

The self-diffusion coefficient of a hard-sphere fluid

Our detailed examination ascertained that the 2PT model bears its validity in estimating the liquid fraction f, which is implicitly defined by

$$f = D(T,\rho)/D^{\mathrm{HS}}(T, f\rho;\sigma), \qquad (1)$$

where D and D^{HS} are the diffusion coefficients for the system in question and the corresponding hard-sphere fluid, respectively. ρ and T are the system's density and temperature. We explicitly include the dependence of D^{HS} on the hard-sphere diameter σ. The neat trick of Goddard *et al.* in deriving a closed equation to determine f was to replace the RHS of Eq. (1) with $D(\rho,T)/D_0^{\mathrm{HS}}(T,\rho;\sigma)$, thereby replacing the definition of f as $f = D(\rho,T)/D_0^{\mathrm{HS}}(T,\rho;\sigma)$. Enskog's theory then allows us to relate D^{HS} to the diffusion coefficient D_0^{HS} and the compressibility factor obtainable from the Carnahan–Starling equation of state. Furthermore, $D_0^{\mathrm{HS}}(T, f\rho) = D_0^{\mathrm{HS}}(T,\rho)/f$ is valid in the zero-pressure limit at which the Chapman–Enskog result is valid. These relations regarding the diffusion coefficients resulted in the cubic equation for f.

Here, we directly solved Eq. (1) instead of solving the cubic equation. We employed the modified Lennard-Jones (mLJ) system with 2048 particles for this judgment. We first evaluated the diffusion coefficient D, Eq. (1) numerator, for the mLJ system at the thermodynamic conditions reported in [4]. Next, we conducted molecular dynamics simulations for a hard-sphere fluid to find D^{HS}. We set $\rho = 0.05$, 0.331, and 0.6 and $\sigma = 1.0$, 1.1, 1.2, and 1.3, where ρ and σ are presented in the mLJ units.

On our way to evaluating the RHS of Eq. (1), we noticed that the empirical formula proposed by Speedy [5] could reproduce the simulated D^{HS} quite satisfactorily. This confirmation enabled us to interpolate the RHS with other fs without carrying out simulations. Finally, we numerically solved Eq. (1), whose RHS was

thus evaluated, to obtain the desired f, which was found to be relatively close to that obtainable from the cubic equation. Therefore, regarding estimating the molecular fraction, we concluded that the treatment of Goddard *et al.* was adequate.

Judging the (dis)continuity of phase transition using ML [6]

Our short-term memory often causes "memory hysteresis" against back-and-forth input of continuously varying input. For example, imagine a series composed of gradually varying pictures from A to B. Suppose that an A-like picture certainly changes to a B-like when we see picture C in the series when we see those pictures from A to B. When we see them in the reverse order, a picture in which we recognize a definite change from B-like to A-like will differ from C, thus inducing memory hysteresis. The size of hysteresis may increase with the smoothness of variation. Because an artificial neural network (ANN) is so constructed that it can reproduce the functionality of a biological neural network (BNN), an ANN would behave like a BNN when a set of continuously changing patterns is input in back-and-forth directions. We then expected that an ANN could distinguish a continuous or discontinuous phase transition from its hysteresis behavior when it sequentially learns a series of phase-transition patterns generated as a function of external parameters such as temperature or external field.

We implemented a convolutional neural network (CNN) to realize an ANN. To test the phase-transition order, we employed two-dimensional Ising and q-state Potts models with $q = 3$ through 6. For the Ising model, we generated spin configurations below and above the critical temperature T_c as a function of the external field h. For the Potts model, we obtained them around the phase-transition point as a function of temperature T. h or T constituted the labels. We let the CNN learn the difference between the configurations with adjacent labels in increasing (decreasing) order of the labels to assess the hysteresis size. The learning effects were stored in the CNN's weights, and we monitored the sum of the weights, W_{sum}, connected to the output layer. For the specifications of the CNN and the models, see [6].

We have already reported the results of the preliminary study [4]. For the Ising crossover transition, hysteresis appeared in W_{sum}'s behavior plotted as a label function, whereas no hysteresis was recognizable for the transition below T_c as expected. However, unlike the Ising case exhibiting an order-to-order transition, the Potts model did not allow the CNN to learn the configurations in reverse order, i.e., from the disordered to the ordered state. The CNN did not seem to capture the disordered state uniquely.

We could resolve this issue by "renormalizing" the q states into a single state to make the CNN facilitate capturing the Potts (dis)ordering aspect [6]. We confirmed that W_{sum}'s hysteresis arose for $q = 3$ and 4, whereas W_{sum} took maximum precisely at the transition point without hysteresis regardless of the learning direction. Interestingly, W_{sum} behaved marginally for the weak first-order transition realized when $q = 5$.

References

[1] S-T. Lin, M. Blanco, and W. A. Goddard: J. Chem. Phys. **119** (2003) 11792.

[2] Y. Katayama *et al.*: Nature **403** (2000) 170.

[3] L. Henry *et al.*: Nature **584** (2020) 382.

[4] K. Fuchizaki *et al.*: ISSP Supercomputer Center Activity Report (2021) 256.

[5] R. J. Speedy *et al.*: Mol. Phys. **66** (1989) 577.

[6] K. Nakamura and K. Fuchizaki: submitted to J. Phys. A.

Numerical Study of Magnetism in the Honeycomb-Lattice Spin Systems

Chitoshi YASUDA
Department of Physics and Earth Sciences, Faculty of Science, University of the Ryukyus, Okinawa 903-0213, Japan

Many low-dimensional antiferromagnets with excitation modes separated from the ground state by a finite energy gap have been synthesized, and effects of impurities on those materials in the gapped state have attracted our interest. In the previous work [1], the spin $S = 1/2$ and $S = 1$ two-dimensional quantum Heisenberg antiferromagnets on a square lattice, which is composed of bond-alternating chains and interchain interactions, have been investigated by the quantum Monte Carlo simulation with the continuous-imaginary-time loop algorithm, and ground-state phase diagrams parametrized by the strength of the bond alternation and that of the interchain coupling have been determined precisely. The phase diagrams reveal under what conditions spin-gapped states and magnetically ordered states are realized. Recently, various honeycomb-lattice systems are interested in relation to quantum spin liquid states. For example, the Kitaev model on the honeycomb lattice has the qunatum spin liquid state as the ground state.

In this project, we research the $S = 1/2$ and $S = 1$ quantum Heisenberg antiferromagnets on the anisotropic dimerized honeycomb lattice using the quantum Monte Carlo simulations with the continuous-imaginary-time loop algorithm [2], and compare the results with those of the square lattice. The honeycomb lattice is composed of bond-alternating chains and interchain interactions. Periodic boundary conditions are imposed in the x and y directions. For the simulation of the $S = 1$ system, the subspin-representation technique is applied [2, 3]. In this technique, the $S = 1$ system is represented by an $S = 1/2$ system with special boundary conditions in the imaginary-time directions. The phase-transition points of the ground state are estimated by the finite-size-scaling analyses of the correlation lengths evaluated by the second-moment method. For valid analyses, it was necessary to calculate up to a system of size $L_x \times L_y = 96 \times 48$, where the temperature is fixed to $T = 1/L_x$. The critical exponent for the correlation length ν is fixed at 0.71 consistent with the value for the three-dimensional classical Heisenberg model. In the $S = 1/2$ system, there are the dimerized state and the antiferromagnetic long-range ordered (AFLRO) state as the ground state. On the other hand, in the $S = 1$ system, there is the Haldane state in addition to the dimerized state and the AFLRO state. The phase diagram parametrized by the strength of the bond alternation and that of the interchain coupling show that the region of the dimerized state of the honeycomb-lattice system is narrower than that of the square-lattice system.

References

[1] M. Matsumoto, C. Yasuda, S. Todo, and H. Takayama, Phys. Rev. B **65**, 014407 (2001).

[2] S. Todo and K. Kato, Phys. Rev. Lett. **87**, 047203 (2001).

[3] K. Harada, M. Troyer, and N. Kawashima, J. Phys. Soc. Jpn. **67**, 1130 (1998).

Spin Dynamics Simulation of the Z_2-vortex Fluctuations

Hikaru KAWAMURA

Molecular Photoscience Research Center, Kobe University, Kobe 657-8501

Yo P. MIZUTA

Graduate School of Engineering Science, Osaka University, Toyonaka 560-8531

Kazushi AOYAMA

Graduate School of Science, Osaka University, Toyonaka, 560-0043

In as early as 1984, it was pointed out that the frustrated isotropic Heisenberg magnets in two dimensions (2D) could possess a novel vortex characterized by the parity-like two-valued topological number corresponding only to its presence/absence, a Z_2 vortex, which drove a topological transition at a finite temperature T_V associated with its binding-unbinding.[1] While the direct experimental observation of the Z_2 vortex has remained elusive for years, a very recent quasi-elastic neutron scattering (QENS) experiment performed on the powder sample of the quasi-two-dimensional (2D) triangular-lattice Heisenberg antiferromagnet $NaCrO_2$ has succeeded in directly probing the signature of the free Z_2 vortex via the observation of a sharp quasi-elastic (QE) scattering of its energy width as narrow as ~10 μeV corresponding to ~0:001J (J the exchange coupling).[2] The observed peak width was even narrower than that in the earlaier model simulation[3] by an order of magnitude. We then have performed further extensive spin-dynamics simulation on the frustrated 2D Heisenberg model by improving the energy resolution by an order of magnitude.[4] The dynamical spin structure factor computed at T slightly above T_V is shown in the figure below, which indeed exhibits a narrow central peak, in addition to the side peaks of spin-wave origin. Quantitative analysis of the data indicates that the width of the central peak indeed becomes as narrow as ~0.001J in the close vicinity of the K-

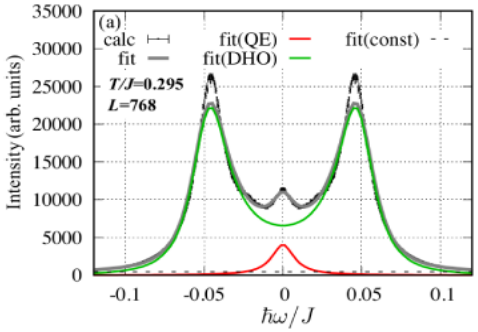

point slightly above T_V (=0.285J), consistently with the recent QENS experiment. [2]

References

[1] H. Kawamura and S. Miyashita, J. Phys. Soc. Jpn. **53**, 4138 (1984). [2] K. Tomiyasu et al, Phys. Rev. B **106,** 054407 (2022). [3] T. Okubo and H. Kawamura, J. Phys. Soc. Jpn. **79**, 084706 (2010). [4] Y.P. Mizuta et al, J. Phys. Soc. Jpn. **91**, 035001 (2022).

Finite temperature calculation of quantum manybody system using random phase product state and neural network wavefunction

Toshiaki IITAKA

Center for Computational Science,

RIKEN, 2-1 Hirosawa, Wako, Saitama, 351-0198 JAPAN

Calculation of thermal average of an observable A of a closed quantum many-body system in its thermal equilibrium at an inverse temperature is one of the most important problems in computational physics. It has, however, two major computational difficulties. The number of quantum states to be included and the dimension of each quantum state vector are both exponentially increases as the temperature and the system size increases, respectively. Each difficulty has been independently attacked using *random state method* [1, 2] and *variational wave function*, respectively.

In this project, we introduced random state method to general form of variational wave functions. Only few papers have investigated the application of random state method to variational wave functions [3-7].

Thermal average of observable *A* at inverse temperature β is calculated using *random state* $|\Phi\rangle$ as

$$\langle A\rangle = \frac{tr[e^{-\beta H}A]}{Z} = \frac{\langle\langle\langle\Phi|A|\Phi\rangle\rangle\rangle}{Z}$$

where

$$Z(\beta) = tr[e^{-\beta H}] = \langle\langle\langle\Phi|\Phi\rangle\rangle\rangle$$

is the *partition function* and the double bracket indicates statistical average over random states. The *thermal state* is defined by the imaginary time evolution of the random state.

$$|\Phi(\beta)\rangle = e^{-\beta H/2}|\Phi\rangle$$

Thermal energy E and specific heat C are expressed as

$$E(\beta) = \langle H\rangle$$

and

$$C(\beta) = k_B\beta^2\left[\langle E^2\rangle - \langle E\rangle^2\right].$$

Variational wave function is a point on a manifold embedded in the Hilbert space,

$$\left|\psi(w)\right\rangle = \sum_{\boldsymbol{\sigma}} c(w,\boldsymbol{\sigma})\left|\boldsymbol{\sigma}\right\rangle$$

which is parameterized with variational parameters, $w = \{w_i\}$, whose number is much less than the dimension of the Hilbert space.

Thermal state has been introduced in some variational wave functions such as MPS and PEPS as

$$\left|\Psi(\beta; w)\right\rangle = e^{-\beta H/2}\left|\Psi(w)\right\rangle$$

where $\left|\Psi(w)\right\rangle$ is random variational wavefunction.

In this project, the above formulation was extended to general form of variational wavefunction by calculating the imaginary time evolution with stochastic reconfiguration[3, 8]. It is noted that the trace is formally taken over the entire Hilbert space in our method while it was limited to its subspace in the previous method[3]. A numerical example for Restricted Boltzmann Machine is computed with NetKet [9] and the result is shown in Fig. 1.

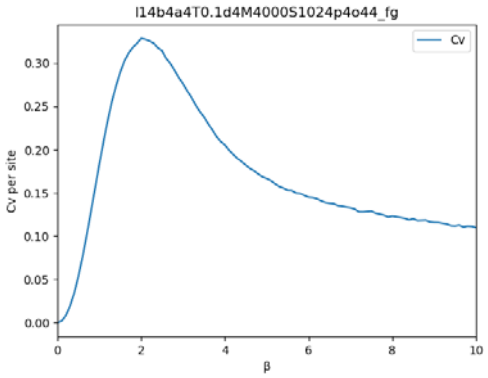

Fig.1 : Specific heat per site for 14 site spin-1/2 antiferromagnetic Heisenberg chain with PBC calculated with RBM($\alpha = 4$) and 1024 samples.

References

[1] T. Iitaka, and T. Ebisuzaki, Phys. Rev. Lett. **90**, 047203 (2003).

[2] T. Iitaka, and T. Ebisuzaki, Phys. Rev. E **69**, 057701 (2004).

[3] K. Takai *et al.*, J Phys Soc Jpn **85**, 034601 (2016).

[4] S. Garnerone, T. R. de Oliveira, and P. Zanardi, Phys. Rev. A **81**, 032336 (2010).

[5] T. Iitaka, arXiv:2006.14459 (2020).

[6] A. Iwaki, A. Shimizu, and C. Hotta, Physical Review Research **3**, L022015 (2021).

[7] S. Goto, R. Kaneko, and I. Danshita, Phys. Rev. B **104**, 045133 (2021).

[8] S. Sorella, Phys. Rev. Lett. **80**, 4558 (1998).

[9] G. Carleo *et al.*, SoftwareX **10**, 100311 (2019).

Tensor data analysis by tensor network

Kenji Harada
Graduate School of Informatics, Kyoto University
Kyoto 606-8501, Japan

Recently, data in various fields have been stored as a multi-dimensional array called a tensor. When the number of attributes (indexes) of a tensor increases, the size of the tensor becomes huge because it increases exponentially as the number of indexes increases. Therefore, we need the high-speed and high-quality use of tensor data of huge sizes.

A tensor network (TN) is an effective tool for representing a huge composite tensor and has been extensively developed in quantum information and statistical physics research. Since the tensor network can effectively represent such high-dimensional data, we may efficiently process the general tensor data.

Previous studies [1, 2] proposed using of a tree tensor network (TTN) for a multi-dimensional probability distribution. In this project, we try to improve the performance of a TTN algorithm for generative modeling to multi-dimensional data distribution.

Here, we consider a generative model based on a quantum state [1, 2]. Following the Born rule, we define $p(\mathbf{x})$ as the square of the amplitude of a wave function:

$$p(\mathbf{x}) = \frac{|\psi(\mathbf{x})|^2}{Z}, \tag{1}$$

where $\psi(\mathbf{x})$ is a wave function and Z is the normalization factor.

MPSs [1] and balance TTNs [2] have been proposed to define the wave function for generative modeling. The number of indexes of a tensor in the balance TTN is equal to that in the MPS. The only difference is the topology of the network; all physical indexes in the TTN, x_i, are connected, and the TTN network has no loop structure. Thus, an MPS is a specialized type of TTN. As shown in [2], the performance depends much on the network topology of TTNs.

We propose a new algorithm to change the network structure of a TTN for generative modeling. Several strategies can be used to select a better choice of local network structure[3]. Our network optimization improves the performance of generative modeling with a TTN.

References

[1] Zhao-Yu Han, Jun Wang, Heng Fan, Lei Wang, and Pan Zhang. Unsupervised Generative Modeling Using Matrix Product States. *Phys. Rev. X*, 8(3):031012, 2018.

[2] Song Cheng, Lei Wang, T. Xiang, and Pan Zhang. Tree tensor networks for generative modeling. *Phys. Rev. B*, 99(15):155131, 2019.

[3] Kenji Harada, Tsuyoshi Okubo, and Naoki Kawashima. Network optimization of tree generative models. in preparation.

Molecular dynamics simulation of $BaTiO_3$ nano structure II

T. Hashimoto
National Institute of Advanced Industrial Science and Technology (AIST), Tsukuba Central 2, 1-1-1 Umezono, Tsukuba, Ibaraki 305-8568, Japan

The ferroelectric domain wall (FDW) has dielectric, electrical, and mechanical properties that differ from those of bulk. It can even be considered a two-dimensional phase different from the bulk. In our previous study, we found that 71° and 109° Ising-like FDWs are observed in $BaTiO_3$ nanoclusters[1]. In this study, we focused on the FDW structures and energies of rhombohedral $BaTiO_3$.

We used a shell model proposed by Tinte et al.[2]. The calculations were performed with the code developed by us. We performed calculations for 71°, 109°, and 180°$\{1\bar{1}0\}$ FDWs in the rhombohedral phase. We used 10×6×6 5-atom unit cells for the 109° FDWs, and 8×6×6 and 10×6×6 10-atom building blocks for the 71° and 180°$\{1\bar{1}0\}$ FDWs, respectively. The initial Ising FDW configurations were made by shifting the Ti atoms in one direction in half of the supercell, and in the other direction in another half. The initial Bloch FDW configurations were made in the same way as the Ising case except that the local dielectric polarization vectors were rotated across the FDW. To mimic the isolated FDW between very thick domains in the supercell calculations, the in-plane lattice constants were set to be the same as those of the single domain phase, while the out-of-plane lattice constant was relaxed.

The domain widths and energies had been calculated with the Ginzburg–Landau–Devonshire (GLD) model and the GLD model with reduced gradient terms (GLD-r) [3]. The GLD and the GLD-r results predict that the 109° Bloch wall is more stable than the 109° Ising wall energy, which is not in accordance with the LDA results. The GLD-r model predicts narrower walls and lower wall energies compared to the GLD model, which improves the energy and width of the 71° Ising wall and the width of the 109° Ising wall, but overshoots the energy of the 109° Ising wall and the energy and width of the 109° Bloch wall. The GLD-r model predicts that the 180° Bloch wall is unstable compared to the 180° Ising wall, which is not in accordance with the LDA results.

The shell model results also have inconsistencies compared to the LDA results: The FDW energy of the 109° Ising wall is too low. The FDW energy of the 180°$\{1\bar{1}0\}$ Bloch wall is too high and the width of it is too narrow. However, it predicted that the 71° Ising wall has the lowest energy, followed by the 109° Ising wall and the 109° Bloch wall.

References

[1] T. Hashimoto and H. Moriwake, Physica B, **656**, 414768 (2023).

[2] S. Tinte, M. Stachiotti, S. Phillpot, M. Sepliarsky, D. Wolf, and R. Migoni: J. Phys.: Condens. Matter **16** (2004) 3495.

[3] M. Taherinejad, D. Vanderbilt, P. Marton, V. Stepkova, and J. Hlinka: Phys. Rev. B **86** (2012) 155138.

Numerical study of quantum many-body scars in bosonic systems

Ryui KANEKO
Department of Physics, Kindai University
Higashi-Osaka, Osaka 577-8502, Japan

Understanding how isolated quantum many-body systems thermalize is of great interest in physics. The eigenstate thermalization hypothesis (ETH) provides a sufficient condition for thermalization and is satisfied in many quantum systems in the presence of interactions [1, 2]. However, recent experiments of nonintegrable systems suggest ETH breaking. This phenomenon originates from the special eigenstates exhibiting extremely slow thermalization [3, 4]. Such quantum many-body scar (QMBS) states exist in various spin models [5–10]. It is desirable to search for the QMBS states in other quantum systems, which can be realized in experiments.

Here we focus on the Bose-Hubbard model suitable for experiments using ultracold atoms on optical lattices. The Hamiltonian is given as

$$\hat{H} = \hat{H}_0 + \hat{H}_{\rm int}, \tag{1}$$

$$\hat{H}_0 = -J\sum_i (\hat{a}_i^\dagger \hat{a}_{i+1} + \hat{a}_{i+1}^\dagger \hat{a}_i), \tag{2}$$

$$\hat{H}_{\rm int} = \frac{U}{2}\sum_i \hat{n}_i(\hat{n}_i - 1). \tag{3}$$

We specifically choose the model in a truncated Hilbert space with the maximum occupation number $n_{\rm max} = 2$. Note that three-body losses of atoms on optical lattices realize this constraint [11, 12].

We numerically diagonalize the Hamiltonian and find the eigenstates with a small entanglement entropy (see Fig. 1). We also analytically show that they are generated by applying the SU(2) ladder operator consisting of a linear combination of two-particle annihilation operators. The construction of the QMBS states is equivalent to the case of the $S = 1$ XY model [13, 14].

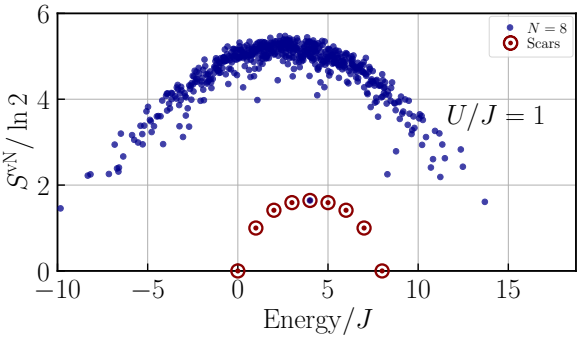

Figure 1: Entanglement entropy as a function of energy. The QMBS states are circled. We consider the system size $L = 8$ and the interaction strength $U/J = 1$ in Eq. (1). The quantum number sector with the particle number $N = L$ and the even parity $\mathcal{I} = +1$ is given by blue dots. Each QMBS state (a red circle with a dot) with the particle number N has the energy $UN/2$ and the expectation values $\langle\sum_{i=1}^L \hat{n}_i\rangle = N$ and $\langle\sum_{i=1}^L \hat{n}_i^2\rangle = 2N$. Its bipartite entanglement entropy at $N = L$, corresponding to a state $|S_{n=L/2}\rangle$, becomes $S_A^{\rm vN} \to [\ln(\pi L/8) + 1]/2$ for $L \to \infty$.

These findings will stimulate further research on the QMBS states in general Bose-Hubbard models without any constraints, which would be more suitable for experiments of ultracold atoms in optical lattices. The construction of the QMBS states in general spin

S systems has been discussed recently [15, 16], which could be extended to the Bose-Hubbard model by utilizing the improved Holstein-Primakoff transformation [17, 18].

References

[1] W. Beugeling *et al.*, Phys. Rev. E **89**, 042112 (2014).

[2] H. Kim *et al.*, Phys. Rev. E **90**, 052105 (2014).

[3] H. Bernien *et al.*, Nature **551**, 579 (2017).

[4] D. Bluvstein *et al.*, Science **371**, 1355 (2021).

[5] C. J. Turner *et al.*, Nat. Phys. **14**, 745 (2018).

[6] C. J. Turner *et al.*, Phys. Rev. B **98**, 155134 (2018).

[7] A. J. A. James *et al.*, Rev. Lett. **122**, 130603 (2019).

[8] N. Shibata *et al.*, Phys. Rev. Lett. **124**, 180604 (2020).

[9] M. Serbyn *et al.*, Nat. Phys. **17**, 675 (2021).

[10] S. Moudgalya *et al.*, Rep. Prog. Phys. **85**, 086501 (2022).

[11] A. J. Daley *et al.*, Phys. Rev. Lett. **102**, 040402 (2009).

[12] M. J. Mark *et al.*, Phys. Rev. Lett. **108**, 215302 (2012).

[13] M. Schecter and T. Iadecola, Phys. Rev. Lett. **123**, 147201 (2019).

[14] S. Chattopadhyay *et al.*, Phys. Rev. B **101**, 174308 (2020).

[15] N. O'Dea *et al.*, Phys. Rev. Research **2**, 043305 (2020).

[16] L.-H. Tang *et al.*, Phys. Rev. Research **4**, 043006 (2022).

[17] M. Vogl *et al.*, Phys. Rev. Research **2**, 043243 (2020).

[18] J. König and A. Hucht, SciPost Phys. **10**, 7 (2021).

Tensor-network study of the quench dynamics of the Kitaev honeycomb model

Ryui KANEKO
Department of Physics, Kindai University
Higashi-Osaka, Osaka 577-8502, Japan

The Kitaev honeycomb model [1] in the magnetic field displays a rich phase diagram of quantum phases [2,3]. These findings stimulate further research on the nonequilibrium dynamics of the model. One of the motivations for studying dynamics is an experimental interest; the Kitaev candidate materials may exhibit unconventional transport [4–6]. The other is an interest in statistical mechanics as to how the integrable Kitaev model, which is rare in quantum 2D systems, thermalizes in the presence of additional interaction [7,8]. These interests motivate us to study the dynamics of the simple Kitaev model with the magnetic field. As a benchmark, we specifically focus on the sudden quench of the ferromagnetic Kitaev model starting from the antiferromagnetic state without the magnetic field. Previous investigations are limited to mean-field calculations or numerical-diagonalization studies for small systems. We use the 2D tensor-network method using the infinite projected entangled state (iPEPS) [9,10], which can directly deal with inifinite systems accurately, to examine how far one can go for the quench dynamics of the Kitaev model.

We prepare the staggered antiferromagnetic state, whose spins are oriented along the z-axis, on a honeycomb lattice as the initial state $|\psi(0)\rangle$. The state can be prepared by the bond dimension $D = 1$, and is time evolved by the $S = 1/2$ Kitaev Hamiltonian

$$\hat{H} = -\sum_{\langle i,j\rangle_\gamma,\gamma\in\{x,y,z\}} J^\gamma \hat{S}_i^\gamma \hat{S}_j^\gamma, \qquad (1)$$

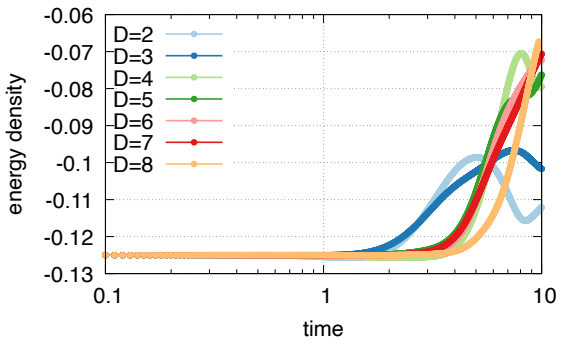

Figure 1: Time evolution of the energy density.

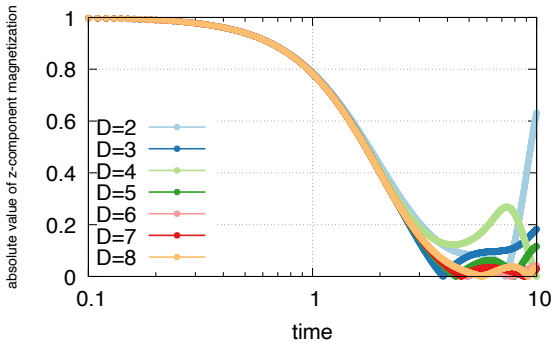

Figure 2: Time evolution of the absolute value of the z-component magnetization.

where γ corresponds to the bond direction and J^γ is the Kitaev interaction. Here we consider the isotropic and ferromagnetic interaction $J^\gamma = 1$. The wave function at each time $|\psi(t)\rangle = \exp(-it\hat{H})|\psi(0)\rangle$ is calculated by the simple update algorithm [11,12] using the tensor-network library TeNeS [13]. The wave function is optimized up to the bond dimension $D = 8$ to examine how physical quantities converge by improving the accuracy of the state

with increasing the bond dimension.

The energy should be conserved for the quench dynamics. We can estimate to what extent the simulation goes well by looking at the degree of conservation. In the present study, the energy is nearly conserved for $tJ^\gamma \lesssim 4$ when $D \gtrsim 4$ (see Fig. 1). Within this reliable time frame, the magnetization nearly vanishes at $tJ^\gamma \approx 4$. This observation is consistent with the previous study, where an emergent non-magnetic steady state has bee proposed [7].

Our study would serve as a reference for understanding the quench dynamics of the Kitaev model and relevant unconventional steady states, which can be identified by utilizing the 2D tensor-network method. It is left for future work to investigate the effect of the magnetic field in the model.

References

[1] A. Kitaev, Ann. Phys. (NY) **321**, 2 (2006).

[2] Z. Zhu *et al.*, Phys. Rev. B **97**, 241110(R) (2018).

[3] C. Hickey and S. Trebst, Nat. Commun. **10**, 530 (2019).

[4] J. Nasu and Y. Motome, Phys. Rev. Research **1**, 033007 (2019).

[5] T. Minakawa *et al.*, Phys. Rev. Lett. **125**, 047204 (2020).

[6] M. Udagawa *et al.*, Phys. Rev. Lett. **126**, 127201 (2021).

[7] L. Rademaker, SciPost Phys. **7**, 071 (2019).

[8] G.-Y. Zhu and M. Heyl, Phys. Rev. Research **3**, L032069 (2021).

[9] T. Nishino *et al.*, Prog. Theo. Phys. **105**, 409 (2001).

[10] F. Verstraete and J. I. Cirac, arXiv:cond-mat/0407066.

[11] J. Jordan *et al.*, Phys. Rev. Lett. **101**, 250602 (2008).

[12] H. C. Jiang *et al.*, Phys. Rev. Lett. **101**, 090603 (2008).

[13] Y. Motoyama *et al.*, Comp. Phys. Commun. **279**, 108437 (2022).

The Study on Superionic Conduction and Phase Transition by Disordering of Complex Hydride

Ryuhei Sato

Advanced Institute for Materials Research,

Tohoku University, 2-1-1 Katahira, Aoba-ku, Sendai 980-8577, Japan

The complex hydrides such as $LiCB_9H_{10}$ are promising candidates for electrolytes due to their high ionic conductivity and stability to metal anodes [1]. Although the development of such complex hydrides is progressing rapidly, the mechanism of superionic conductivity induced by the phase transition due to the disordering (≈ the change in rotational motion) of the complex anions is not clear. Therefore, the purpose of this study is to clarify the effect of the disordering on the ion conduction and the phase transition by using *ab initio* molecular dynamics (AIMD) and neural-net potential molecular dynamics (NNP-MD) simulations.

AIMD simulation at 1000K confirmed that $LiCB_9H_{10}$ exhibits concerted motion, in which multiple Li ions migrate simultaneously with the rotation of the complex anion. To clarify the effect of the $CB_9H_{10}^-$ rotation, we analyzed the change in diffusion coefficient with and without the rotation using NNP-MD simulations (Fig. 1). As shown in the figure, the activation energy increases when the anion rotation is stopped, and the conductivity decreases by nearly one order of magnitude at around room temperature [2].

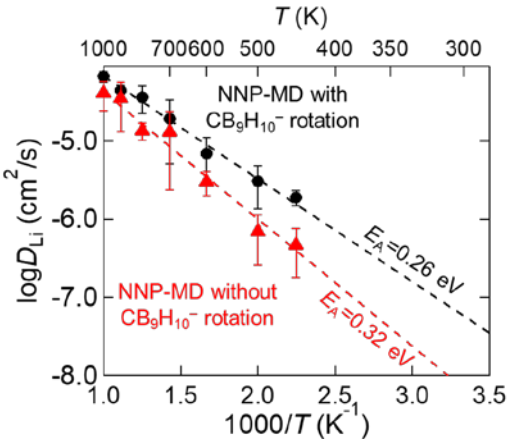

Figure 1 Arrhenius plot of Li self-diffusion coefficient during NNP-MD simulations of $LiCB_9H_{10}$ with and without $CB_9H_{10}^-$ rotation [2].

As shown in the discussion above, it is possible to quantitatively analyze the changes in ion transport caused by anion-rotation using NNP-MD simulations. However, it is difficult to obtain a specific relationship between the anion rotation and Li migration. Therefore, in order to visualize the ion transport mechanism in such a disordered system, we have developed an ion-migration-mechanism analysis method using topological data analysis based on persistent homology.

This year, we investigated the applicability of topological data analysis on ion migration mechanism [3]. Here, we choose α-AgI as a benchmark, because this system retains the ordered I bcc lattice while Ag ions are disordered in the system and shows complex concerted ion migration. MD simulations at various temperatures confirmed specific ring (one-dimensional hole in terms of homology) structures appear only when the system shows high ionic conductivity. Inverse analysis of these ring structures revealed that they were four-membered rings consisting of two Ag and I ions. By deforming these four-membered rings along the probability density distribution of the ring structure obtained by topological data analysis, we succeeded in visualizing the representative concerted ion migration of Ag ions in α-AgI[3]. In the future, we plan to apply this technique to complex hydride systems to clarify the relationship between anion rotation and ion migration.

Recently, complex hydrides are expected to be applied as multivalent-ion (ex. Zn^{2+} and Mg^{2+}) conductors [4]. Although the insertion of neutral molecules into complex hydrides is known to be effective to improve the ion conductivity for these multivalent-ion systems, there is no clear guideline to choose most effective neutral molecules for these complex hydrides. In addition, the specific mechanism of how the insertion of neutral molecules improves ionic conductivity is also unclear. Therefore, we created a workflow to analyze the effect of such neutral molecules on complex hydrides. Given a composition including neutral molecules, complex anions, and cations, a structure search method based on genetic algorithms (USPEX) can estimate the stable and reasonable structure including neutral molecules after several hundred DFT calculations. The activation energies of ion migration estimated from metadynamics simulations using the obtained structures are in good agreement with experimental values. The obtained trajectories of ion migration during the metadynamics simulation confirm that the coordination structure of the neutral molecule during ion migration has a significant effect on the activation energy. As a result of machine learning using the estimated activation energies, it was confirmed that the distance between anions and the electronegativity are important ones for the activation energy [5].

References

[1] W. Tang et al., *Adv. Eng. Mater.*, 6 (2016) 1502237.

[2] R. Sato et. al., to be submitted.

[3] R. Sato et al., *J. Chem. Phys.*, 158, (2023) 144116.

[4] K. Kisu et al., *J. Mater Chem. A*, 10 (2022) 24877.

[5] S. Egon, R. Sato et al. submitted to *NPJ. Comput. Mater.*

Theoretical studies on dynamics in biomolecular and liquid systems

Shinji Saito

Graduate University for Advanced Studies (Sokendai) / Institute for Molecular Science, 38 Nishigo-Naka, Myodaiji, Okazaki 444-8585, Japan

Fluctuations are inherent in condensed phase systems, such as liquid and biomolecular systems, and occur across diverse spatio-temporal scales. These fluctuations play a significant role in structural changes and reaction dynamics, thereby influencing various properties and functions. Consequently, an understanding of fluctuations is crucial for a comprehensive understanding of the relevant chemical/biological processes. In the second half of the fiscal year of 2022, our group utilized the supercomputer resources at ISSP for mainly two related projects, 1) the ion permeation process of potassium channel Kv1.2, and 2) the excitation energy transfer of light harvesting complex II (LHCII) in higher plants.

Kv1.2 is a mammalian voltage-controlled potassium channel from the Shaker K^+ channel family which regulates the cellular membrane potential by conditionally releasing the intracellular K^+ ions. Since its crystal structure was resolved about twenty years ago, it has become a typical and representative model for the study of ion channels. Here, we focus on the dynamical disorder revealed in the ion permeation processes under various ion concentrations and external voltages and attempt to understand the conformational origins of such dynamical disorder.

In the second half of the 2022 fiscal year, we constructed a Kv.12 model of about 140k atoms at the electrophysiological concentration of 0.15 M and performed roughly 100 μs molecular dynamics (MD) simulations at an external electric field of 500 mV using GROMACS. During the MD simulation, about 2300 potassium permeation events were observed. The time series analysis showed that these permeation events roughly followed the pattern of a Poisson process with a slight deviation from it. Further analyses and MD simulations at different ion concentrations and external electric field strength are to be performed for a complete picture of the dynamic disorder in the ion permeation process of Kv1.2.

LHCII, where the first step of the photosynthetic process occurs, has a complex structure which makes its excitation energy transfer (EET) difficult to be elucidated experimentally. In order to understand the EET dynamics of LHCII, we performed quantum mechanics (QM) calculation using the CAM-B3LYP functional and determined the optimal range separate parameters (between CAM and B3LYP) that reproduced the experimental

excitation energies of Chl *a* and *b* in three solvents [1]. With these optimized parameters, we refined the structures for 14 chlorophylls (Chl) in LHCII by using a modified version of GAMESS on the supercomputer at ISSP. In order to study the dynamical properties, we introduced a model called Molecular Mechanics Shepard interpolation Correction (MMSIC) that can give the approximate excitation energies during MD simulation based on the interpolation of optimized structures using the above-mentioned functional theory. The parallelized MMSIC-MD simulation sufficiently reproduced the QM/MM excitation energies on the fly and showed that the excitation energies of Chl *a* in LHCII varies wider than in solvents.

References

[1] Zhu, Zhe, Masahiro Higashi, Shinji Saito, Excited states of chlorophyll a and b in solution by time-dependent density functional theory, The Journal of Chemical Physics 156(12) (2022) 124111.

Structural formation of inverse patchy particles

Takamichi TERAO

Department of Electrical, Electronic and Computer Engineering,

Gifu University, Yanagido 1-1, Gifu, 501-1132

Inverse patchy colloids are those in which the anisotropy of interparticle interactions is due to inhomogeneous surface charges [1]. Previous studies of colloidal particle systems have largely dealt with the problem of aggregates, which are dominated by attractive interparticle interactions, and colloidal crystals, which are dominated by repulsive interactions. Conventional patchy particles are dominated by anisotropic attractive interactions. Inverse patchy particles, on the other hand, consist of heterogeneously charged units where the pair potentials between particles contain both attractive and repulsive properties. They are expected to exhibit novel properties and their properties with respect to structure formation are of interest.

In this study, we focused on the structural formation of inverse charged patchy particles. The surface of these particles is charged and the sign of the charge is reversed between the bipolar part and the other parts. The structure formation in these systems was studied by molecular dynamics simulations. The simulations were performed with the LAMMPS simulation package in the NVT ensemble. In thermal equilibrium, inverse patchy particles exhibit a variety of configurations by changing the ratio of positive and negative charges on the surface.

Figure 1 shows a snapshot of inverse patchy colloids when the motion of each sphere was confined between a pair of two-dimensional planes. From these results, we have revealed the dependence of the orientation order of the colloids on the charge coverage ratio, as well as the phase diagram of the system.

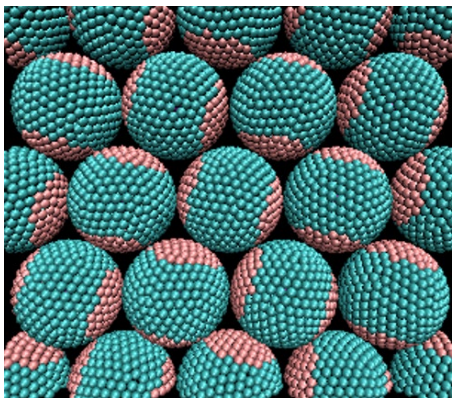

Fig. 1: Snapshot of inverse patchy colloids under geometrical confinement.

References

[1] P. D. J. van Oostrum, M. Hejazifar, C. Niedermayer, and E. Reimhult: J. Phys.: Condens. Matter 27 (2015) 2341.

Effect of chain crossing prohibition on phase-separated structure of block copolymers

Katsumi HAGITA,[1] and Takahiro MURASHIMA[2]

[1]*Department of Applied Physics, National Defense Academy, Yokosuka 239-8686*

[2]*Department of Physics, Tohoku University, Sendai 980-8578*

We have studied phase-separated structures of block copolymers in order to clarify topological effect of chain crossing prohibition. To achieve this aim, we firstly considered MP-SRP extensions [1,2] of dissipative particle dynamics (DPD) simulations [3]. We found that a slight change in the potential (force field) between original DPD [3] and MP-SRP extensions [1,2] affects weakly the lamellar domain spacing. The numerical precision is related to potential validity problems, and comparisons between different physics, Gaussian and excluded volume chains, may not be appropriate. Thus, we switched our approach to the development of force field parameters in order to treat directly with the phase separation phenomenon in the coarse-grained molecular dynamics (CGMD) simulations of the Kremer-Grest (KG) model [4]. Although implementations of the MP-SRP extensions [1,2] were developed using LAMMPS [5], the CGMD approach has the advantage of being free from the implementation and able to use HOOMD-blue [6] on the GPU. Notably, HOOMD-blue has a good performance for the standard DPD simulations [3].

To confirm fundamental behaviors using Gaussian chains, we performed large scale DPD simulations to estimate lamellar domain spacing of symmetric linear, ring, and four-arm-star block copolymer blends [7]. We also confirmed practical compatibility of lamellar domain spacing between self-consistent field theory and DPD simulations [8]. For fundamental understandings of topological effects by chain crossing prohibition, we performed CGMD simulations of polymers with rings. In [9], ring-filling effect on stress–strain curves of randomly end-linked tetra-arm prepolymers was studied. In [10], we discovered topological transition in multicyclic chains with structural symmetry inducing stress-overshoot phenomena in multicyclic/linear blends under biaxial elongational flow. In addition, we investigated topological barriers on the crystallization behavior of ring polyethylene melts with trefoil knots via united atom MD simulations [11].

Currently, we investigated interaction parameters of AB di-block copolymers for CGMD simulations. To consider a connection to Flory-Huggins χ parameter, we are studying

relationships among interaction parameters, lamellar domain spacing, and chain length (N). First, we performed CGMD simulations of AB di-BCP starting from the lamellar structures as shown in Fig. 1 (a). We confirmed the behaviors of domain spacing from weak to strong segregation conditions were consistent with theories, simulations, and experiments.

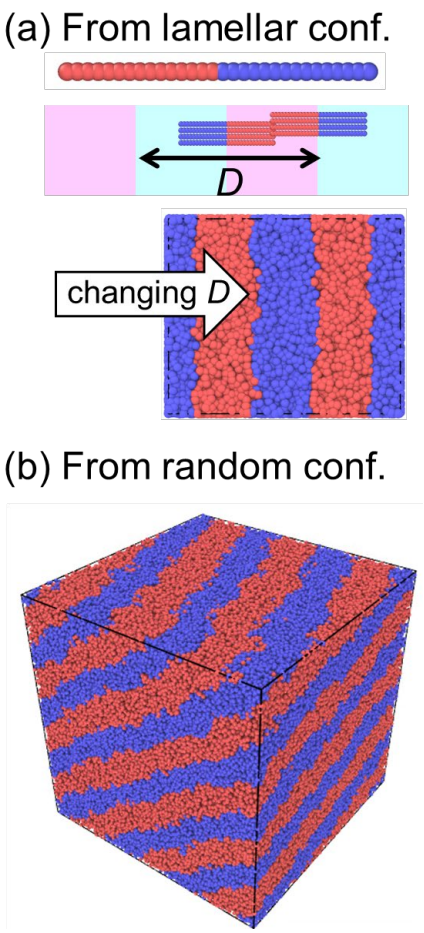

Fig. 1: Snapshots of CGMD models of AB di-BCP forming lamellar structures.

Second, we found that the AB-BCP in CGMD simulations spontaneously forms a lamellar structure as shown in Fig. 1 (b). We also confirmed that the lamellar domain spacing depends on the interaction parameters. After further studies on the interaction parameters, we will investigate topological constrain effect of polymers such as rings via CGMD simulations.

References

[1] R. D. Groot and P. B. Warren: J. Chem. Phys. **107** (1997) 4423.

[2] N. Iwaoka, K. Hagita and H. Takano: J. Chem. Phys. **149** (2018)114901.

[3] K. Hagita, T. Murashima, H. Shiba, N. Iwaoka, and T. Kawakatsu: Comput. Mater. Sci., **203** (2022) 111104.

[4] K. Kremer and G. S. Grest: J. Chem. Phys. **92** (1990) 5057.

[5] S. Plimpton: J. Comp. Phys. 117 (1995) 117.

[6] J. A. Anderson, J. Glaser, and S. C. Glotzer, Comput. Mat. Sci. **173**, 109363 (2020).

[7] K. Hagita, T. Murashima, and T. Kawakatsu, Macromolecules **55**, 8021 (2022).

[8] K. Hagita, and T. Murashima, Polymer **269**, 125733 (2023).

[9] K. Hagita, T. Murashima, T. Ohkuma, and H. Jinnai, Macromolecules **55**, 6547 (2022).

[10] T. Murashima, K. Hagita, and T. Kawakatsu, Macromolecules **55**, 9358 (2022).

[11] K. Hagita, T. Murashima, N. Sakata, K. Shimokawa, T. Deguchi, E. Uehara, and S. Fujiwara, Macromolecules **56**, 15 (2023).

Analysis of Various Crystal Forms of Glycine Nanocrystals by Large-Scale Metadynamics Simulations

Hiroki NADA

Faculty of Engineering, Tottori University, 4-101 Koyama-Minami, Tottori 680-8552

The control of structure and shape of glycine nanocrystals is important in connection with pharmaceutical engineering [1]. In this project, a classical molecular dynamics (MD) simulation combined with the metadynamics (MTD) method (hereafter, MTD simulation) was performed to elucidate stable structures and shapes of a glycine nanocrystal.

The MTD simulation was performed for a cubic system in which an α glycine nanocrystal consisting of 64 glycine molecules was placed at its center. The remainder of the system was filled with water molecules. AMBER force field was used for estimation of the intermolecular interaction energy and force acting between glycine molecules. The MTD simulation was carried out with DL_POLY 2.20 [2], in which PLUMED 1.3 [3] was implemented to permit combination with the MTD method, using System C of ISSP Supercomputer Center.

A free energy surface (FES) obtained using discrete C^{α}-C^{α} and N-N radial distribution functions represented by Gaussian window functions as collective variables indicated a few local minima. Each local minimum corresponded to a crystal-like structure with a different molecular arrangement of glycine molecules. Moreover, the shape of the nanocrystal was also different between those local minima. These results suggest that not only the structure of nanocrystals but also the shape of them can be analyzed using the MTD method.

In summary, the MTD method is a helpful tool to search for stable structures and shapes of nanocrystals consisting of complex molecules.

References

[1] X. Yang and A. S. Myerson: CrystEngComm. **17** (2015) 723.

[2] W. Smith and T. R. Forester: J. Mol. Graph. **14** (1996) 136.

[3] M. Bonomi et al.: Comput. Phys. Commun. **180** (2009) 1961.

Structural Analysis of Amorphous Silicon Monoxide by a Metadynamics Method with Unsupervised Machine Learning

Hiroki NADA

Faculty of Engineering, Tottori University, 4-101 Koyama-Minami, Tottori 680-8552

Amorphous SiO has been studied by many research groups because it can be functional materials [1]. However, molecular-scale structure of it remains elusive. The purpose of this project was elucidating molecular-scale structure of amorphous SiO using a classical molecular dynamics (MD) simulation combined with the metadynamics (MTD) method (hereafter, MTD simulation [2]).

MTD is an enhanced sampling method that increases the probability of reaching high free-energy states by adding a Gaussian bias potential to the Hamiltonian of a state. The MTD method affords a free energy surface (FES) in a space of collective variables (CVs) for a system of interest. This FES quantitatively represents the relative thermodynamic stabilities of many different states of the system.

The MTD simulation was carried out for each of amorphous Si, SiO and SiO_2 phases with DL_POLY 2.20 [3], in which PLUMED 1.3 [4] was implemented to permit combination with the MTD method, using System B of ISSP Supercomputer Center. In this project, we focused on the structural similarity between the examined amorphous phases. The structural similarity was analyzed by evaluating the geometrical similarity of Si-Si, Si-O, and Si-O pair-distribution functions. In this project, the geometrical similarity was evaluated using a method of unsupervised machine learning, dimensional reduction technique [5].

We confirmed that the present methodology is helpful to investigate detailed structures of multicomponent amorphous phases.

References

[1] A. Hirata et al.: Nat. Commun. **7** (2016) 11591.

[2] A. Laio and M. Parrinello: Proc. Natl. Acad. Sci. U. S. A. **99** (2002) 12562.

[3] W. Smith and T. R. Forester: J. Mol. Graph. **14** (1996) 136.

[4] M. Bonomi et al.: Comput. Phys. Commun. **180** (2009) 1961.

[5] H. Nada: ACS Omega **3** (2018) 5789.

Quantum algorithm for combinatorial optimization

Tatsuhiko SHIRAI
Department of Computer Science and Communications Engineering, Waseda University
Ookubo, Shinjuku-ku, Tokyo 169-8555

We have developed a quantum algorithm for QAOA (Quantum approximate optimization algorithm), which solves combinatorial optimization problems (COPs) in gate-based quantum computers. This year, we proposed a new method called spin-variable reduction method for formulating a constrained COP as an Ising model [1] and compared the performance with conventional methods in maximum glaph coloring problems.

QAOA is a hybrid quantum-classical algorithm designed to approximate the ground state of a Hamiltonian H. QAOA consists of calculations in a quantum computer and classical computer. The quantum computer calculates the expectation value of H over a variational state, which is given by

$$|\vec{\beta},\vec{\gamma}\rangle := e^{-i\beta_p H}e^{-i\gamma_p X}\cdots e^{-i\beta_1 H}e^{-i\gamma_1 X}|+\rangle\,, \tag{1}$$

where $\vec{\beta}=(\beta_1,\ldots,\beta_p)$ and $\vec{\gamma}=(\gamma_1,\ldots,\gamma_p)$. p denotes a circuit depth. X is called a mixer and adopted as $X=\sum_i \sigma_i^x$ where $\vec{\sigma}_i=(\sigma_i^x,\sigma_i^y,\sigma_i^z)$ is the Pauli operator acting on site i. $|+\rangle$ is defined as $\sigma_i^x|+\rangle=|+\rangle$ for all i. The classical computer optimizes $(\vec{\beta},\vec{\gamma})$ to minimize the value of $\langle\vec{\beta},\vec{\gamma}|\,H\,|\vec{\beta},\vec{\gamma}\rangle$. We solve the quantum dynamics on the super computer using openMP.

Maximum graph coloring problem colors each node of a given graph $G=(V,E)$ using n colors so that the number of edges connecting the nodes with different colors is maximized. This problem has a constraint that one color is assigned to each node. When solving a COP with constraints by QAOA, the Hamiltonian is given as $H=H_{\rm obj}+H_{\rm cst}$. Here, $H_{\rm obj}$ and $H_{\rm cst}$ denote the Hamiltonians for objective function and constraints of the COP, respectively. There are three methods to give the Hamiltonians: penalty method, domain-wall method, and spin-variable reduction method.

Figure 1 shows p dependences of success probability p_s. Here, we set $n=4$ and $|V|=6$, and generate 10 random graphs with edge density 0.75. We found that domain-wall method and spin-variable method outperforms penalty method.

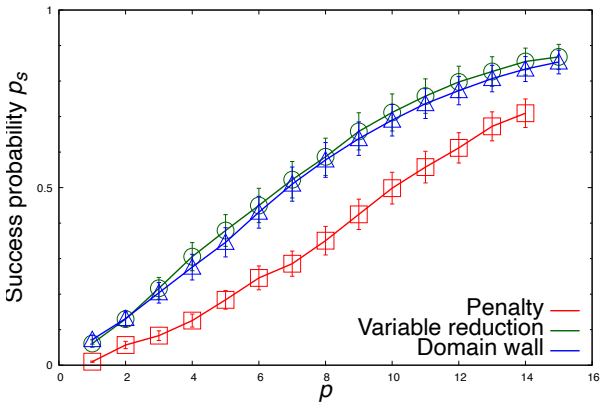

Figure 1: Performance comparison among penalty method (squares), spin-variable reduction method (circles), and domain-wall method (triangles).

References

[1] T. Shirai and N. Togawa: IEEE Transactions on Computers (Early Access).

Topological chirality order and its stability in breathing-kagome antiferromagnets

Kazushi AOYAMA
Department of Earth and Space Science, Graduate School of Science, Osaka University
Machikaneyama-cho, Toyonaka-shi, Osaka 560-0043

The quest for topological spin textures in solids is one of the central issues in condensed matter physics because of their possible applications to spin-electronic devices. A typical example of such topological spin textures is the so-called skyrmion crystal (SkX) where the total solid angle subtended by all the spin in the magnetic unit cell takes an integer topological in units of 4π. Noting that the scalar spin chirality $\chi_{ijk} = \mathbf{S}_i \cdot (\mathbf{S}_j \times \mathbf{S}_k)$ is related to the solid angle, the SkX could be regarded as a topological chiral order. Although the SkX is usually realized in the presence of a magnetic field being irrespective of whether the the Dzaloshinskii-Moriya interaction is active or not [1], a zero-field SkX is also possible in a specific metallic system [2]. Previously, we theoretically demonstrated that a breathing bond-alternation of the underlying lattice can induce a zero-field topological chiral order which can be viewed as a miniature version of the SkX [3]. In the work, we investigate effects of an additional single-ion magnetic anisotropy which more or less exists in real materials.

We consider the following classical J_1-J_3 model on the breathing kagome lattice with the single-ion magnetic anisotropy:

$$\mathcal{H} = J_1 \sum_{\langle i,j\rangle_S} \mathbf{S}_i \cdot \mathbf{S}_j + J_1' \sum_{\langle i,j\rangle_L} \mathbf{S}_i \cdot \mathbf{S}_j + J_3 \sum_{\langle\langle i,j\rangle\rangle} \mathbf{S}_i \cdot \mathbf{S}_j + D \sum_i (S_i^z)^2, \quad (1)$$

where $\mathbf{S}_i$ is a classical spin, the summation $\sum_{\langle\rangle_{S(L)}}$ runs over site pairs on small (large) triangles having the nearest neighbor (NN) interaction J_1 (J_1'), $J_3 > 0$ is the third NN antiferromagnetic interaction along the bond direction, and $D < 0$ ($D > 0$) represents an easy-axis (easy-plane) anisotropy. In the isotropic case of $D = 0$, a triple-$\mathbf{Q}$ state appearing for a relatively large J_3 takes the miniature SkX structure having a nonzero uniform total chirality [3]. By performing Monte Carlo simulations, we investigate the stability of this topological chiral order against the anisotropy D. In our simulations, 1×10^6 - 2×10^6 MC sweeps are carried out under the periodic boundary condition, and the first half is discarded for thermalization. $\mathbf{S}_i$ at each site is updated in a conventional random and a successive over-relaxation-like processes, where in the former (latter) process, we try to rotate a spin in a randomly proposed direction (by the angle π around the local mean field) by using the Metropolis algorithm. Observations are done at every MC sweep, and the statistical average is taken over 4 independent runs starting from different random initial configurations.

It is found that the zero-field topological chiral order with the miniature SkX structure is relatively robust against easy-axis ($D < 0$) and easy-plane ($D > 0$) anisotropies, although for strong easy-axis (easy-plane) anisotropy, a triple-$\mathbf{Q}$ collinear (coplanar) state is favored. Since the SkX and anti-SkX each having positive or negative chirality are energetically degenerate, the topological Hall effect of alternative sign is possible at zero field. For moderate

$D < 0$ ($D > 0$), the collinear (coplanar) phase preempts the SkX phase and in the chiral sector, it shows a random domain structure consisting of positive- and negative-chirality clusters [4]. It is also found that the miniature SkX is robust against the external magnetic field, but further analysis is necessary to clarify the in-field properties of the model.

References

[1] T. Okubo, S. Chung, and H. Kawamura, Phys. Rev. Lett. **108**, (2012) 017206.

[2] R. Ozawa, S. Hayami, and Y. Motome, Phys. Rev. Lett. **118**, 147205 (2017).

[3] K. Aoyama and H. Kawamura, Phys. Rev. B **105**, (2022) L100407.

[4] K. Aoyama and H. Kawamura, J. Phys. Soc. Jpn. **92**, (2023) 033701.

Molecular modeling of ferroelectric nematic phase

Takeaki ARAKI, and Matheus DE MELLO

Department of Physics,

Kyoto University, Kitashirakawa-Oiwake-cho, Sakyo, Kyoto 606-8502

Ferroelectric liquid crystals are partially ordered anisotropic fluids with ferroelectricity. Its experimental realization has not been reported for a long time. Recently, some experimental groups have succeeded in synthesizing molecules which possibly show ferroelectric nematic order [1-2].

Even though the molecular features required to stabilize the ferroelectric phase were systematically studied, the origins of the spontaneous polar ordering remain still unclear. In this work, we study a molecular liquid DIO, which were synthesized by Nishikawa *et al*., focusing on which of the dipole-dipole electrostactic interaction or the polar shape of the molecules is dominant for the polar ordering.

We performed all-atom molecular dynamics simulations of 1000-2000 DIO molecules with GROMACS. The partial charge on each atom is estimated by using Gaussian. In order to see the effect of the electrostatic interaction, we carried out the simulations of the DIO without the electric charges. We analyzed the nematic, polar order parameters, the spatial distribution, and the correlation between the molecular axes.

Our simulation results indicate the spontaneous polar ordering at a low temperature. The distribution function suggests the molecule shape can be regarded as a rod without the remarkable head-tail asymmetry. Owing to the electric charges, the local parallel-parallel alignment is favored than the parallel-anti parallel alignment, which is usually observed in the conventional nematic phase.

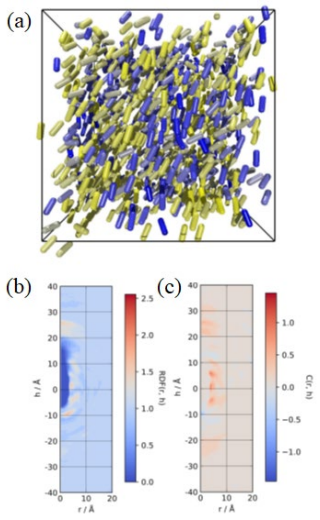

Fig. 1: (a) A snapshot of the liquid crystal phase of DIO at 330K. The molecule is represented with a rod whose color shows the orientation. (b) The distribution function. (c) The correlation function.

References

[1] H. Nishikawa, *et al.* Adv. Mater. 29, 1702354 (2017).

[2] R. J. Mandle, *et al.*, Chem. Eur. J. 23, 14554 (2017).

Aggregation of polyelectrolytes in mixed solvents

Takeaki ARAKI, and Dai Matsubara

Department of Physics,

Kyoto University, Kitashirakawa-Oiwake-cho, Sakyo, Kyoto 606-8502

Polymer systems often exhibit phase-separated structures with diverse patterns from microscopic to macroscopic length scales. In particular, diblock copolymer melts and polyelectrolyte in poor solvents are expected to be applied to nanostructures.

In this study, we consider mesoscopic pattern formation of weakly charged polyelectrolytes in binary mixture solvents by means of field theoretic polymer simulations in lattice space. The polymer is modeled as a continuous Gaussian chain, and is described by path integrals. The solvent-polyelectrolyte and solvent-solvent interactions are given by Flory Huggins parameters. The electrostatic interaction is obtained by solving Poisson-Boltzmann equation. The binary solvent itself is mixed. But the affinities of the solvents to the polyelectrolyte is different. One of the solvents prefers the polyelectrolyte more than the other.

Figure 1 shows the concentration field of the polyelectrolyte in the binary solvent mixtures. The composition of the more preferred solvent is increased from top to bottom with fixing the polyelectrolyte concentration. When the more preferred component is rich in the solvent (bottom), the polyelectrolyte is mixed homogeneously. As its composition is decreased (top), the system is phase-separated and a labyrinth pattern is formed. In the polymer-rich phase, a stripe concentration modulation pattern is observed.

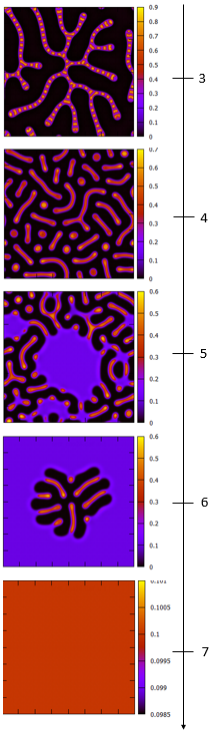

Fig. 1: Snapshots of the phase-separated pattern of the polyelectrolyte in binary mixture solvents. The concentration of the more preferred component is increased from top to bottom.

References

[1] G. H. Fredrickson, The Equilibrium Theory of Inhomogeneous Polymers, *Oxford University Press*, 2013.

Rheology Simulation of Dynamically Cross-linked Networks

Yusuke Yasuda

Research Center for Computational Design of Advanced Functional Materials.

National Institute for Advanced Industrial Science and Technology, Ibaraki 305-8568.

Recently a new type of dynamic bond elastomers called entropy-driven has gained attention for showing superior self-healing and toughness compared to conventional dynamic bond elastomers [1], but detailed understanding is not reached yet. Last year, we succeeded in fabricating a new coarse-grained model which can reproduce typical hysteresis and self-healing properties of conventional dynamic bond elastomer. This year, we introduced entropy-driven properties to the coarse-grained model.

In this work, we made coarse-grained model for dynamic bond elastomers based on Kremer-Grest model [1]. For cross-links between reactive bead, we introduced harmonic potential with associating and dissociating condition (Fig. 1). We tuned harmonic constant K and bond fracture energy ε_d. Under this condition we conducted equilibration simulation and mechanical tests. Calculation was conducted using molecular dynamics simulation software packages OCTA, and LAMMPS on ISSP Supercomputer System.

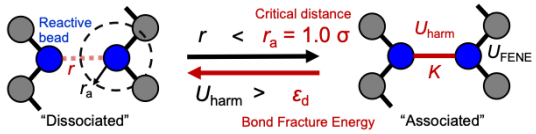

Fig.1, Schematic illustration of the coarse-grained model of dynamic bond elastomers.

From equilibration simulation, we found that equilibrium constant K_a has proportional dependence to 1/T, consistent to Gibbs equation. From the slopes and y-intercepts of the 1/T dependence of K_a, we defined ΔS_a and ΔU_a. From this analysis, we found that ΔU_a are influenced primarily by ε_d, and ΔS_a are predominantly influenced by on K. As K decreases, ΔS_a increases, confirming smaller K represents entropy-driven systems.

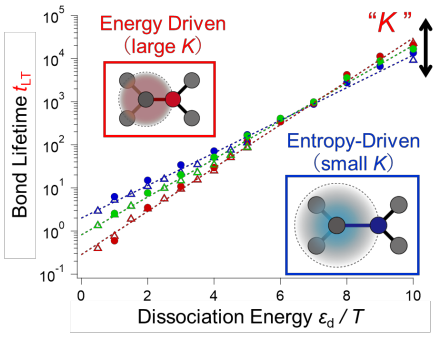

Fig. 2, the relationship among Bond lifetime, dissociation energy, and harmonic constant K

We also conducted lifetime analysis for different Ks. Then we found that average bond lifetime follows Arrhenius equation depending on K (Fig. 2), and dynamic bonds with smaller K shows shorter lifetime in high ε_d region, concluding that entropy-driven dynamic bond elastomers with high ε_d owing to smaller dissociation activation energy.

We also conducted mechanical and stress-recovery test. Both models show typical large hysteresis, and stress recovery at high temperature. Then we analyzed stress-relaxation behavior by analyzing relationship between stress and healing time, to find that stress-relaxation times are closely related to bond lifetime. Then we conclude that faster self-healing in entropy-driven dynamic bond elastomers originates from faster dissociation / association dynamics, which comes from lower activation energy for dissociation [3].

References [1] Kim et al. *Macromolecules* **2020**, *53*, 4121. [2] K, Kremer et al., *J. Chem. Phys.*, **1990**, *92*, 5057. [3] Y. Yasuda et al., *under review*.

Acknowledgement This work is partially supported by a project JPNP18016, commissioned by the New Energy and Industrial Technology Development Organization(NEDO)

Structural Analysis and Mechanical Properties Simulations of Polymer Networks with Various Network Structures

Yusuke Yasuda

Research Center for Computational Design of Advanced Functional Materials.

National Institute for Advanced Industrial Science and Technology, Ibaraki 305-8568.

Rubber elasticity theories proposed so far qualitatively reproduces the mechanical properties of vulcanized rubbers and cross-linked gels, but it is not quantitative. One reason of this is that the actual polymer networks contain inhomogeneity, and it is difficult to detect it by experiments. Then theoretically, homogeneous network is assumed.

In this work, we aimed to develop a methodology to handle network inhomogeneity, focusing on detecting structural defects in the network. We performed coarse-grained molecular dynamics simulations for networks with various inhomogeneity. Then we analyzed the structure during the crosslinking process and the mechanical properties under uniaxial deformation. We tried to extract substructures that contribute to the mechanical properties.

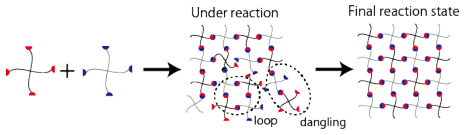

Fig, 1. Schematic illustration of the fabrication method of the system.

In this research, we fabricated coarse-grained model of star-shaped end-crosslinked elastomers which is known as a homogeneous network, was created based of the repulsive Kremer-Grest model. We prepared 3-arm and 4-arm systems referring to tetra-PEG, tri-PEG gel [1] tuning the arm length. Two terminal types A, B are prepared. Total number of beads in system are set approximately 1.0×10^5. τ density condition is set as $0.85\,\sigma^{-3}$Then system relaxation calculation and reaction calculations. For fabrication of networks with various inhomogeneity, we terminate the reaction calculation when reaction ratio reaches certain value in range of 0.24 – 0.96. Then we conducted uni-axial elongation test (λ=1-4) , and obtain stress-extension ratio curves. Then we calculated elastic modulus G_{sim} by fitting the initial shape of stress-extension ratio curves.

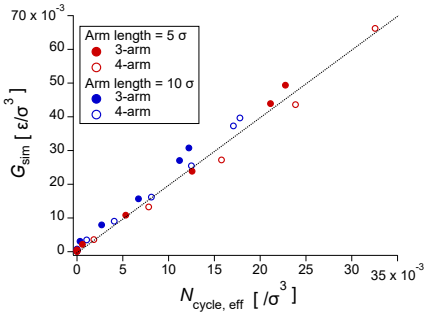

Fig. 2 Elastic moduli G_{sim} against the number of effective closed loops $N_{cycle,eff.}$

Then we tried to calculate the structure which contribute to elastic moduli. Based on the Scanlan-Case [2,3] criterion, we analyzed the network structure. We counted only effective chain s between branching points with three or more branches, excluding dangling, loop, super-dangling, super-loop structure and eliminate, including bridge and super-bridge structures. In the network constructed by effective chains, we counted the number of closed loops in network based on phantom network theory, finding that elastic moduli are proportional to $N_{cycle,eff}$ for all branch num and arm length.

References 1. 1. Fujiyabu et al., Sci Adv. 2022, 8(14), eabk0010 2. Scanlan, J. Polym. Sci., 1960, 43, 501, 3. Case, J. Polym. Sci., 1960, 45,

Acknowledgement This work is supported by a Grant-in-Aid for Young Scientists (22K14740)

Theory of microwave scattering in a dissipative superconducting circuit element

TSUYOSHI YAMAMOTO
Faculty of Pure and Applied Sciences, University of Tsukuba
Tsukuba, Ibaraki 305-8571

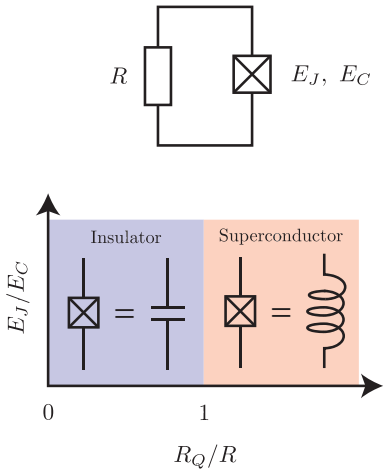

Figure 1: (top) A Josephson junction with the Josephson energy E_J and the charging energy E_C shunted by a resistor with the resistance R. (bottom) Illustration of the phase diagram of the Schmid-Buldagaev transition.

A Josephson junction is a building block of superconducting circuits. Thanks to its characteristic nonlinearity, we can develop a great variety of superconducting devices, such as a superconducting qubit and a parametric amplifier. Although the property of the isolated Josephson junction is understood well, it is little known, especially its many-body effects, when it contacts electromagnetic environments. The most notable phenomenon is a dissipation-induced quantum phase transition. Forty years ago, Schmid and Buldagaev theoretically found that a single Josephson junction shunted to a resistor, a resistively-shunted Josephson junction, undergoes a superconductor-insulator transition [1, 2]. When the resistance is larger than a resistance quantum ($R > R_Q = h/4e^2$), the Josephson junction becomes an insulator, while when $R < R_Q$, it becomes a superconductor, interestingly not being controlled by junction parameters (see Figure 1).

Although the theoretical works on the DC transport checked the Schmid-Bulgadaev transition [3, 4], there is no decisive evidence for the experimental observation [5], stirring up controversy. The recent development of superconducting circuits allows experimentalists to measure the AC-impedance of the resistively-shunted Josephson junction using microwave spectroscopy and then to obtain important properties, such as the excitation spectrum or the dynamical property. This endeavor would be a key to solving the ongoing debate problem.

In this project, we numerically investigated the AC-impedance of the resistively-shunted Josephson junction [6]. To obtain the AC-impedance, we calculated the phase-phase correlation function defined on the imaginary-time axis using the path-integral quantum Monte Carlo (PIQMC) simulation and then performed the analytical continuation for the PIQMC data using the Padé approximation. Since the Padè approximation needs highly-accurate calculations for the applying data, we performed the parallel computing for the Monte Carlo sampling mainly using “F2cpu”, succeeding in collecting a large enough Monte

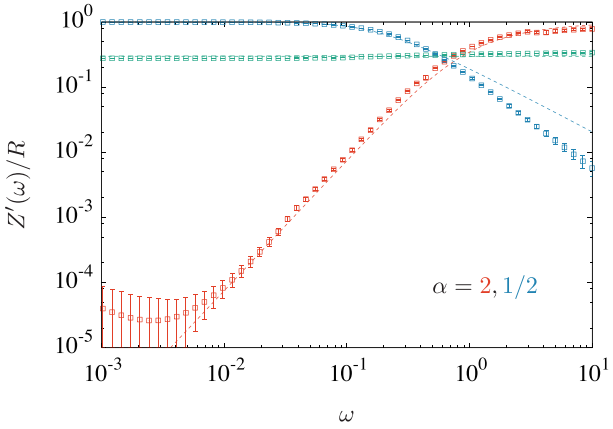

Figure 2: Frequency dependence of the real part of the AC-impedance $Z'(\omega)$ for various values of $\alpha = R_Q/R = 2$ (red), 1 (green), and 1/2 (blue), obtained by the PIQMC. At the DC limit ($\omega \to 0$), the AC-impedance goes to 0 and R for $\alpha > 1$ and $\alpha < 1$, respectively, which is a signature of the Schmid-Bulgadaev transition. The dashed lines represents the analytical formulas.

Carlo steps, typically $\sim 5 \times 10^7$, to provide the accurate calculations for the AC-impedance. Our numerical results for the AC-impedance as a function of frequency or Matsubara frequency (the Fourier space of the imaginary time) confirmed the superconductor-insulator transition, as originally predicted by Schmid and Bulgadaev and revealed the low- and high-energy physics and their crossover (see Figure 2) [7]. This work would give a deep understanding of the dissipative Josephson junction, which pushes further development for superconducting devices using Josephson junctions.

References

[1] A. Schmid, Phys. Rev. Lett. **51**, 1506 (1983).

[2] S. A. Bulgadaev, JETP Lett. **39**, 264 (1984).

[3] N. Kimura and T. Kato, Phys. Rev. B **69**, 012504 (2004).

[4] S. L. Lukyanov and P. Werner, J. Stat. Mech. P06002 (2007).

[5] A. Murani *et al.*, Phys. Rev. X **10**, 021003 (2020).

[6] P. Werner and M. Troyer, Phys. Rev. Lett. **95**, 060201 (2005).

[7] T. Yamamoto, T. Kato, L. I. Glazman, and M. Houzet, in preparation.

Grain boundary Li ion conductivity in NASICON-type Solid Electrolytes

Masanobu NAKAYAMA

Department of Advanced Ceramics,

Nagoya Institute of Technology, Gokiso, Showa-ku, Nagoya, Aichi 466-8555

$LiZr_2(PO_4)_3$ (LZP) related materials are promising solid electrolyte materials with high ionic conductivity and chemical stability.[1] Many material calculations have been applied to lithium ion-conducting NASICON-type solid electrolytes, but most of them are concerned with bulk conduction, and grain boundaries have rarely been investigated.[2], [3] In this study, the effect of dopant Ca on the ionic conductivity is discussed.

To calculate lithium ion diffusion in the grain boundary model of LZP, we used the Bond Valence Force Field (BVFF) proposed by Adams et al.[4] plus a Stillinger-Weber (SW) type force field representing three-body interactions. Parameters included in the force field were evaluated by a cuckoo search to match the results of first-principles calculations. The same was employed: force-field molecular dynamics (FFMD) calculations using the NVT ensemble were performed for 1 ns every 50 K from 400 K to 900 K. The results are presented in Table 1. The software package NAP[5], [6] was used for the above.

Figure 1 shows the grain boundary model used in this study. (a) and (b) have the same composition, but (a) with Ca ions randomly arranged and (b) with Ca ions segregated at the grain boundary, as experimentally confirmed. For these models, molecular dynamics was performed to evaluate the diffusion coefficient versus temperature, and the results are shown in Figure 2 as an Arrhenius plot. The obtained results show that the ionic conductivity (room temperature) of the segregated structure (b) is 5 x 10^{-4} cm^2 s^{-1}, which is about twice the diffusion coefficient of the random structure (a). On the other hand, no significant change in activation energy was observed. This suggests that the grain boundary conductivity can be controlled by controlling the arrangement of dopants.

A more detailed analysis of the obtained results shows that Li ions have a trapping effect near Ca ions. In previous studies, the grain boundary structure also has the effect of trapping Li ions. Therefore, it is suggested that Li ions become excessively concentrated near the grain boundary. We believe that such excess of lithium ions contributes to the enhancement of ionic conduction at the grain boundary.

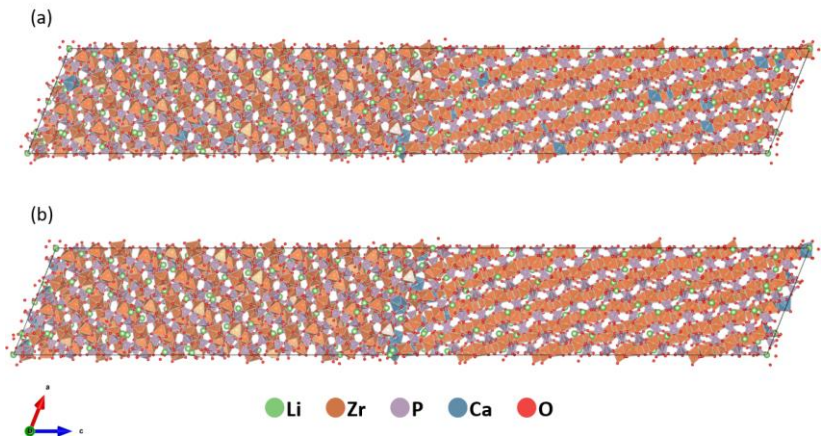

Figure 1 Grain boundary structure model for Ca-doped LZP. (a) Random substitution of Ca to Zr sites and (b) Ca segregation model near grain boundaries.

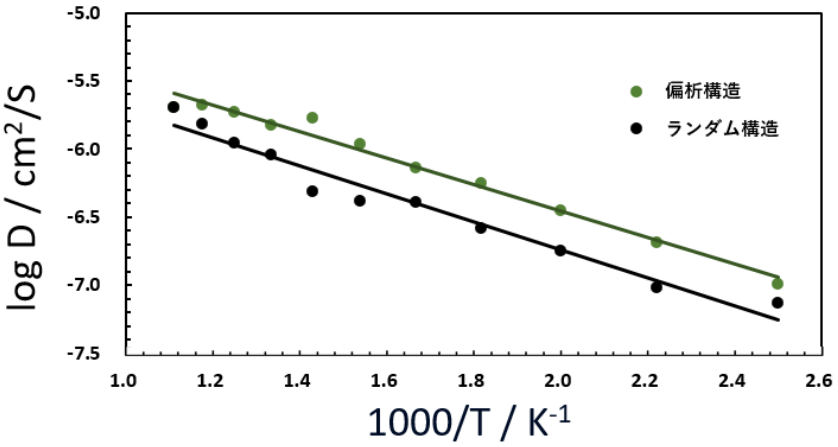

Figure 2 Comparison of diffusion coefficients of Li in two-types of grain boundary models of Ca-doped LZP. (Black symbol: random Ca arrangement model; Green symbol: Ca segregation model near to grain boundary.

References

[1] M. Nakayama et al., Chem. Commun., **58**, 9328–9340, (2022)

[2] K. Nakano et al., J. Phys. Chem. C, **125**, 23604–23612 (2021)

[3] R. Kobayashi et al., Acta Mater., **226**,117596 (2022)

[4] S. Adams et al., Phys. Stat. Sol. A, **208**, 1745-1753 (2011)

[5] R. Kobayashi, J. Open Source Softw.,**6**, 2768, (2020)

[6] R. Kobayashi et al., APL Mater., **8**, 081111, (2020)

Surface Tension Stabilizing Cell Motion Order

Katsuyoshi Matsushtia, Naoya Kamamoto, Maki Sudo, Taiko Arakaki
Depertment of Biological Science, Graduate School of Science, Osaka University
Machikaneyama, Toyonaka, Osaka 560-0043

Cells collectively move in particular scaffolds in various biological phenomena, including organ morphogenesis [1]. For example, neuronal cells move by interacting with surrounding glial tissue[2]. The collective motion reflects the interaction between the tissue and the surrounding scaffold. The ordering mechanism in this collective motion needs sufficient examination through the computer simulation based on statistical physics. In particular, the essential interaction in statistical physics is the surface tension between the cells and scaffolds, which should be incorporated into the simulation. To clarify the effect of the interface tension, we consider a collective motion of a cell cluster and its dependence on the surface tension.

We employed the cellular Potts model [3] and extended its cells with the polarity of cell-cell adhesion [4]. This model induces the spontaneous order of the cellular motion and successfully explains the collective migration of cells [5]. We changed the surface tension between the scaffold and the cells and observed the collective motion. In the case of low surface tension, the cells have an affinity with the scaffolds and individually exhibit a random walk. When the surface tension increases above the Graner-Glazier surface tension, the cells form a cluster and collectively move, In this case, the collective motion has a persistence time, in which the cluster almost straightly moves. As the surface tension increases, the switching from the straight motion to the rotational motion and inverse switching appears. In the case of large surface tension, the collective motion becomes the rotation, the center of which corresponds to the center of the cluster. Due to the rotational motion, the center of the cluster exhibits only diffusion.

This result explains the previous result of the cluster consisting of the two types of cells, which is reported in the previous project [6]. The cell cluster transitions from the rotational to straight motion as the differentiation of cells progresses. The present result implies that this motion transition originates from the surface tension decreases associated with the cell type changes in the differentiation.

We appreciate Prof. H. Kuwayama, Prof. S. Yabunaka, Dr. H. Hashimura, Prof. Sawamoto, Dr. Matsuda, Prof. H. Yoshino, and Prof. M. Kikuchi their various support on this work.

References

[1] P. Rørth, Ann. Rev. Cell Develop. Biol. **25**, 407 (2009).

[2] C. Nakajima, M. Sawada, K. Sawamoto, Curr. Opi. Neurobio. **66**, 1 (2021).

[3] F. Graner and J. Glazier, Phys. Rev. Lett. **69**, 2013 (1992).

[4] K Matsushita, Phys. Rev. E **95**, 032415 (2017).

[5] K Matsushita, Phys. Rev. E **97**, 042413 (2018).

[6] K. Matsushita, N. Kamamoto, M. Sudo, K. Fujimoto, Proc. Sympo. Traffic Flow Self-driven Parti. **27**, 23 (2021).

Calculation of ordered structures, dynamics and optical properties of soft materials

Jun-ichi FUKUDA

Department of Physics, Kyushu University, Motooka 744, Nishi-ku, Fukuoka 819-0395

We continued our study that started in the previous year on the structure of a cholesteric blue phase liquid crystal (BPLC) under an electric field. Our study was motivated by a recent experimental study [1] demonstrating the formation of various (meta)stable ordering with different periodicity in a reproducible manner by applying an electric field. Particularly, a tetragonal structure with $I4_122$ symmetry was shown to be (meta)stable even after the cessation of the electric field, which had not been reported.

Our numerical study focused on the role of planar surfaces that confine BPLC on its structure and stability, and was based on the Landau-de Gennes continuum theory that describes the orientational order by a second rank tensor. Calculations were carried out on a regular mesh, which facilitated the parallelization (in our case OpenMP was used). We also calculated the optical properties of the structures obtained (more specifically, how monochromatic incident light with a given wavevector is reflected and transmitted) by directly solving the Maxwell equations for the electromagnetic field of light. We employ plane-wave expansions in the directions normal to the thickness direction, and the Maxwell equations were discretized so that the matrix representing the Maxwell equation is of block tridiagonal form.

Our calculations [2] showed that structures with different and discretized periodicity are indeed (meta)stable. The free energy evaluation of these structures revealed that the periodicity of the most stable structure depends systematically on the electric field strength. We also calculated [2] the reflection spectra of the structures. We found strong selective reflection depending on the circular polarization of the incident light arising from the chirality of BPLC, and the variation of the reflection peak position in response to the electric field.

References

[1] D.-Y. Guo et al., Nature Mater. **19**, 94 (2020).

[2] J. Fukuda, Front. Soft Matter **2** 1011618 (2022).

Measurement-induced phase transitions in $U(1)$-symmetric monitored circuits

Yohei FUJI
Department of Applied Physics, University of Tokyo, Tokyo 113-8656

Many-body quantum systems evolved under repeated measurements have recently been shown to reveal a novel type of nonequilibrium phase transition called the measurement-induced phase transition [1, 2]. A paradigmatic example is the entanglement transition from a volume-law to an area-law entangled phase, which is induced by the competition between unitary dynamics and projective measurements. Surprisingly, the entanglement transition exhibits critical phenomena described by conformal field theory as in equilibrium phase transitions. It is then natural to ask whether universality classes due to symmetry or dimensionality also arise in measurement-induced phase transitions.

In this study, we considered one-dimensional random quantum circuits consisting of two-site unitary gates and projective measurements of single qubits, both of which are design to preserve a $U(1)$ charge corresponding to the total number of flipped qubits [3]. By employing parallel sampling implemented in Julia on Supercomputer System B at ISSP, we computed steady-state physical quantities averaged over many circuit realizations and measurement outcomes. In addition to the entanglement transition characterized by the logarithmic scaling of the entanglement entropy, we found a charge-fluctuation transition characterized by the logarithmic scaling of the bipartite charge fluctuation as shown in Fig. 1. The latter transition exhibits critical phenomena akin to the Tomonaga-Luttinger liquid theory, much like critical phenomena for the ground state of one-dimensional quantum systems preserving $U(1)$ symmetry. This result thus highlights the importance of symmetry for classifying and understanding the measurement-induced phase transitions.

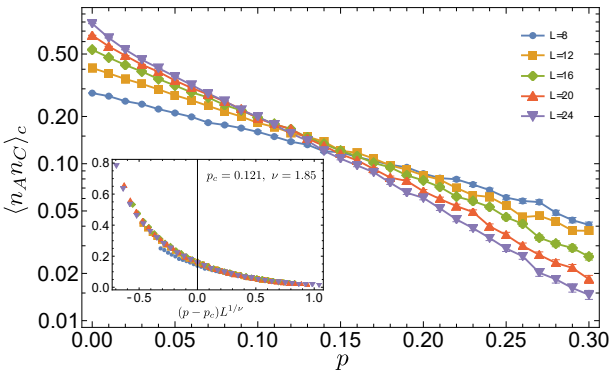

Figure 1: Subsystem charge correlation function $\langle n_A n_C \rangle_c$ between two disjoint subsystems A and C is plotted as a function of the measurement rate p. It is related to the bipartite charge fluctuation F_A by $\langle n_A n_C \rangle_c = F_A + F_C - F_{A \cup C}$.

References

[1] A. C. Potter and R. Vasseur, Entanglement Dynamics in Hybrid Quantum Circuits in *Entanglement in Spin Chains: From Theory to Quantum Technology Applications*, edited by A. Bayat, S. Bose, and H. Johannesson (Springer International Publishing, Cham, 2022) pp. 211–249.

[2] M. P. A. Fisher, V. Khemani, A. Nahum, and S. Vijay, Random Quantum Circuits, Annu. Rev. Condens. Matter Phys. **14**, 335 (2023).

[3] H. Oshima and Y. Fuji, Charge fluctuation and charge-resolved entanglement in a monitored quantum circuit with $U(1)$ symmetry, Phys. Rev. B **107**, 014308 (2023).

First principles studies of electronic structures in armchair-edged graphene nanoribbons

Junhuan LI, Kenta ARIMA

Graduate School of Engineering, Osaka University, Yamada-oka, Suita, Osaka 565-0871

Local electronic structures of graphene nanosheets have been intensively studied so far [1, 2]. However, the relationship between the electronic structure and atomic arrangement is still unclear. In this study, we simulated scanning tunneling microscopy (STM) images of armchair-edged graphene nanoribbons (AGNRs) by the first principles calculations.

Calculations were performed by STATE (Simulation Tool for Atom TEchnology) package. The AGNR we simulated was terminated by hydrogen atoms as shown in Figure 1. Periodic boundary conditions were applied to a supercell setup with length l_{cell}.

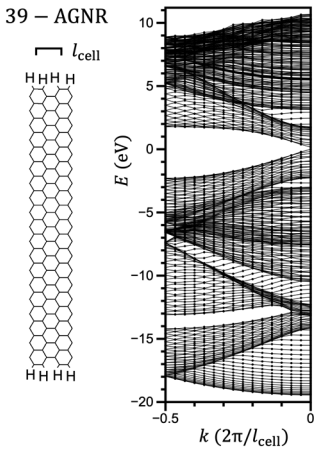

Fig. 1: The ribbon configuration and band structure of 39-AGNR.

The band structure of 39-AGNR (where 39 is the width measure by the number of rows of carbon atoms across the AGNR) is shown in the right panel of Figure 1. Based on the simulated band structure, the STM images were calculated using different sample biases. At a sample bias of -1 V, the simulated STM image exhibit hexagonal patterns as shown in Figure 2.

This work has been performed on System B of the Supercomputer Center, the Institute for Solid State Physics, the University of Tokyo.

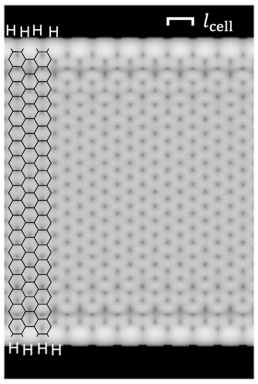

Fig. 2: The simulated STM image of 39-AGNR.

References

[1] T. Wassmann et al., J. Am. Chem. Soc. **132**, 3440 (2010).

[2] J. Li et al., Phys. Rev. B **103**, 245433 (2021).

Numerical studies on thermodynamics and excitation spectra in Heisenberg antiferromagnets on the triangular and kagome lattices

Yoshiyuki Fukumoto
Department of Physics, Faculty of Science and Technology, Tokyo University of Science
2641 Yamazaki, Noda, Chiba 278-8510

Neutron scattering experiments on two-dimensional frustrated spin systems with spontaneous magnetizations, such as a triangular-lattice system $Ba_3CoSb_2O_9$ [1] and a kagome-lattice system $Cs_2Cu_3SnF_{12}$ with the $\boldsymbol{q} = 0$ type ordering stabilized by Dzyaloshinskii-Moriya (DM) interactions [2,3], have revealed that the dynamic structure factors consist of not only collective magnon excitations but also spinon continuums.

As for the triangular-lattice system, Zhang and Li used the fermionic spinon operator to calculate dynamic structure factors within the RPA approximation [4]. They argued that the structure of the spinon continuum is closely related to the roton minimum of the magnon spectrum, and also found an amplitude mode composed from two spinons that cannot be captured by the spin wave approximation.

As for the kagome-lattice system, magnon dispersions obtained from a neutron scattering experiment on $Cs_2Cu_3SnF_{12}$ were analyzed based on the linear spin wave (LSW) approximation, and reported that the spin-wave interactions led to a large negative-renormalization, where the exchange parameter was found to be about 40% smaller than a reliable value, $J = 20.7$ meV, determined from magnetic susceptibility measurements [2]. Also, a recent neutron scattering experiment has observed a fourth collective excitation that is thought to be an amplitude mode [3].

In this article, we report our recent results of an Ising expansion (IEP) study on the large negative-renormalization observed in $Cs_2Cu_3SnF_{12}$. In order to stabilize the $\boldsymbol{q} = 0$ ordering, which is assumed in the xy plane, we incorporate the DM interaction with the D vector of $\boldsymbol{D} = (0, 0, D^{\parallel})$ and write a minimal Hamiltonian for this material as

$$H = J \sum_{\langle i,j \rangle} \boldsymbol{S}_i \cdot \boldsymbol{S}_j + \sum_{\langle i,j \rangle} \boldsymbol{D} \cdot (\boldsymbol{S}_i \times \boldsymbol{S}_j), \quad (1)$$

where $\boldsymbol{S}_i$ represents the $S = 1/2$ operator at site i. Introducing a perturbation parameter λ, we write $H_\lambda = H_0 + \lambda H_1$, where H_0 is an Ising model and we assume $\lambda \to 1$ recovers eq. (1). The perturbation calculation was performed using the connected cluster expansion method, including all clusters up to 9 links and 10 sites. Multi-block diagonalization was performed in the calculation of the effective Hamiltonian [5]. We also incorporated a local field term to improve convergence of the series [5]. The local field term is the form of staggered magnetic field stabilizing the $\boldsymbol{q} = 0$ ordering and its strength is defined as t. We include the local field term into H_0 and that with opposite sign into H_1, so as to cancel out with each other at $\lambda \to 1$. If we set $t = 0$, then we have unphysical results such as the magnon energies being negative in most of the wave vectors. When $t > 0$, the results change significantly at first, and the region of negative magnon energy decreases. When t increases to some extent, the region of negative magnon energy disappears and the result does not depend on t very much. As such value of t, we choose $t/J = 1$ in this study. As t is further increased, the resulting t dependence increases slowly, be-

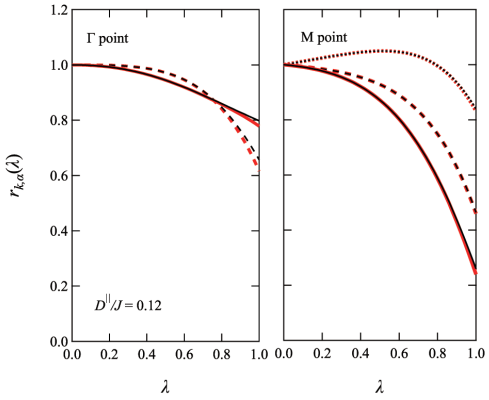

Figure 1: Renormalization factors $r_{\boldsymbol{k},\alpha}(\lambda)$. The black and red lines, respectively, represent the ninth and eighth order results.

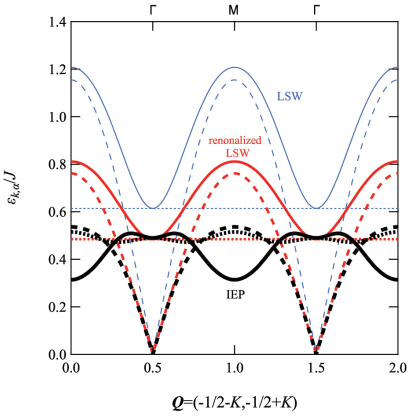

Figure 2: Comparison of magnon dispersions between the IEP and LSW. The choice of line type is the same as in Fig. 1.

cause it becomes harder to correctly handle the local field term included in the perturbation.

Let $\epsilon_{\boldsymbol{k},\alpha}$ be the magnon excitation energy to be obtained, where $\boldsymbol{k}$ is the wave vector and α is the identifier for three modes in the kagome lattice. We set $\epsilon_{\boldsymbol{k},\alpha} = r_{\boldsymbol{k},\alpha}(1) \times \epsilon^{\mathrm{LSW}}_{\boldsymbol{k},\alpha}$, where $\epsilon^{\mathrm{LSW}}_{\boldsymbol{k},\alpha}$ is the magnon excitation energy in the LSW and $r_{\boldsymbol{k},\alpha}(\lambda)$ is "renormalization factor". We calculate $r_{\boldsymbol{k},\alpha}(\lambda)$ by the IEP up to the ninth order, and evaluate value of $r_{\boldsymbol{k},\alpha}(1)$ by naive summation of the obtained series. In Fig. 1 we show the eighth and ninth order results of $r_{\boldsymbol{k},\alpha}(\lambda)$ at Γ and M points as a function of λ, and find a good convergence. In particular, for M point, the renormalization factor represented by the solid line amounts to 0.26 at $\lambda \to 1$, which demonstrates that large negative renormalization occurs in the kagome system.

Experimental results for $Cs_2Cu_3SnF_{12}$ show that the two high-energy modes are almost degenerate at the Γ point, and their energies are about 10 meV [2,3]. By fixing $J = 20.7$meV, which has been determined from magnetic susceptibility measurements [2], and searching the value of $D^{\parallel}$ so that the calculated energy of the high-energy modes at Γ point is 10 meV, we obtain $D^{\parallel}/J = 0.12$.

Figure 2 shows a comparison of the magnon dispersions between the IEP and the LSW. The path on the wave-vector plane, which connects Γ and M points, is chosen in the same way as in the experiment [3]. The black and blue lines are, respectively, the ninth-order IEP and LSW results, where $D^{\parallel}/J = 0.12$. On the other hand, the red lines are the results of the LSW with renormalized parameters where $D^{\parallel}/J = 0.18$ and the energy scale is modified by a factor 0.62 [2]. Figure 2 tells us that the dispersion relations calculated by the LSW undergo not only renormalization of the interaction parameters but also flattening of the high-energy part and the appearance of roton-like minimum around M point due to spin-wave interactions. As for the triangular lattice system, we had modification of high-energy part but no renormalization of interaction parameters [5].

In summary, we have used the IEP to investigate how spin-wave interactions modify the LSW predictions of magnon dispersions. We have successfully calculated the renormalization factor $r_{\boldsymbol{k},\alpha}(\lambda)$ by the IEP. As a result, in the kagome lattice system, in addition to the renormalization of the interaction parameter pointed out by Ono *et al.* [2], we have found that the high-energy part around M point undergoes strong deformation. In the near future, we plan to incorporate more realistic DM interactions to reproduce the detailed structure of experimental magnon spectrum data.

[1] S. Ito *et al.*, Nat. commn. 8, 235, 2017.
[2] T. Ono *et al.*, JPSJ 83, 043701, 2014.
[3] M. Saito *et al.*, PRB 105, 064424, 2022.
[4] C. Zhang *et al.*, PRB 102, 075108, 2020.
[5] W. Zheng *et al.*, PRB 74, 224420, 2006.

Numerical study of the effect of large bond randomness on the magnetization process and magnetic susceptibility in the spherical Kagome system $\{W_{72}V_{30}\}$

Yoshiyuki Fukumoto
Department of Physics, Faculty of Science and Technology, Tokyo University of Science
2641 Yamazaki, Noda, Chiba 278-8510

The spherical kagome system $\{W_{72}V_{30}\}$ is a frustrated cluster magnet consisting of thirty V^{4+} with $S = 1/2$ [1]. The exchange interaction has been estimated as $J = 115$K. In the experimental study of the low-temperature magnetization process, a step structure unique to cluster magnets has not been found [2]. To understand this result, the effects of bond randomness [2] and Dzyaloshinskii-Moriya (DM) interactions [3] were examined.

Subsequently, specific heat measurements were performed by Kihara *et al.* at temperatures $T < 11$K and magnetic fields up to 15T [4]. Although the magnitude of the specific heat is comparable to that expected in the Heisenberg model, the shape of the specific heat curve is completely different. In particular, in the Heisenberg-model calculation, a peak appeared near 2K, and it was found that even a magnetic field up to 15T affected the shape of the specific heat curve. However, in the experiment, the specific heat curve had no peak and was not affected by the magnetic field up to 15T. To resolve this problem, the specific heat calculation was performed considering bond randomness or DM interaction. Each strength is assumed to be about $0.1J$. However, it did not lead to an explanation of the experimental results.

In a previous study investigating the effect of bond randomness in a triangular lattice system [5], it was reported that when the randomness is large compared to the energy scale of the magnetic field, the magnetic field dependence of the specific heat disappears. Therefore, we decided to investigate the effect of strong bond randomness also in the spherical kagome system. As a result, it was clarified that the experimental results can be explained by assuming that the strength of the bond randomness is 40-50% of the exchange interaction. The results were published as a paper [6].

It is also interesting to study if the model Hamiltonian with the large bond randomness and a modest DM interaction reproduces experimental magnetic susceptibility. Magnetic susceptibility calculation in the presence of the both terms is a challenging problem in terms of computational complexity. If we have DM interactions, we need to work with vectors of dimension 2^{30}. In addition, when DM interaction exists, the magnetic susceptibility is obtained by applying a small magnetic field and calculating the expected value of magnetization by the cTPQ method. Then, it is necessary to average the direction of the magnetic field, the bond randomness, and the random vector of the cTPQ method. We will continue our research on efficient implementation of these averaging operations.

[1] A. M. Todae *et al.*, ChemComm, 3351 (2009).
[2] J. Schnack *et al.*, arXiv:1304.2603v1.
[2] Y. Fukumoto *et al.*, JPSJ 87, 124710 (2018).
[4] T. Kihara *et al.*, PRB 99, 064430 (2019).
[5] K. Watanabe *et al.*, JPSJ 83, 034714 (2014).
[6] M. Motohashi *et al.*, PTEP, 113I01 (2022).

Nematic Tomonaga-Luttinger Liquid Phase in an $S=1/2$ Ferromagnetic-Antiferromagnetic Bond-Alternating Chain with Next-Nearest-Neighbor Interactions

Takashi Tonegawa

Kobe University, University of Hyogo, and Osaka Metropolitan University

Recently, using mainly numerical methods, we [1] have investigated the ground-state phase diagram of an anisotropic $S=1/2$ two-leg ladder with different leg interactions. The xy and z components of the leg interactions between nearest-neighbor spins in the a (b) leg are denoted, respectively, by $J_{\mathrm{l},a}$ and $\Delta_{\mathrm{l}}J_{\mathrm{l},a}$ ($J_{\mathrm{l},b}$ and $\Delta_{\mathrm{l}}J_{\mathrm{l},b}$). On the other hand, the xy and z components of the uniform rung interactions are, respectively, denoted by $\Gamma_{\mathrm{r}}J_{\mathrm{r}}$ and J_{r}. In the above, Δ_{l} and Γ_{r} are the XXZ-type anisotropy parameters for the leg and rung interactions, respectively. This system has a frustration when $J_{\mathrm{l},a}J_{\mathrm{l},b}<0$ irrespective of the sign of J_{r}.

We [1] have numerically determined the phase diagram on the Δ_{l} ($0.0\le|\Delta_{\mathrm{l}}|\le1.0$) versus $J_{\mathrm{l},b}$ ($-2.0\le J_{\mathrm{l},b}\le3.0$) plane in the case where $J_{\mathrm{l},a}=0.2$, $J_{\mathrm{r}}=-1.0$, and $\Gamma_{\mathrm{r}}=0.5$. It is noted that the rung interaction is ferromagnetic and its anisotropy is of the Ising-type. Furthermore, the a leg interaction is antiferromagnetic, while the b leg interaction are either ferromagnetic or antiferromagnetic, the anisotropies of both leg interactions being of the XY-type. We have employed the physical consideration, and the level spectroscopy and phenomenological renormalization-group analyses of the numerical date obtained by the exact diagonalization method. Interestingly enough, we have found that two kinds of nematic Tomonaga-Luttinger Liquid (nTLL) phases appear; one of which appears in the unfrustrated and the other in the frustrated one. The nTLL state is characterized not only by the formation of two-magnon bound pairs but also by the dominant nematic four-spin correlation function. It should be emphasized that the asymptotic form of this correlation function in the unfrustrated region and that in the frustrated region show the power-law decay with the uniform character and the power-law decay with the staggered character, respectively. Thus, both nTLL phases are different phases, and the latter nTLL phase may be called the staggered nTLL phase.

According to the above result, it is reasonably expected that the nTLL state appears as the zero-field ground state in general $S=1/2$ unfrustrated one-dimensional systems in which pairs of $S=1/2$ spins coupled strongly with the Ising-type ferromagnetic interaction are connected by the weak XY-type antiferromagnetic interactions. Some examples of such systems are (A) the $S=1/2$ ferromagnetic-antiferromagnetic bond-alternating chain, (B) the $S=1/2$ two-leg ladder with ferromagnetic rung and antiferromagnetic leg interactions, (C) the $S=1/2$ Kondo necklace chain with ferromagnetic rung and antiferromagnetic leg interactions, and so on.

The purpose of this report is to discuss the system (A) with next-nearest-neighbor interactions, which is described by the Hamiltonian

$$\mathcal{H}=-J_{\mathrm{F}}\sum_{j=1}^{N/2}[\vec{S}_{2j-1},\vec{S}_{2j}]+J_{\mathrm{AF}}\sum_{j=1}^{N/2}[\vec{S}_{2j},\vec{S}_{2j+1}]+J_2\sum_{j=1}^{N}[\vec{S}_j,\vec{S}_{j+2}]$$

with

$$[\vec{S}_{2j-1},\vec{S}_{2j}]=\Gamma_{\mathrm{F}}\left(S^x_{2j-1}S^x_{2j}+S^y_{2j-1}S^y_{2j}\right)+S^z_{2j-1}S^z_{2j}\,,$$

$$[\vec{S}_{2j},\vec{S}_{2j+1}]=S^x_{2j}S^x_{2j+1}+S^y_{2j}S^y_{2j+1}+\Delta_{\mathrm{AF}}S^z_{2j}S^z_{2j+1}\,,$$

$$[\vec{S}_j,\vec{S}_{j+2}]=S^x_jS^x_{j+2}+S^y_jS^y_{j+2}+\Delta_{\mathrm{AF}}S^z_jS^z_{j+2}\,,$$

where $J_{\mathrm{F}}\gg J_{\mathrm{AF}}>0.0$, $1.0\ge\Gamma_{\mathrm{F}}\ge0.0$, $1.0\ge|\Delta_{\mathrm{AF}}|\ge0.0$, and N, being assumed to be a multiple of four, is the number of spins in the system. We note that the nearest-neighbor ferromagnetic interactions are stronger than the nearest-neighbor antiferromagnetic ones, and the anisotropies of the former and latter interactions are of the Ising-type and the XY-type, respectively. Furthermore, the anisptropies of the nearest-neighbor antiferromagnetic interactions and next-nearest-neighbor ones have the same form.

Using a variety of numerical methods based on the exact diagonalization calculation, we have determined the ground-state phase diagram on the J_2 versus Δ_{AF} plane in the case where $J_{\mathrm{F}}=-1.0$,

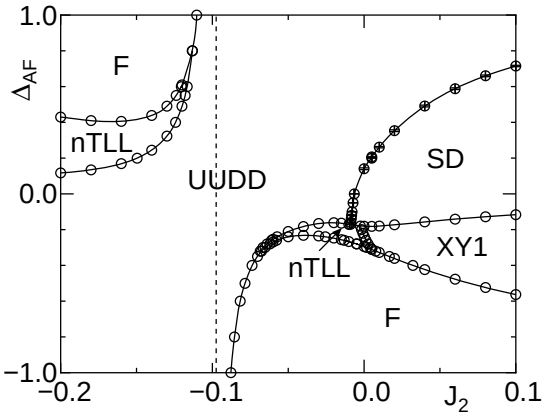

Figure 1: Ground-state phase diagram for $J_{\rm F}=-1.0$, $J_{\rm AF}=0.195$, and $\Gamma_{\rm F}=0.8$.

$J_{\rm AF}=0.195$, and $\Gamma_{\rm F}=0.8$. The obtained phase diagram, where the solid lines show the phase boundary lines, is depicted in Fig. 1. This phase diagram consists of the ferromagnetic (F), $XY1$, singlet-dimer (SD), and up-up-down-down (UUDD) phases as well as the nematic Tomonaga-Luttinger liquid (nTLL) phase. It should be emphasized that the one of the nTLL phases which appears in the frustrated region ($J_2<-1.0$) is the the staggered nTLL phase discussed above.

Finally, we discuss how to obtain the phase boundary lines in these phase diagrams. We denote, respectively, by $E_0^{\rm P}(N,M)$ and $E_1^{\rm P}(N,M)$, the lowest and second-lowest energy eigenvalues of the Hamiltonian $\mathcal{H}$ under the periodic boundary condition within the subspace of N and M, where $M(=0,\pm1,\cdots,\pm N/2)$ is the total magnetization. Furthermore, we denote by $E_0^{\rm T}(N,M,P)$ the lowest eigenvalue of $\mathcal{H}$ under the twisted boundary condition within the subspace of N, M, and P, where $P(=\pm1)$ is the eigenvalue of the space inversion operator with respect to the twisted bond. We have numerically calculated these energies for finite-size systems with up to $N=28$ spins by means of the exact-diagonalization method. The ground-state energy of the finite-N system is given by $E_0^{\rm P}(N,N/2)$ in the F region and by $E_0^{\rm P}(N,0)$ in the other regions. In the following way, we have estimated the finite-size critical values of the interaction parameters for each phase transition. Then, the phase boundary line for the transition has been obtained by connecting the results for the $N\to\infty$ extrapolation of the finite-size critical values.

First, the phase transitions between the $XY1$ and SD phases and between the nTLL and UUDD phases are the Berezinskii-Kosterlitz-Thouless transition [2]. In these transitions, the level spectroscopy method developed by Nomura and Kitazawa [3] is very powerful for calculating the finite-size critical values, which are estimated from $E_0^{\rm P}(N,0)=E_0^{\rm T}(N,M,-1)$. Secondly, the phase transition between the SD and UUDD phases is the 2D Ising-type transition. It is well known that the phase transition line is determined by the phenomenological renormalization-group (PRG) method [4]. Then, to estimate the finite-size critical values, we solve the PRG equation, $N\,\Delta_{00}(N)=(N+4)\,\Delta_{00}(N+4)$, where $\Delta_{00}(N)=E_1^{\rm P}(N,0)-E_0^{\rm P}(N,0)$. Thirdly, the nTLL state accompanies two-magnon bound-states, while the $XY1$ state does not. Then, in the ground-state magnetization curve for the finite-size system, the magnetization increases from $M=0$ to $M=2$ in the former state and from $M=0$ to $M=1$ in the latter state. Thus, the finite-size critical values are estimated from $\Delta_{10}(N)=\Delta_{20}(N)/2$, where $\Delta_{M0}(N)=E_0^{\rm P}(N,M)-E_0^{\rm P}(N,0)$. Lastly, it is apparent that the finite-size critical values for the phase transitions between the F phase and one of the nTLL, $XY1$, and UUDD phases are estimated from $E_0^{\rm P}(N,N/2)=E_0^{\rm P}(N,0)$.

In conclusion, we remark that the phase diagram shown in Fig. 1 is nearly point-symmetric around the point $(J_2,\,\Delta_{\rm AF})=(-J_{\rm AF}/2.0=-0.0975,\,0.0)$ (see the dotted line) and the F and nTLL phases appear in two places. This characteristic feature of the phase diagram can be well explained by the perturbation calculation from the strong ferromagnetic coupling limit [5]. The key point is the fact that the anisptropies of the nearest-neighbor antiferromagnetic interactions and next-nearest-neighbor ones have the same form.

The present work has been done in collaboration with Kiyomi Okamoto, Kiyohide Nomura, and Tôru Sakai.

[1] T. Tonegawa, T. Hikihara, K. Okamoto, S. C. Furuya, and T. Sakai, J. Phys. Soc. Jpn. **87**, 104002 (2018).
[2] Z. L. Berezinskii, Sov. Phys. JETP **34**, 610 (1971); J. M. Kosterlitz and D. J. Thouless, J. Phys. C **6**, 1181 (1973).
[3] K. Nomura and A. Kitazawa, J. Phys. A **31**, 7341 (1998).
[4] M. P. Nightingale, Physica A **83**, 561 (1976).
[5] K. Okamoto, T. Tonegawa, K. Nomura, and T. Sakai, Presentation at the Autumn Meeting of the Physical Society of Japan, September 12∼15, 2022.

Phase separation dynamics in hydrodynamic models

Kyosuke ADACHI

Nonequilibrium Physics of Living Matter RIKEN Hakubi Research Team, RIKEN Center for Biosystems Dynamics Research (BDR), 2-2-3 Minatojima-minamimachi, Chuo-ku, Kobe 650-0047, Japan

RIKEN Interdisciplinary Theoretical and Mathematical Sciences Program (iTHEMS), 2-1 Hirosawa, Wako 351-0198, Japan

Liquid-liquid phase separation (LLPS), which is widely recognized in condensed matter and soft matter physics, has gained renewed attention in cell biology. Several kinds of protein condensates have been found in a cell, and LLPS is discussed as a possible mechanism of the formation and dynamics of condensates [1]. To understand how the amino acid sequence of proteins and intracellular nonequilibrium environments can affect the phase separation dynamics, numerical simulations of polymer models and hydrodynamic models should be useful.

This year, as a preliminary study, we performed several numerical simulations of hydrodynamic models, which are PDE models of the particle density field. We first tested the Model B dynamics [2] by the Euler-Maruyama method with discretization of time and space. Using parallel computing to collect many samples with different initial conditions and noise realizations, we confirmed the Lifshitz-Slyozov-Wagner (LSW) scaling for the growth of the cluster size. Then, as a simple extension to nonequilibrium conditions that can be relevant to intracellular situations, we considered a model that breaks the fluctuation-dissipation relation. This model is similar to Active Model B+ [3], which have been originally proposed as a model of active matter. Performing numerical simulations with small additional terms to improve numerical stability, we found that the cluster growth is slower than that in Model B, suggesting the suppression of the phase separation dynamics due to the nonequilibrium conditions.

References

[1] S. F. Banani *et al*., Nat. Rev. Mol. Cell Biol. **18**, 285 (2017).

[2] P. C. Hohenberg and B. I. Halperin, Rev. Mod. Phys. **49**, 435 (1977).

[3] C. Nardini *et al*., Phys. Rev. X **7**, 021007 (2017).

Solution of the Eliashberg equation with the electron-electron Coulomb interaction

Ryosuke AKASHI
National Institutes for Quantum Science and Technology

The Eliashberg theory[1] with the Migdal approximation [2] is the state-of-the-art framework for the first-principles calculations of phonon-mediated superconductors. In principle, the competition between the phonon-mediated pairing attraction and screened Coulomb repulsion is accurately treated there for weakly correlated metals, which is crucial for reliable estimation of the superconducting transition temperature $T_{\rm c}$. However, the latter part has been mostly treated as a single empirical parameter μ^*[3], with which one cannot apply the theory to undiscovered systems where the $T_{\rm c}$ measurement does not exist. It is only recent that the effect of the screened Coulomb interaction on the pairing has been explored non-empirically.

The author has recently studied the effect of frequency dependent screened Coulomb interaction within the random -phase approximation. He has revealed the cooperative mechanism of the plasmonic and phononic pairing attractions from first principles, by analysing the non-diagonal (pairing) part of the self energy [4, 5]. On the other hand, a part of diagonal self energy due to the plasmons were shown to have negative effect, partially cancelling the former pairing [6]. However, the full treatment of all the components of the screened Coulomb-induced frequency dependent self energy was missing. In this project, we calculated the Eliashberg equations with all the screened Coulomb self energy parts included for uniform electron gas [7].

The Eliashberg equations with the Migdal approximation are written as follows:

$$Z_i(i\omega_j) = 1 - T\sum_{i'j'} \frac{\omega_{j'}}{\omega_j} \frac{Z_{i'}(\omega_{j'})}{\Theta_{j'}(i\omega_{j'})} W_{ii'}(\omega_j - \omega_{j'}), \quad (1)$$

$$\chi_i(i\omega_j) = T\sum_{i'j'} \frac{\xi_{i'} + \chi_{i'}(\omega_{j'})}{\Theta_{j'}(i\omega_{j'})} W_{ii'}(\omega_j - \omega_{j'}), \quad (2)$$

$$\phi_i(i\omega_j) = -T\sum_{i'j'} \frac{\phi_{i'}(\omega_{j'})}{\Theta_{j'}(i\omega_{j'})} W_{ii'}(\omega_j - \omega_{j'}), \quad (3)$$

$$\Theta_i(i\omega_j) = [\omega_j Z_i(i\omega_j)]^2 + [\xi_i + \chi_i(i\omega_j)]^2 + [\phi_i(i\omega_j)]^2 . \quad (4)$$

Indices i (i') and j (j') denote the basis state and Matsubara frequency, respectively. ξ_i is the energy eigenvalue of the state i measured from the chemical potential. $W_{ii'}(\nu_j)$ is the matrix element of the interaction between the Cooper pair states labeled by i and $i*$ with the Bosonic Matsubara frequency ν_j.

For homogeneous electron gas the basis i corresponds to the plane-wave state. We have implemented a code package that solves the above equations with an approximate manner. The interaction $W_{ii'}(\nu_j)$ was set to the screened Coulomb interaction $W_{\rm el}$ within the random phase approximation plus the attraction mediated by the Einstein phonon with definite frequency and electron-phonon coupling $W_{\rm ph}$. The diagonal terms Z and χ were evaluated at $T = 0$ noniteratively with initial value $Z = 1$ and $\chi = 0$ and without $W_{\rm ph}$, which corresponds to the G_0W_0 approximation. The equation for the nondiagonal term ϕ was later linearized with $W_{\rm ph}$ and its largest eigenvalue, which becomes unity at the transition temperature, was calculated. The iterative method

was used, which required only no more than a few hours in a serial run at *system B* at $T \sim 100K$.

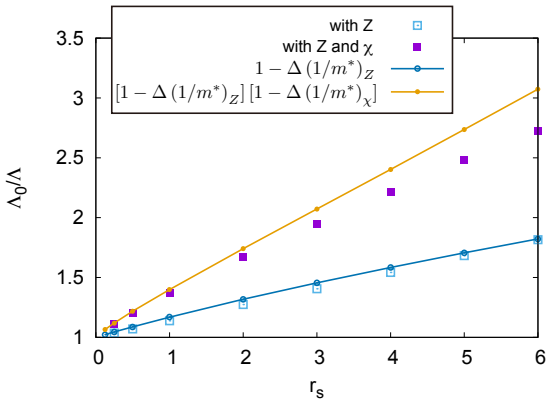

Figure 1: Ratio of the largest eigenvalues of the linearized Eliashberg equation with and without the self-energy corrections. Lines indicate approximate formulas. Taken from Ref. [7]

We show the results of the corrections to the pairing strength in Fig. 1. The blue open (purple closed) squares denote the inverse ratio of the largest eigenvalues with Z (Z and χ) to the non-interacting value. The values larger than unity indicate suppression of the pairing by the Coulomb self energy. The χ term has been known to cancel the effect of Z for the effective mass. In contrast, our result shows that χ cooperate with Z for the pairing suppression. This result highlight the importance of χ for superconducting calculations, which is computationally demanding and has mostly been ignored in the previous studies.

We also analyzed the band structure of a compound HgCr2Se4 [8]. The calculations were performed using Quantum Espresso [9] with norm conserving pseudopotentials from *Pseudo dojo* [10]. Self consistent calculations using the HSE06 exchange-correlation functional [11] and spin-orbit coupling required half a day per run with 2 nodes in *fat* group in *Ohtaka*. For the memory requirement the jobs could not run in *cpu* queue group. The band structure was interpolated using Wannier90 [12].

References

[1] G. M. Eliashberg, Zh. Eksp. Teor. Fiz. **38**, (1960) 966.

[2] A. B. Migdal, Zh. Eksp. Teor. Fiz. **34**, (1958) 1438.

[3] P. Morel and P. W. Anderson, Phys. Rev. **125**, (1962) 1263.

[4] Y. Takada, J. Phys. Soc. Jpn. **45** (1978) 786.

[5] R. Akashi and R. Arita, Phys. Rev. Lett. **111** (2013) 057006.

[6] A. Davydov, A. Sanna, C. Pellegrini, J. K. Dewhurst, S. Sharma, and E. K. U. Gross, Phys. Rev. B **102**, (2020) 214508.

[7] R. Akashi, Phys. Rev. B **105** (2022) 104510.

[8] H. Tanaka *et al.*, Phys. Rev. Lett. accepted.

[9] P. Giannozzi *et al.*, J. Phys. Condens. Matter **29**, (2017) 465901.

[10] G. Pizzi *et al.*, J. Phys. Condens. Matter **32**, (2020) 165902.

[11] J. Heyd, G. E. Scuseria, and M. Ernzerhof, J. Chem. Phys. 436 124, (2006) 219906.

[12] N. Marzari and D. Vanderbilt, Phys. Rev. B **56** (1997) 12847.

Gapless symmetry-protected topological phase of quantum antiferromagnets on anisotropic triangular strip

Yuichiro HIDAKA[1], Shunsuke C. FURUYA[2], Atsushi UEDA[1], and Yasuhiro TADA[3]
[1]*Institute for Solid State Physics, University of Tokyo*
Kashiwa-no-ha, Kashiwa, Chiba 277-8581
[2]*Department of Basic Science, University of Tokyo*
Meguro, Tokyo 153-8902
[3]*Quantum Matter Program, Graduate School of Advanced Science and Engineering, Hiroshima University, Higashihiroshima, Hiroshima 739-8530*

Classifying phases of matter is one of the paramount issues in condensed matter physics. One of the important classes of the quantum phase of matter is a symmetry-protected topological (SPT) phase. An SPT phase is a gapped phase that preserves some given symmetries but is not adiabatically connected to a trivial phase without breaking the symmetries [1]. Recently many researchers attempt to extend the concept of the SPT phase into gapless systems [2, 3].

One of the gapless SPT phases we study is the anisotropic triangular strip (ATS) model, which is the three-leg XXZ spin ladder with the frustrated XXZ rung interaction. The lattice is shown in Fig.1. According to the field-theoretic analysis, if the rung coupling is sufficiently small, the ground state of the ATS model is the gapless SPT state, in that the ground state has simultaneously the properties of the Haldane state and the Tomonaga-Luttinger liquid. This property is also supported by the numerical calculation [4].

In the present study, we investigate the ground state of the ATS model, where we expand the region of the parameters. We used the ITensor and TeNPy libraries [5, 6]. We found that the entanglement spectrum of the ATS model is doubly degenerate, which is the important feature of the Haldane state if the rung coupling $J_\times$ is sufficiently small (Fig.2). Moreover, from the calculation of the entanglement entropy, we found that the ground state has the central charge $c = 1$. On the other hand, if the rung coupling $J_\times$ is sufficiently larger than the ladder coupling J, the ground state becomes the ferrimagnetic state. This is checked by the calculation of magnetization. Finally, if the rung coupling $J_\times$ is of the same order as the ladder coupling, the ground state is in the trivial phase, in which we cannot see the even-fold degeneracy of the entanglement spectrum, and is in a gapless phase. The phase diagram of the ATS model is determined as shown in Fig.3 [7].

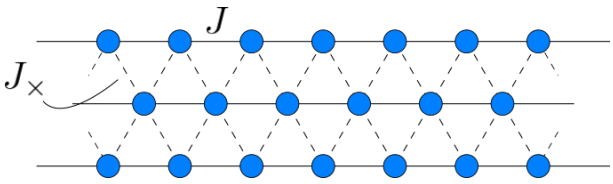

Figure 1: The anisotropic triangular strip (ATS) XXZ model. J denotes the ladder coupling and $J_\times$ denotes the frustrated rung coupling. All coupling is the XXZ interaction: $S_i^x S_j^x + S_i^y S_j^y + \Delta S_i^z S_j^z$.

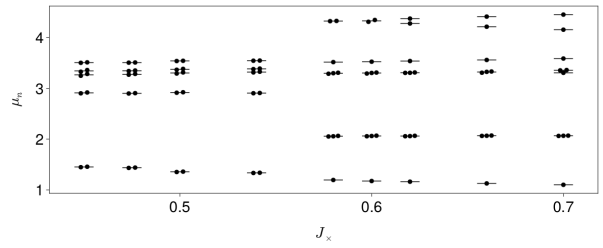

Figure 2: The entanglement spectrum of the ATS model with $\Delta = 0.8$. When $J_\times < 0.54$ we can see the even-fold degeneracy of the entanglement spectrum, which implies the Haldane state.

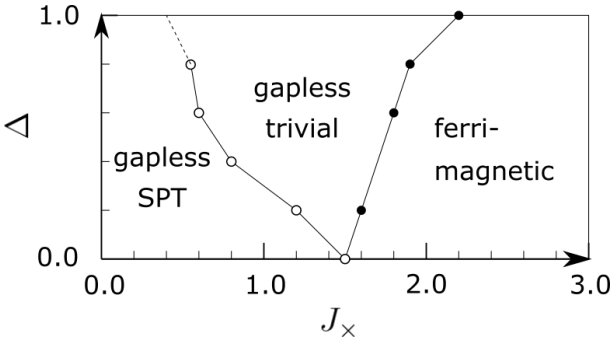

Figure 3: The phase diagram of the ATS model.

References

[1] X. Chen, Z.-C. Gu, and X.-G. Wen, Phys. Rev. B 83, 035107 (2011).

[2] T. Scaffidi, D. E. Parker, and R. Vasseur, Phys. Rev. X 7, 041048 (2017).

[3] S. C. Furuya and M. Oshikawa, Phys. Rev. Lett. 118, 021601(2017).

[4] Y. Hidaka, S. C. Furuya, A. Ueda, and Y. Tada, Phys. Rev. B 106, 144436(2022).

[5] M. Fishman, S. R. White, and E. M. Stoudenmire, arXiv:2007.14 (2020).

[6] J. Hauschild and F. Pollmann, SciPost Phys. Lect. Notes , 5 (2018).

[7] Y. Hidaka, S. C. Furuya, A. Ueda, and Y. Tada, in preparation.

Finite temperature calculations of frustrated quantum spin systems

Katsuhiro MORITA
Department of Physics and Astronomy, Faculty of Science and Technology, Tokyo University of Science, Noda, Chiba 278-8510

The $S = 1/2$ kagome antiferromagnets are known to have exotic properties even at finite temperatures. The specific heat has a multiple-peak structure [1], and the 1/3 magnetization plateau is expected to melt asymmetrically at finite temperatures [2, 3]. These properties do not appear in the triangular lattice model, for example. Therefore, these properties are considered to be unique to the kagome lattice model.

In this study, we have calculated the magnetic specific heat, entropy, magnetic susceptibility, and finite temperature magnetization curves for the $S = 1/2$ $J_1 - J_2$ kagome lattice Heisenberg model using the orthogonalized finite temperature Lanczos method [4, 5] on Supercomputer System B at the ISSP. J_1 represents the nearest-neighbor interaction and J_2 represents the next nearest-neighbor interaction. Here we set $J_1 = 1$ as the energy unit. In this study, the calculations were performed with a 36-site kagome cluster.

We have found that the entropy remains at low for $-0.06 < J_2 < 0.02$, and outside this range, the entropy decreases rapidly. At $J_2 \simeq 0$, the magnetic specific heat has a triple-peak structure, but as $|J_2|$ increases, the specific heat tends to have a double-peak structure. In the finite temperature magnetization curves, there is asymmetric melting of the 1/3 magnetization plateau around $J_2 = 0$, but the 1/3 plateau becomes clearly visible as $|J_2|$ increases. This is because the $\mathbf{q} = \mathbf{0}$, up-up-down state stabilizes for $J_2 > 0$, the $\sqrt{3} \times \sqrt{3}$ up-up-down state stabilizes for $J_2 < 0$, and the plateau becomes unstable around the boundary.

These results will be compared with experimental results in the future to clarify the magnetic properties of the compounds.

References

[1] T. Shimokawa and H. Kawamura, J. Phys. Soc. Jpn. **85**, 113702 (2016).

[2] J. Schnack, J. Schulenburg, and J. Richter: Phys. Rev. B **98**, 094423 (2018).

[3] T. Misawa, Y. Motoyama, and Y. Yamaji: Phys. Rev. B **102**, 094419 (2020).

[4] K. Morita and T. Tohyama: Phys. Rev. Research **2**, 013205 (2020).

[5] K. Morita: Phys. Rev. B **105**, 064428 (2022).

Machine learning molecular dynamics studies of complex structural materials

Masahiko OKUMURA[1], Hayato SHIBA[2], Masatoshi HANAI[3], Yasunobu ANDO[4], Akiko YAMAGUCHI[1], Keita KOBAYASHI[1], and Hiroki NAKAMURA[1]

[1]*Center for Computational Science and e-Systems, Japan Atomic Energy Agency, Wakashiba, Kashiwa, Chiba 277-0871*

[2]*Information Technology Center, University of Tokyo, Chiba 277-0882*

[3]*Graduate School of Information Science and Technology, University of Tokyo, Tokyo 133-8658*

[4]*Research Center for Computational Design of Advanced Functional Materials, National Institute of Advanced Industrial Science and Technology, Tsukuba, Ibaraki 305-8568*

Machine learning molecular dynamics (MLMD) is a promising simulation method with high accuracy and low computational costs [1]. Artificial neural networks (ANNs) are used to reproduce the results of first-principles calculations (FPCs). The ANNs are trained using datasets that consist of a lot of the results of FPCs. For this method, supercomputers are used for 1) making huge amounts of the FPC results, 2) training the ANNs, and 3) conducting molecular dynamics (MD) simulations with the ANN potentials. Density functional calculations are popular for making the training data. Several methods are used to train the ANNs, e.g., stochastic gradient descent, adaptive momentum estimation, extended Kalman filter (EKF), etc. The EKF method is known as one of the best optimizers for the ANN potential. However, the calculation speed for an epoch is slower than the other methods. To overcome this weak point, the multi-stream EKF method is often used with parallel computers [2]. The MD simulations with the ANN potentials for large systems are usually conducted on a supercomputer.

Preparing the training dataset and training the ANNs are the time-consuming steps of MLMD. Notably, the ANNs for complex materials require a large dataset, because many atom configurations are realized, where the complex materials are, in this report, defined as those with large unit cells with periodic boundary conditions. For making a dataset of complex materials, a large number of FPCs with many atom configurations in large unit cells are required. With the large dataset, heavy ANN training is needed. Density functional calculations are popular to make the data, which are popular calculations on the ISSP

supercomputer. But the ANN training calculations may not be popular. Therefore, we evaluated the scaling of the ANN training on System B, and the results are compared with those given by Oakbridge-cx operated by the Information Technology Center, The University of Tokyo. We prepared 7,007 data of ThO_2, which shows superionic transition below its melting point [3]. Therefore, large unit cells are needed to reproduce the superionic transition and melt, i.e., ThO_2 can be considered a complex material although the structure of its solid state is simple. The dataset contains the configurations of solid, super-ionic, and liquid states of ThO_2. The n2p2 open-source software for MLMD [4] was used, which provides the multistream EKF method using MPI.

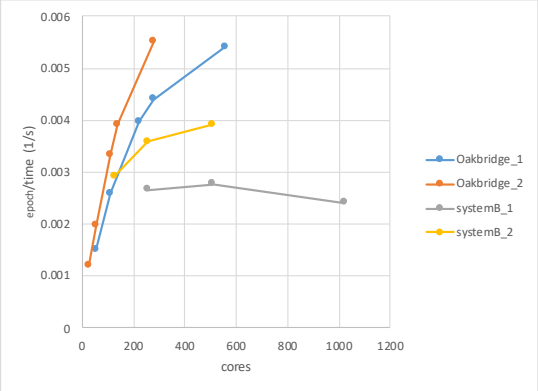

Fig. 1 The relation between the number of cores and the number of steps per second is shown. The blue and orange plots represent full- and half-core calculations on Oakbridge-cs, respectively. The gray and yellow pots represent full- and half-core calculations on Oakbridge-cs, respectively.

Figure 1 shows the relation between the number of cores and epoch/time (1/s) for System B and Oakbridge-cs. The blue and orange plots show the results of Oakbridge-cx, where the former and the latter are the results of calculations using all and half of the cores on a CPU, respectively. We found that the reduction of the active cores improves the performance. This may be because the relative memory size was increased by the reduction of the active cores. The gray and yellow plots represent the results of System B, where the former and the latter are the results of calculations using all and half of the cores on a CPU, respectively. For System B, the same tendency was obtained, i.e., the reduction of the active cores accelerates the learning speed.

We investigated the relation between the number of cores and the number of epochs per second. We found that the reduction of active cores improves the calculation speed both for System B and Oakbridge-cx.

References

[1] J. Behler and M. Parrinello, Phys. Rev. Lett. **98**, 146401 (2007).

[2] A. Singraber *et al.*, J. Chem. Theo. Comp. **15**, 3075 (2019).

[3] K. Kobayashi *et al.*, Sci. Rep. **12**, 9808 (2022).

[4] A. Singraber *et al.*, J. Chem. Theo. Comp. **15**, 1827 (2019).

Multi-impurity method for bond-weighted tensor renormalization group

Satoshi MORITA
Graduate School of Science and Technology, Keio University
Kohoku-ku, Yokohama, Kanagawa 223-8522

Tensor network (TN) methods are attracting much attention as powerful tools for computing strongly correlated many-body problems. The partition function of classical statistical systems can be represented by the TN form. However, the contraction of a large TN still requires an exponentially large computational effort. The concept of the real-space renormalization group resolves this problem. The tensor renormalization group (TRG) method and its variants calculate a coarse-grained tensor by information compression using the singular value decomposition [1, 2]. These methods can calculate the partition function approximately in logarithmic time for the system size. Recently, Adachi, et al. have proposed the bond-weighted TRG (BWTRG) method, which improves the accuracy of TRG by introducing a bond weight and distributing it appropriately [3].

In this study, we propose an algorithm to calculate higher-order moments of physical quantities based on BWTRG. We introduce a bond-weight impurity which represents a physical quantity. With the appropriate update rules, coarse-grained bond-weights containing multiple impurities can be generated to calculate the higher-order moments of the physical quantity. Our proposed method is compared with conventional methods on the two-dimensional classical spin model. The proposed method achieves higher accuracy at lower computational cost than the higher-order TRG algorithm [4]. We also show that the finite-size scaling analysis of the squared magnetization provides critical exponents and distinguishes the weakly first-order and continuous phase transitions.

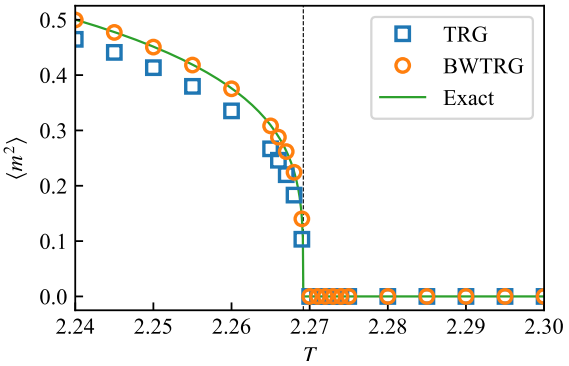

Figure 1: The squared magnetization of the Ising model on the square lattice calculated by TRG and BWTRG with the bond dimension $\chi = 128$ and the system size $L = 2^{25}$. The green solid curve shows the exact solution in the thermodynamic limit.

References

[1] M. Levin and C. P. Nave, Phys. Rev. Lett. **99**, 120601 (2007).

[2] Z. Y. Xie, J. Chen, M. P. Qin, J. W. Zhu, L. P. Yang, and T. Xiang, Phys. Rev. B **86**, 1 (2012).

[3] D. Adachi, T. Okubo, and S. Todo, Phys. Rev. B **105**, L060402 (2022).

[4] S. Morita and N. Kawashima, Comput. Phys. Commun. **236**, 65 (2019).

Majorana Kramers Qubits and Yang-Lee Anyons in Topological Superconductors

Takeshi MIZUSHIMA
Department of Materials Engineering Science, Osaka University
Toyonaka, Osaka 560-8531

We have investigated non-Abelian statistics of Majorana Kramers pairs (MKPs) in time-reversal invariant topological superconductors (TRITSCs) [1]. Numerically solving the time-dependent Bogoliubov-de Gennes equation, we have simulated the braiding dynamics of MKPs in a network of one-dimensional TRITSCs. We have first considered the tolerance of MKPs against a perturbation with broken time-reversal symmetry such as a magnetic field and demonstrated the robustness of the non-Abelian braiding of MKPs when the initial and final states of a braiding process maintain the combined symmetry of time reversal and mirror reflection symmetries. The Majorana Kramers qubit is tolerant even when intermediate states break the combined symmetry. We have also discussed the effect of gate-induced inhomogeneous potentials at junctions between superconducting nanowires. Such a potential generally induces a non-Majorana nearly zero-energy Andreev bound state at the junctions. Our numerical simulation shows that the dynamics of MKPs accumulate significant errors when such non-Majorana states exist and interfere with MKPs. Although we concentrated on Majorana particles in a TRITSC in this work, it is expected that effects of non-Majorana states generated by inhomogeneous gate potentials on the non-Abelian braiding are ubiquitous for any topological superconductors with broken time-reversal symmetry.

We have also demonstrated that a Yang-Lee anyon system is constructed from collective Majorana bound states in a network of topological superconducting nanowires [2]. Yang-Lee anyons are nonunitary counterparts of Fibonacci anyons, obeying the same fusion rule. Because of nonunitarity, the central charge and the scaling dimension for the one nontrivial primary field are negative, $c = -22/5$ and $\Delta = -2/5$, respectively. The nonunitary conformal field theory with $c = -22/5$ describes the nonunitary critical phenomenon known as the Yang-Lee edge singularity. In Ref. [2], we consider a topological superconductor junction system coupled with dissipative electron baths as a non-hermitian platform for interacting Majorana quasiparticles. Numerically calculating the central charge and scaling dimension, we find the condition that the non-Hermitian Majorana system can simulate the Ising spin model of the Yang-Lee edge singularity and confirmed that, by controlling model parameters in a feasible way, the Yang-Lee edge criticality is realized. We also discuss the scheme for the measurement and the braiding of Yang-Lee anyons, aiming at the application to universal quantum computation.

References

[1] Y. Tanaka, T. Sanno, T. Mizushima, and S. Fujimoto: Phys. Rev. B **106**, 014522 (2022).

[2] T. Sanno, M. G. Yamada, T. Mizushima, and S. Fujimoto: Phys. Rev. B **106**, 174517 (2022).

Quantum Monte Carlo simulations of Spin Hall magnetoresistance in quasi-two-dimensional antiferromagnetic insulator/metal bilayer systems

Takeo Kato

Institute for Solid State Physics,

The University of Tokyo, Kashiwa-no-ha, Kashiwa, Chiba 277-8581

Spin Hall magnetoresistance (SMR) is a novel type of magnetoresistance caused by spin current. SMR was firstly observed in 2013 by Nakayama in a bilayer system composed of a metal and a magnetic insulator [1]. The phenomenological theory for SMR [2] is widely used for analysis of SMR, but it can't describe the temperature dependence of SMR in a bilayer system composed of a metal and an antiferromagnetic-insulator [3] .

In this study, we discuss the SMR dependence of temperature, thickness of AFI, and randomness of exchange interaction. To discuss about these features, we expand the microscopic theory of SMR based on Keldysh Greens function [4]. In this theory the spin current is expressed in terms of the spin susceptibility of the antiferromagnetic insulator, but analytical calculation based on spin-wave theory are available for only low temperature. Due to calculate widely temperature dependence of SMR by the quantum Monte Carlo method, we obtained the spin conductance formulation by Matsubara Greens function [5].

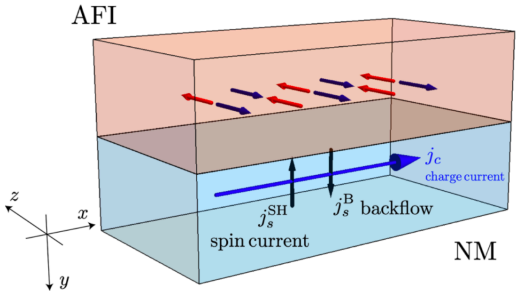

Fig. 1:Setup for SMR calculation cited from[5].

We used DSQSS for the quantum Monte Carlo method, and we adjustment some code to be able to calculate the local spin susceptibility. The accuracy for the calculation is proportional to the number of Monte Carlo steps, so We performed parallelization calculations with MPI, which is included in DSQSS, to achieve a high degree of accuracy.

We show the result of this calculations based on the paper [5]. The temperature and thickness dependence of SMR is shown in Fig. 2. The black points indicate the total SMR signal, whereas the red and blue plots are contribution from *z*-component and *xy*-components of spin susceptibility. Green arrows indicate the ordering temperature.

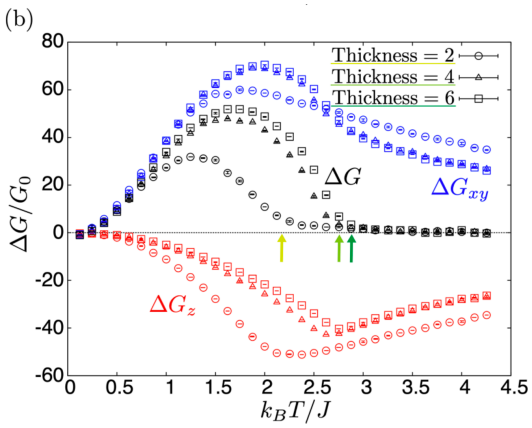

Fig. 2: S=1 result for SMR cited from [5].

It shows that at high temperature SMR signals vanish in consistent with the analytical calculation by the high temperature expansion. SMR has a peak less than the ordering temperature and the thickness dependence becomes weaker for four or more layers.

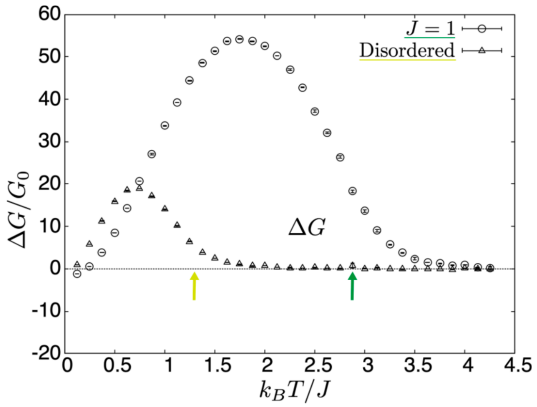

Fig. 3: Disordered case of result cited from [5].

The effect of randomness by disordered exchange interactions is shown in Fig. 3. It shows that the ordering temperature is suppressed and the SMR signal becomes small in the disordered case.

We calculated SMR in AFI by quantum Monte Carlo simulations, and we discussed about the SMR dependence of temperature, thickness of AFI, and randomness of exchange interaction.

References

[1] H. Nakayama, et al., Phys. Rev. Lett. **110**, 206601 (2013).

[2] Y. T. Chen, et al., Phys. Rev. B **87**, 144411 (2013).

[3] D. Hou, et al., Phys. Rev. Lett. **118**, 147202 (2017).

[4] T. Kato, Y. Ohnuma, and M. Matsuo, Phys. Rev. B **102**, 094437 (2020).

[5] T. Ishikawa, M. Matsuo, and T. Kato, Phys. Rev. B **107**, 054426 (2023).

Precise structural analysis of atomic arrangement of hydrogen-adsorbed ceria surfaces by using 2DMAT

Izumi MOCHIZUKI

Slow Positron Facility, Institute of Materials Structure Science, High Energy Accelerator Research Organization (KEK), Oho 1-1, Tsukuba, Ibaraki, 305-0801, Japan

We used 2DMAT [1-7], an open-source data-analysis software that is preinstalled on the ISSP supercomputers, developed by the PASUMS project at FY2020 and 2021 for data analyses of total-reflection high-energy positron diffraction (TRHEPD). TRHEPD is an innovative method for the precise determination of atomic arrangement of crystal surfaces due to its exceeding surface sensitivity. It is realized at Slow Positron Facility, IMSS, KEK [8].

We applied 2DMAT to the structural analysis of a Ge(001)-c(4×2) surface as a test of the analysis method by an optimization procedure, Nelder-Method method [5, 7].

We also investigated a hydrogen (H) adsorbed CeO_2(111)-(1×1) surface [9]. It was a challenge for the detection of surface hydrogen since it is quite difficult for other experimental measurements. In this study, we first calculated the structure of the bare CeO_2(111)-(1×1) surface and that of the H-adsorbed one by using Quantum ESPRESSO in the DFT+U method. The results were then compared with those obtained by the TRHEPD experiment. We found that the TRHEPD can detect the surface hydrogen properly with the data-driven analysis, as an innovative feature of TRHEPD. More detailed analysis is ongoing.

References

[1] https://www.pasums.issp.utokyo.ac.jp/2DMAT

[2] K. Tanaka, *et al*. (I. Mochizuki), Acta. Phys. Pol. A 137, 188 (2020).

[3] T. Hoshi, *et al*. (I. Mochizuki), Comp. Phys. Commun. 271, 108186 (2022).

[4] T. Hanada, *et al*., Comp. Phys. Commun. 277 108371 (2022).

[5] Y. Motoyama, *et al*. (I. Mochizuki), Comp. Phys. Commun. 280, 108465 (2022).

[6] K. Tanaka, *et al*. (I. Mochizuki), JJAP Conf. Series 9, 011301 (2023).

[7] N. Kinoshita, *et al*. (I. Mochizuki), in JPS meeting, 22-25, Mar. 2023.

[8] https://www2.kek.jp/imss/spf/eng/

[9] I. Mochizuki, in *Innovation catalysis science through the integration of high-performance data-driven science and advanced measurement technology*, online mini-symposium, Joint Usage/Research Center for Catalysis (JURCC), 30. Mar. 2023, https://sites.google.com/view/hpc-catal2023

Equilibration and glass transition in the dense hard sphere systems

Masaharu ISOBE
Nagoya Institute of Technology
Gokiso-cho, Showa-ku, Nagoya, 466-8555

As the simplest models, the hard disk/sphere systems have been investigated via molecular simulation in both equilibrium and non-equilibrium phenomena [1]. In this project, we focus on the equilibration and the non-equilibrium phase transition in the hard disk/sphere model system with modern algorithms, *i.e.*, Event-Chain Monte Carlo (ECMC) [2, 3], Newtonian ECMC (NEC) [4] and Event-Driven Molecular Dynamics(EDMD) [5].

Efficiency of Newtonian Event-Chain Monte Carlo in dense hard disk systems

In the statistical mechanics of many body systems, the physical properties at the true equilibrium state are crucial. To invent efficient method of equilibration in the molecular simulation is one of fascinating topics where the simple model systems such as hard-spheres and Ising spins have been investigated actively and made important contribution. In 2009, Event-Chain Monte Carlo (ECMC) [2] was invented in hard disk systems that updates the particle position with sequential collisions (i.e., event-chain) and has been applied to the many typical models studied in statistical physics [3]. ECMC has several variants depending on how the direction of movement of the particles after the collision is determined. Recently, Newtonian-ECMC (NEC) [4] was invented by applying the velocity collision rule to each collision event to dictate the direction of particle movement; this is often used in the Event-Driven Molecular Dynamics (EDMD) of hard-sphere systems. NEC outperformed not only other variants of ECMC but EDMD in the diffusion coefficient and melting process in hard sphere systems. However, the optimal performance strongly depends on the physical properties and chain length (or duration) of ECMC (and its variants). Previously, we found the high efficiency of NEC in diffusion coefficient of liquid state in hard disk systems for all chain lengths and various system sizes, which is caused by the spatially homogeneous sampling of the displacement (i.e., collision) [7]. To figure out the mechanism of equilibration of NEC in dense systems, we focus on the equilibrium state of dense hard disk systems above the fluid-to-solid transition point, which show the relaxation via hopping motion even in the packing fraction at the solid phase in hard disk systems for each methods. We also found profoundly efficient diffusion coefficient by NEC even when the relaxation becomes only successive hopping motion in highly dense systems.

Free volume estimator (NELF-A) in dense poly-disperse hard disk systems — local structure analysis on pressure and inherent structure

In many-particle systems, the free volume of a tagged particle constructed from excluded volume by surrounding particles made a crucial contribution to describing the macroscopic properties in the history of liquid state theory. Several numerical algorithms for calculating the free volume (FV) have been invented, such

as Monte Carlo (MC) sampling and Voronoi tessellation. However, MC is an approximate calculation, and the Voronoi tessellation requires high computational costs (especially for poly-disperse systems). As an alternative algorithm, we propose the simple, efficient, and precise method, Neighbors for Enclosing Local Free Area (called NELF-A), which is easily applied to dense poly-disperse hard disk systems often used in glassy model systems [8].

As an application of the NELF-A, we implement an alternative method to obtain the inherent structure instead of short-time averaged coarse-graining trajectories. The summary of the algorithm is as follows: (i) The displacement vectors from a particle position to a geometric center of FV estimated by NELF-A for each particle are drawn. (ii) The positions in a whole system are updated with the displacement vectors multiplied by a scaling parameter β less than unity. (iii) Repeat (ii) until the positions converge toward an inherent structure. The FV in equilibrium state eventually converging positions after (i)-(iii) procedure and the isotropic shape of FV located on a triangular lattice could be observed (i.e., inherent structure). Even in a typical non-equimolar binary mixture hard disk system, the probability density distribution obtained by (i)-(iii) procedure is fairly consistent with the conventional method based on the short-time averaged coarse-graining trajectories. We also confirmed the accuracy of this method by estimating pressure based on FV-based as compared with the other conventional methods.

Anomalous phase transition in self-propelled hard disk systems

In this study, we investigate the phase behavior of the self-propelled hard disk systems with the Vecsek-type interaction via EDMD simulation systematically. In addition to the ordinal order-disorder transition of the collective velocity field known in the original point particle of the Vicsek model, we observed the novel competition driven by the global positional order (so-called Alder transition) due to the exclusive effect of hard disk, which causes anomalous fluctuations around phase transition and transition shifts [9].

References

[1] M. Isobe: Mol. Sim. **42** (2016) 1317.

[2] E. P. Bernard, W. Krauth, and D. B. Wilson: Phys. Rev. E **80** (2009) 056704.

[3] W. Krauth: Front. Phys. **9** (2021) 229.

[4] M. Klement and M. Engel: J. Chem. Phys. **150** (2019) 174108.

[5] M. Isobe: Int. J. Mod. Phys. C **10** (1999) 1281.

[6] M. Klement, S. Lee, J. A. Anderson and M. Engel: J. Chem. Theor. and Comp. **17** (2021) 4686.

[7] H. Banno, D. Mugita, and M. Isobe: J. of Phys.: Conf. Ser. **2207** (2022) 012011.

[8] K. Souno, H. Koyama, D. Mugita, and M. Isobe: *in preparation.*

[9] N. Murase and M. Isobe: Proceedings of the 28th Symposium on Traffic Flow and Self-driven Particles, **28** (2023) 9. (in Japanese)

Molecular dynamics analyses of ion migration at electrode-electrolyte interfaces and grain boundaries in electrolytes

Ryo KOBAYASHI

Department of Applied Physics, Nagoya Institute of Technology,

Gokiso-cho, Showa-ku, Nagoya, Aichi 466-8555

All-solid-state batteries (ASSBs) are considered as a promising candidate for next-generation lithium-ion batteries. They use a solid-state electrolyte instead of the liquid-state electrolyte used in conventional lithium-ion batteries. The key to achieving high performance in ASSBs is to reduce or control the resistivity at interfaces such as the electrode/electrolyte interface and grain boundaries (GBs) within the electrolyte. To achieve this, we need a deeper understanding of the atomic structure and precise mechanisms of ion migration at GBs. The goal of this project is to obtain new insights into these processes by using large-scale molecular dynamics (MD) simulations.

In order to obtain atomistic insights on Li-ion migration mechanism at GBs, we performed non-equilibrium MD simulation of large-scale poly-crystalline Li2Zr(PO4)3 (LZP) system containing half a million atoms using a interatomic potential generated using a meta-heuristic approach [1,2,3] and extracted local ion flux information around GBs [4]. From the simulation and local ion-flux analyses, we showed that, in poly-crystalline materials, the ions migrate towards the lower reaches of grain and go through spots at GBs, and the high-flux spots contain migration paths as low energy as the bulk ones.

This methodology can be applicable to a wide variety of systems for electrolytes and interfaces between electrode and electrolyte.

References

[1] R. Kobayashi, Y. Miyaji, Nakano, K. M. Nakayama, *APL Materials* **8**, 081111 (2020)

[2] Nagoya Atomistic-simulation Package (nap) http://github.com/ryokbys/nap

[3] Optzer, http://github.com/ryokbys/optzer

[4] R. Kobayashi, K. Nakano, M. Nakayama, Acta Materialia, 226 (2022) 117596.

[5] M. Nakayama, K. Nakano, M. Harada, N. Tanibata, H. Takeda, Y. Noda, R. Kobayashi, M. Karasuyama, I. Takeuchi, M. Kotobuki, *Chem. Commun.* **58**, 9328–9340 (2022)

Theoretical study for firefly bioluminescence substrate analogs and related molecules

Miyabi HIYAMA
Graduate School of Science and Technology, Gunma University
Tenjin-cho, Kiryu, Gunma 376-8515

In this year, we studied the stable structures of adenosine triphosphate (ATP)-metal complexes in aqueous solutions and the theoretical absorption spectra for the firefly luciferin analog named "seMpai".

It is believed that the cofactor ATP and Mg^{2+} form a complex and react with the substrate luciferin in firefly bioluminescence. Wang et al. [1] reported that the bioluminescence quantum yields decreased with increasing cadmium or zinc concentration when these metal ions were used instead of magnesium one. The effects of metals on luciferin, on ATP, and on proteins may be responsible for this feature. We expected that the effect of metals on ATP was most significant than the others because the ATP is directly related to the bioluminescence reaction. Thus, the optimized structures of ATP-Mg^{2+}, ATP-Zn^{2+}, and ATP-Cd^{2+} in aqueous solutions were obtained using the density functional theory (DFT). For the initial structures for these calculations, the results from Global Reaction Mapping (GRRM11) calculations [2] were used because there were many local minimum structures of these complexes. We found that there was no clear difference in the structure of these metal ion coordination to ATP. It also found that ATP-Zn^{2+} and ATP-Cd^{2+} were unstable in aqueous solutions, unlike ATP-Mg^{2+} .

In these days, one of the firefly luciferin analogs named "seMpai", which is prepared with the aim of improving water solubility and produces red luminescence with firefly luciferase, was reported [3]. To elucidate the absorption characteristics of this analog, the optimization structure of its ground state for its conjugate acids and bases expected to be main component in the aqueous solutions were obtained from DFT calculations. The time dependent DFT (TDDFT) calculations were carried out to estimate the theoretical absorption spectra for these structures.

The computational chemistry software package, Gaussian09 [4], was used for DFT and TDDFT calculations. All calculations using Gaussian09 and GRRM11 were performed on system B of Super Computer Center in ISSP.

References

[1] Y. Wang, H. Kubota, N. Yamada, T. Irie, H. Akiyama: Photochem. Photobiol. **87**, 846 (2011).

[2] K. Ohno, S. Maeda: Chem. Phys. Lett. **384**, 277 (2023). S. Maeda, K. Ohno,: J. Phys. Chem. A, **109** 5742 (2005). K. Ohno, S. Maeda, J. Phys. Chem. A, **110** 8933 (2006).

[3] R. Saito, T. Kuchimaru, S. Higashi, S. W. Lu,M. Kiyama, S. Iwano, R. Obata, T. Hirano, S. Kizaka-Kondoh, S. A. Maki: Bull. Chem. Soc. Jpn. **92**, 608 (2019).

[4] Gaussian09 Revision D.01, M. J. Frisch et al.

Analysis of Ising model in statistical-mechanical informatics

Yuya SEKI

Graduate School of Science and Technology, Keio University, Kanagawa 223-8522

We have developed an optimization method for discrete black-box optimization problems by combining machine learning, simulated annealing, and integer encoding methods [1]. Our approach is based on factorization machine with annealing (FMA) [2] that uses factorization machines as machine learning model. Factorization machine with annealing approximates an objective function of a black-box optimization problem by training a factorization machine. Instead of minimizing the objective function that requires high cost to evaluate it, FMA minimizes a model equation of FM. Here, simulated annealing can be used for the minimization because the model equation of FM has a QUBO form that is equivalent to Ising model. Since FM is an important factor in performance of FMA, we analyze properties of model equations of FM, which are Ising models, by using numerical simulations on the supercomputer.

Tuning parameters in the FMA method is required to achive a high performance. To this end, we performed the calculation in parallel by changing the parameters with multiple processes on the supercomputer. In addition to the parallel computing mentioned above, we use multithreading to reduce computational time for the Monte Carlo simulation to minimizes the model equation of the trained FM. By using the parallel computing on the supercomputer, we obtained numerical results efficiently.

This year we investigated the performance of FMA for integer-variable black-box optimization problems in detail [1]. Integer variables can be represented as binary variables through integer encoding methods such as binary encoding, one-hot encoding, and domain-wall encoding. Since the encoded bit strings differ depending on the encoding methods, the performance of FMA is determined by the choice of the encoding method. Through a numerical simulation, we found that the FMA with one-hot encoding method has higher performance than FMA with other encoding methods. By using simulation on the supercomputer, we revealed the relationship between sparsity of bit string and the performance of FMA.

References

[1] Y. Seki *et al.*: arXiv:2209.01016 (2022).

[2] K. Kitai *et al.*: Phys. Rev. Research **2** (2020) 013319.

Quantum Pyrochrole Magnet

H. Kadowaki
Department of Physics, Tokyo Metropolitan University
Hachioji, Tokyo 192-0397, Japan

We are investigating static correlations $\langle \sigma^z_{\boldsymbol{Q}} \sigma^z_{-\boldsymbol{Q}} \rangle$ and dynamic correlations $\langle \sigma^z_{\boldsymbol{Q}}(0) \sigma^z_{-\boldsymbol{Q}}(t) \rangle$ characterized by the modulation wave vector $\boldsymbol{k} \sim (\frac{1}{2}, \frac{1}{2}, \frac{1}{2})$, which were observed by neutron scattering experiments, e.g. Ref. [1, 2], in the frustrated pyrochlore magnet $Tb_{2+x}Ti_{2-x}O_{7+y}$ (TTO). TTO with $x < x_c \simeq -0.0025$ is very interesting because of their quantum spin liquid (QSL) ground state. A simple question "why TTO shows the static short-range order with $\boldsymbol{k} \sim (\frac{1}{2}, \frac{1}{2}, \frac{1}{2})$?" has been a difficult problem for many years [3]. Recently we have solved this problem using quantum simulation based on thermal pure quantum (TPQ) states, and proposed that small three-spin interaction terms of a form $\sigma^{\pm}_{\boldsymbol{r}} \sigma^z_{\boldsymbol{r}'} \sigma^z_{\boldsymbol{r}''}$ are a key ingredient of both $\boldsymbol{k} \sim (\frac{1}{2}, \frac{1}{2}, \frac{1}{2})$ and the QSL state of TTO at low temperatures [4].

We are now extending the quantum simulation for $\langle \sigma^z_{\boldsymbol{Q}} \sigma^z_{-\boldsymbol{Q}} \rangle$ to inelastic neutron spectra, i.e., simulating $\langle \sigma^z_{\boldsymbol{Q}}(0) \sigma^z_{-\boldsymbol{Q}}(t) \rangle$ using a TPQ method [5]. We have written a simulation program, which now works very well, and are performing time-consuming calculations, which we would like to continue in 2023.

References

[1] H. Takatsu et al. Phys. Rev. Lett. **116**, (2016) 217201.

[2] H. Kadowaki et al. J. Phys. Soc. Jpn. **87** (2018) 064704.

[3] H. Kadowaki et al. Phys. Rev. B **99** (2019) 014406.

[4] H. Kadowaki, M. Wakita, B. Fåk, J. Ollivier, and S. Ohira-Kawamura, Phys. Rev. B **105** (2022) 014439.

[5] H. Endo et al. Phys. Rev. Lett. **121** (2018) 220601.

Atomistic model study on the coercivity mechanism of permanent magnets

Hiroshi Hayasaka[1], Masamichi Nishino[2, 1], and Seiji Miyashita[3,4,1]

[1]*Elements Strategy Initiative Center for Magnetic Materials, National Institute for Materials Science, 1-2-1 Sengen, Tsukuba, Ibaraki 305-0047, Japan*

[2]*Research Center for Advanced Measurement and Characterization, National Institute for Materials Science, 1-2-1 Sengen, Tsukuba, Ibaraki 305-0047, Japan*

[3]*Institute for Solid State Physics, The University of Tokyo, 5-1-5 Kashiwanoha, Kashiwa 277-8581, Japan*

[4]*The Physical Society of Japan, 2-31-22 Yushima, Tokyo 113-0033, Japan*

1. Angular dependence of coercivity

We investigated angular dependences of nucleation and pinning fields in anisotropic Heisenberg model. Unlike a deterministic process in magnetization reversal at zero temperature, reversal is a stochastic process for barrier crossing at finite temperatures. We studied the thermal fluctuation effect using the stochastic LLG equation method [1].

At zero temperature, the normalized nucleation field shows an asymmetric bowl-like angular dependence, and the value at large angles rapidly increases. On the other hand, the pining field shows almost constant dependence at $\theta < 40^\circ$ and increases at larger θ. The thermal fluctuation effect reduces the nucleation and pinning fields. At higher temperatures, the thermal effect makes both fields closer, in which the surface nucleation at the hard magnet plays an important role [2].

2. Coercivity enhancement by dysprosium substitution into neodymium permanent magnets

We investigated the features and mechanisms of the enhancement of the threshold field for magnetization reversal in atomistic Nd-Fe-B model with Dy substitution. The results showed that a change from surface to bulk nucleation occurs when the number of substituted layers increases and the anisotropy energy of Dy is resistant to temperature increase, which significantly enhances coercivity, especially at high temperatures [3].

References

[1] M. Nishino, and S. Miyashita, Phys. Rev. B **91**, 134411 (2015)

[2] H. Hayasaka, M. Nishino, and S. Miyashita, Phys. Rev. B **105**, 224414 (2022)

[3] M. Nishino, H. Hayasaka, and S. Miyashita, Phys. Rev. B **106**, 054422 (2022)

Large-scale molecular-dynamics simulation of pressure-induced coordination change in silica glass with ANN potentials

Daisuke WAKABAYASHI

Photon Factory, Institute of Materials Structure Science,

High Energy Accelerator Research Organization (KEK), Tsukuba 305-0801

Silica is well known as an archetypal oxide and the compression behavior of silica glass and melt has attracted considerable attention in various research fields. Theoretical studies using molecular-dynamics simulations have been actively conducted to obtain information on the atomic arrangements and bonding states of silica glass under high pressure. Since there is no long-range order in amorphous materials as exists in crystals, calculations on a large number of atoms are required to reproduce the structural changes. There is a limit to the size of the system which can be calculated by ab-initio methods.

In this study, we have fitted the potential with a machine-learning technique (ANN potential) on the basis of the results of ab-initio calculations, and have applied it for the calculations with an extended system. However, in our previous projects, it has been observed that the large-scale calculations of melt were difficult to stabilize and quickly diverged, making them impossible to continue. In this project, potential averaging and active learning are employed in combination to avoid computational instability efficiently [1].

The test calculations were performed for the solidification process of silica melt under high pressure. The ANN potential was determined with the total potential energy, atomic force, and pressure data obtained by ab-initio calculations for a temperature range of 300-5,000 K at 60 GPa with 144 atoms. Using the potential, we made molecular-dynamics calculations on silica melt at 60 GPa and 4,000 K for a system of about 30,000 atoms.

The use of multiple interatomic potentials averaged together stabilizes the calculations. The initial parameter sets for the fitting were randomly generated, and five ANN potentials were determined from the five parameter sets, respectively. In order to avoid extreme results, molecular-dynamics simulations were performed in an extended system using the average value of the atomic forces calculated by the five ANN potentials.

In addition, active learning was carried out to efficiently compensate for the lack of data. First, molecular-dynamics simulations were performed at 60 GPa and 4,000 K with the averaged ANN potentials in a system of the same size as in the ab initio calculations. The atomic

forces calculated from each ANN potential should agree, and therefore it is likely that atomic configurations at steps having a large variation in atomic force among the five potentials have not been well learned. Then, the standard deviation of the atomic forces was estimated for all atoms at each step, and the atomic configurations for which the maximum value was larger than 0.25 eV/Å were extracted [2]. The total potential energies, atomic forces, and pressure in the extracted configurations were calculated by an ab initio method and added to the initial dataset. Active learning was carried out twice in total.

The averaged ANN potential obtained after two active-learning cycles did not cause any computational instability during the simulations at 60 GPa and 4,000 K and in the subsequent simulations of the cooling process down to 300 K. Without active learning, the calculation becomes unstable before 2,000 steps and cannot reproduce the results of the ab initio calculations. The time at which the destabilization occurs is significantly delayed with each active-learning cycle.

The calculations on silica glass at 60 GPa and 300 K have not only reproduced ab initio calculations, but have also been found to significantly improve the precision of the intermediate-range structure and reproduce the experimental data in the literature [3]. This suggests that the experimentally observed structural transformation of silica glass, in which the coordination number of Si changes from 4 to 6 with increasing pressure [4], can be simulated in more detail. In fact, the calculations of the depressurization process down to 0 GPa were successful with the ANN potentials determined in the same method as for the cooling process and reproduced the change in coordination number from 6 to 4.

References

[1] D. Wakabayashi, K. Shimamura, A. Koura, and F. Shimojo, submitted to J. Phys. Soc. Jpn.

[2] Y. Zhang, H. Wang, W. Chen, J. Zeng, L. Zhang, H. Wang, and W. E, Comput. Phys. Comm. **253**, 107206 (2020).

[3] D. Wakabayashi, N. Funamori, T. Sato, and T. Taniguchi, Phys. Rev. B **84**, 144103 (2011).

[4] T. Sato and N. Funamori, Phys. Rev. B **82**, 184102 (2010).

First-principles investigation of ductile deformation mechanism in silver sulfide

Masaaki MISAWA
Department of Intelligent Mechanical Engineering, Fukuoka Institute of Technology
Wajiro-higashi, Higashi-ku, Fukuoka 811-0295

β-Ag_2S, a low-temperature phase of silver sulfide, exhibits metal-like ductility at room temperature even though it is an inorganic semiconductor[1]. Elucidating the origin of this ductility will be extremely useful for designing materials for flexible next-generation semiconductor devices. Although several theoretical investigations have been done to elucidate the mechanism of ductile deformation of β-Ag_2S from the viewpoint of bonding states in crystals [1, 2], theoretical verification considering dynamics under finite temperatures has not yet been performed. Therefore we have investigated the behavior of β-Ag_2S under shear stress based on first-principles molecular dynamics method [3].

In this study, we have performed first-principles molecular dynamics simulations for the six types of deformations of β-Ag_2S crystals: the (100)[010], (100)[001], (010)[100], (010)[001], (001)[100], and (001)[010] shear, where $(KLM)[klm]$ shear means that simple shear deformation in which the crystal's (KLM) plane slides toward the $[klm]$ direction. The shear rate in the simulations was equivalent to $d\gamma/dt = 0.05$ ps^{-1}, and shear deformations up to $\gamma = 0.50$ were performed under room temperature (300 K). The radial distribution function of the sulfur ion sublattice during the deformation process was analyzed to elucidate atomistic behaviors of β-Ag_2S under shear stress, and it was observed that peaks that once disappeared during deformation were restored in the four systems: (100)[001], (010)[100], (001)[100], and (001)[010] shear. In addition, we performed a more detailed study for the (100)[010] and (010)[001] shear systems, in which structural recovery did not occur, by slowing the shear rate, and observed structural recovery in these systems as well. A common feature of these structural recovery mechanisms is that the fracture is repaired by the mass movement of sulfur atoms in a particular crystal plane.

We also pointed out that the BCC-like structure of the sulfur sublattice in β-Ag_2S may be responsible for this atomistic behavior. Ag_2Se, which is not ductile, does not have such a highly symmetric anion-sublattice and thus cannot undergo the mass movement of atoms in response to shear stress, resulting in difficulty in structural recovery. Such atomistic understanding is expected to accelerate research and open a possibility in designing a wide variety of inorganic ductile semiconductors for future flexible electronics based on silver chalcogenides.

References

[1] X. Shi *et al.*: Nat. Mater. **17**, 421 (2018).

[2] G. Li *et al.*: npj Comput. Mater. **4**, 44 (2018).

[3] M. Misawa *et al.*: Sci. Rep. **12**, 19458 (2022).

Development of machine-learning-based phase diagram construction method for high-throughput batch experiments

Ryo TAMURA
International Center for Materials Nanoarchitectonics,
National Institute for Materials Science,
1-1 Namiki, Tsukuba, Ibaraki, 305-0044

Phase diagrams are valuable guidelines for the development of new materials. Through experiments, phase diagrams have been determined in various spaces, such as between processes, between external fields, and between compositions. In the field of materials informatics, tools focusing on phase diagrams have been developed using machine learning (ML). Among these tools, we have developed an ML method based on uncertainty sampling (US)[1] to efficiently construct phase diagrams, which we call the Phase Diagram Construction (PDC) package[2]. This method evaluates the uncertainty based on the ML model learned under the conditions that the phase domain is specified. Using evaluated uncertainty, the experimental condition with most uncertainty in the phase diagram is selected as the next experimental condition. Based on this suggestion, an experiment will be conducted and the corresponding phase domain is identified. The number of known points is then increased and the next experimental condition is proposed using the updated ML model. By applying the PDC to the known phase diagram, it was demonstrated that this iterative process can rapidly construct an accurate phase diagram and discover new phase domains[1]. For further validation, PDC was applied to construct a new diagram for obtaining Zn-Sn-P films by molecular beam epitaxy[3]. The PDC experiments detected new phases that were not observed in the initial stage, and detailed phase boundaries were quickly determined. Thus, the PDC proved to be useful in the case where one condition is proposed in ML and one experiment is performed in each iteration. Further speed-up can be achieved by incorporating the knowledges of materials science[4].

In addition, we developed PDC for high-throughput batch experiments[6]. To address the performance of the method, the target was a Cu-Mg-Zn ternary alloy. Both isothermal sections of this system (two-dimensional) and its temperature-dependent phase diagram as a whole (three-dimensional) were considered. We showed that PDC is suitable for high-throughput batch experiments to efficiently construct phase diagrams. Using this version, a temperature-composition phase diagram of a crosslinked polymer was constructed, and its usefulness was confirmed[5].

References

[1] K. Terayama, R. Tamura, Y. Nose, H. Hiramatsu, H. Hosono, Y. Okuno, and K. Tsuda, Physical Review Materials **3**, 033802 (2019).

[2] https://github.com/tsudalab/PDC

[3] R. Katsube, K. Terayama, R. Tamura, and Y. Nose, ACS Materials Letters **2**, 571-575 (2020).

[4] K. Terayama, K. Han, R. Katsube, I. Ohnuma, T. Abe, Y. Nose, and R. Tamura, Scripta Materialia **208**, 114335 (2022).

[5] W. Hu, T. Chen, R. Tamura, K. Terayama, S. Wang, I. Watanabe, and M. Naito, Science and Technology of Advanced Materials **23**, 66-75 (2022).

[6] R. Tamura, G. Deffrennes, K. Han, T. Abe, H. Morito, Y. Nakamura, M. Naito, R. Katsube, Y. Nose, and K. Terayama, Science and Technology of Advanced Materials: Methods **2**, 153-161 (2022).

Study on Novel Algorithm for Ising Machines

Shu Tanaka

Department of Applied Physics and Physico-Informatics, Keio University

Hiyoshi, Yokohama, Kanagawa, 223-8522

Ising machines are special computers for combinatorial optimization problems. The Ising machine expresses the objective function and constraints of a combinatorial optimization problem in terms of an Ising model, and searches for low-energy states of the Ising model. Since the Ising machine operates on the basis of stochastic behavior, it is necessary to develop various internal algorithms to improve the solution accuracy. In this research project, we investigated algorithms to improve the performance of the Ising machine from the viewpoint of statistical mechanics.

(I) Dynamical properties of bit-width reduction algorithms for simulated-annealing-based Ising machine

Ising machines have several hardware limitations. We have focused on cases where the possible values of the interaction coefficients and local field coefficients in the Ising model are limited and have proposed a method to make Ising machines work properly even in the presence of such limitations [1]. Reference [1] confirms the validity of the proposed method by comparing the ground states. On the other hand, the dynamic properties of the proposed method were not clarified. We have used the method of a previous study [2,3] to study the slow relaxation due to entropy effects, temperature-dependent effective interactions, and local magnetic fields. As a result, it was confirmed that there is a change in the time scale depending on the bit-width to be reduced [4].

(II) Black-box optimization using Ising machines

An Ising machine is a piece of hardware that takes an Ising model or equivalent Quadratic Unconstrained Binary Optimization (QUBO) representation as an input format and operates to find its ground state. Ising machines have been applied in various situations to combinatorial optimization problems that can be represented by Ising models or QUBOs. On the other hand, a method to use Ising machines for black-box discrete optimization, i.e., discrete optimization problems where the objective function is not explicitly given, was proposed by us in 2020 [5]. We extended it and proposed a method to perform integer-valued black-box optimization with Ising machines [6].

References

[1] D. Oku, M. Tawada, S. Tanaka, and N. Togawa, IEEE Trans. Comp. **71**, 223 (2020).

[2] S. Miyashita, S. Tanaka, M. Hirano, J. Phys. Soc. Jpn. **76**, 083001 (2007).

[3] S. Tanaka and S. Miyashita, J. Phys. Soc. Jpn. **78**, 084002 (2009).

[4] S. Kikuchi, N. Togawa, and S. Tanaka, arXiv:2304.12796 (2023).

[5] K. Kitai, J. Guo, S. Ju, S. Tanaka, K. Tsuda, J. Shiomi, and R. Tamura, Phys. Rev. Res. **2** (2020) 013319.

[6] Y. Seki, R. Tamura, and S. Tanaka, arXiv:2209.01016 (2022).

Charge distribution in metallic and charge order phase in organic crystals

Masatoshi SAKAI, Hiroki WATANABE, Ryosuke ANDO, Ryo WATANUKI

Department of Electrical and Electronic Engineering,

Chiba University, 1-33 Yayoi-cho Inage, Chiba 263-8522

Our research group conducts developments of novel electronic devices using organic charge order materials. In our previous work, we observed obvious field effect transistor (FET) characteristics of α-(BEDT-TTF)$_2$I$_3$[1] with 4-probe electrical measurement and small FET modulation of β-(BEDT-TTF)$_2$PF$_6$ [2] with 2-terminal electrical measurement. To analyze these experimental results, we are trying to calculate the electronic state of α-(BEDT-TTF)$_2$I$_3$ and β-(BEDT-TTF)$_2$PF$_6$. This report is a interim report of this research work in progress.

At first, about the electronic state of α-(BEDT-TTF)$_2$I$_3$ crystal, we adopted new parameter sets[3] of *t*, *U*, *V* because the previous parameter set could not reproduce the experimentally observed charge order structure. This time we adopted the parameter set considering the breaking of inversion symmetry. By adopting these novel parameters, we obtained calculated charge distribution of which the charge distribution trend agrees with that of the experimentally obtained one. And we could marshal the trend of the parameter set, which can obtain the charge order phase and metallic phase. Next, we are planning to try calculating real-time evolution from the insulator to the metallic phase and vice versa..

Furthermore, we also proceeded the calculation of the charge order phase of β-(BEDT-TTF)$_2$PF$_6$ crystal. This calculation started from the first-principle calculation (Quantum Espresso), and we obtained parameters using RESPACK. By using the obtained parameters, we tried to represent the charge distribution of the experimentally observed charge order. At present, we are making a superlattice structure to represent the real charge order. We are also trying to calculate the process and probability between the insulator and metallic phase of β-(BEDT-TTF)$_2$PF$_6$ to analyze our phase transition device characteristics.

---

[1] under preparation

[2] M. Sakai et al., Nanosci. and Nanotechnol. 16, 3267 (2016).

[3] D. Ohki et al., Phys. Rev. B 107, L041108 (2023).

Magnetic structures on the thin films made by the dipolar interaction and the frictional force stemming from these structures

Hisato Komatsu

Kyushu University, Kasuga, Fukuoka 816-8580 *

Masamichi Nishino and Yoshihiko Nonomura

National Institute for Materials Science, Tsukuba, Ibaraki 305-0044

We applied for the usage of the ISSP Supercomputer planning to investigate the magnetic structures of the dipolar system. However, we have not got notable results on this subject. Instead, we studied a theoretical model of the magnetic friction.

Magnetic friction, the frictional force generated from the magnetic interaction between spin variables, has been extensively studied in recent years. These studies aimed not only to investigate the behavior of the magnetic systems, but also to reveal the microscopic mechanisms of the friction. For this purpose, many types of theoretical models have been proposed and investigated[1, 2].

In the case of the normal solid surfaces, there is a well-known empirical law called the Dieterich-Ruina law[3, 4]. In our previous studies, we proposed models of magnetic friction that seemed to obey this law, at least in the steady state[5, 6]. These studies revealed that magnetic structures can behave as a kind of potential barrier that prevent the lattice motion. In the study of this academic year, we investigated a simplified model of the magnetic friction to consider the finite-size effect, which cannot be discussed in our previous studies. Specifically, we introduced a model composed of N Ising spin variables $\{\sigma_i\}$ interacting with each other by the following Hamiltonian:

$$H = -\frac{J(x)}{N}\sum_{i,j}\sigma_i\sigma_j = -NJ(x)m^2. \qquad (1)$$

Here, x is a real value representing the shift of the lattice, m is the magnetization per spin: $m \equiv \sum_i \sigma_i/N$, and $J(x)$ is the periodic function of x. For simplicity, we impose a periodic boundary condition on x. As a concrete form of $J(x)$, two types, A and B, are considered. Type-A is a piecewise linear function, and type-B is a sinusoidal function.

We introduce the time development of spin variables by the Glauber dynamics, and define one Monte Carlo step (MCS) as the unit time. In addition, the time development of x under this Hamiltonian and external force $F_{\rm ex}$ are introduced as the following overdamped Langevin equation:

$$\gamma N\frac{dx}{dt} = F_{\rm ex} - \frac{\partial H}{\partial x} + \sqrt{2\gamma NT}R(t), \qquad (2)$$

where $R(t)$ is the white Gaussian noise, $\langle R(t)R(t')\rangle = \delta(t-t')$. Here, we introduce coefficient N, considering the situation that N spins move simultaneously.

*Present address : Shiga-university, Hikone, Shiga 522-0069

We investigated this system by numerical simulation using ISSP Supercomputer, and found that this system shows two different behaviors depending on the damping constant γ. When γ is small, the stick and slip states are separated as the metastable states, and the probability that each state appears determines the relation between F_{ex} and the lattice velocity v. When γ is large, on the other hand, such separation does not appear and v is determined by the thermal activation process. We calculated the histogram of m and x like Fig. 1 and the F_{ex}-v relation, by the simulation. Furthurmore, we also estimated these quantities under sufficiently large or small γ theoretically using approximations, and compared it with the result of the simulation.

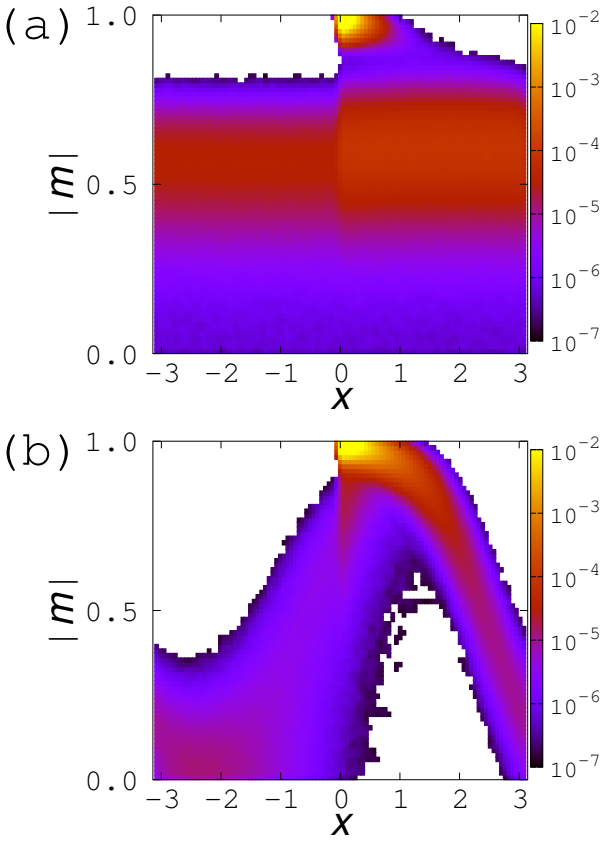

Figure 1: Examples of the histogram of the magnetization m and shift of the lattice x under (a)small γ and (b)large γ. In the case that γ is small, stick and slip states are separated as the metastable states like graph (a). These graphs are the results of the type-A model, type-B model also shows the similar result.

References

[1] D. Kadau, A. Hucht, and D. E. Wolf, Phys. Rev. Lett. **101**, 137205 (2008).

[2] M. P. Magiera, L. Brendel, D. E. Wolf, and U. Nowak, Europhys. Lett. **87**, 26002 (2009).

[3] A. Ruina, J. Geophys. Res. **88**, 10359 (1983)

[4] J. H. Dieterich, Tectonophysics **144**, 127 (1987)

[5] H. Komatsu, Phys. Rev. E. **100**, 052130 (2019)

[6] H. Komatsu, Phys. Rev. E. **102**, 062131 (2020)

[7] B. N. J. Persson, O. Albohr, F. Mancosu, V. Peveri, V. N. Samoilov, and I. M. Sivebaek, Wear **254** 835 (2003).

Numerical Study of One Dimensional Frustrated Quantum Spin Systems

Kazuo HIDA
Professor Emeritus, Division of Material Science,
Graduate School of Science and Engineering,
Saitama University, Saitama, Saitama 338-8570

1 Model

We investigate the ground-state phases of mixed diamond chains described by the following Hamiltonian:

$$\mathcal{H} = \sum_{l=1}^{L} \Big[(1+\delta)\boldsymbol{S}_l(\boldsymbol{\tau}_l^{(1)} + \boldsymbol{\tau}_{l-1}^{(1)}) + (1-\delta)\boldsymbol{S}_l(\boldsymbol{\tau}_l^{(2)} + \boldsymbol{\tau}_{l-1}^{(2)}) + \lambda \boldsymbol{\tau}_l^{(1)}\boldsymbol{\tau}_l^{(2)} \Big], \quad (1)$$

where $\boldsymbol{S}_l, \boldsymbol{\tau}_l^{(1)}$ and $\boldsymbol{\tau}_l^{(2)}$ are spin operators with magnitudes $S_l = \tau_l^{(1)} = 1/2$ and $\tau_l^{(2)} = 1$, respectively. The number of unit cells is denoted by L, and the total number of sites is $3L$. The lattice structure is depicted in Fig. 1. We consider the region $\lambda \geq 0$ and

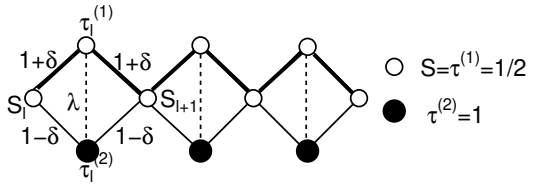

Figure 1: Structure of the diamond chain investigated in this work.

$1 \geq \delta \geq -1$. For $\delta = 0$, $\boldsymbol{\tau}_l^{(1)} + \boldsymbol{\tau}_l^{(2)}$ commutes with the Hamiltonian (1) for all l. In [1], we made use of this property to determine the ground-state phase diagram. In addition to the Lieb-Mattis(LM) type ferrimagnetic phase and the nonmagnetic Tomonaga-Luttinger liquid (TLL) phase, an infinite series of ferrimagnetic phases with spontaneous magnetizations $m_{\rm sp} = 1/p$, where $p(= 1, 2, ..., \infty)$ is the spatial periodicity of the ground state. Since the spin operators $\boldsymbol{\tau}^{(1)}$ and $\boldsymbol{\tau}^{(2)}$ have different magnitudes, however, it is not natural to assume $\delta = 0$ in a realistic situation. Hence, we examine more general cases with $\delta \neq 0$ in the present work.

2 Analytical Results

Let us start with the analytic consideration of several limiting cases.

1. $\lambda \gg 1+\delta, 1-\delta$: All pairs of $\boldsymbol{\tau}_l^{(1)}$ and $\boldsymbol{\tau}_l^{(2)}$ form spin-1/2 states. If the effective interaction between them is antiferromagnetic, the ground state is a TTL state. If it is ferromagnetic, the ground state is the LM-type ferrimagnetic state with $m_{\rm sp} = 1$. Using the perturbation calculation with respect to $(1 \pm \delta)/\lambda$, we find the phase boundary between these two phases is given by $\delta = 0.6$.

2. $\lambda \leq 0$、$1 \pm \delta > 0$: The system is unfrustrated and the ground state is the LM-type ferrimagnetic state with $m_{\rm sp} = 1$. A similar ground state is expected for $0 < \lambda \ll 1 \pm \delta$.

3. $1 + \delta \simeq 0$ and $\lambda \simeq 0$: For $1 + \delta = \lambda = 0$, $\boldsymbol{S_l}$ snd $\boldsymbol{\tau}_l^{(2)}$ form a ferrimagnetic chain with $m_{\rm sp} = 1/2$ and $\boldsymbol{\tau}_l^{(1)}$ are free spins with magnitude 1/2. For small $1 + \delta$ and λ, we can determine the phase boundary between the LM-type ferrimagnetic

phase with $m_{\rm sp} = 1$ and the nonmagnetic phase as $\lambda/(1+\delta) \simeq 0.738$ by the perturbation calculation with respect to these small parameters $1+\delta$ and λ combined with the numerical exact diagonalization (NED) calculation of the ferrimagnetic chain.

4. $1-\delta = 0$ or $\lambda = 0$: If $1-\delta = \lambda = 0$, $\boldsymbol{S}_l$ and $\boldsymbol{\tau}_l^{(1)}$ form a spin-1/2 antiferromagnetic Heisenberg chain aand $\boldsymbol{\tau}_l^{(2)}$ are free spins. If $\lambda > 0$ and $\delta = 1$, the ground state is the LM-type ferrimagnetic phase with $m_{\rm sp} = 1$. The same is true if $\delta < 1$ and $\lambda = 0$. However, if $\lambda > 0$ and $\delta < 1$, these two interactions frustrate, and a nontrivial ground state is realized.

3 Numerical Results

We have carried out the NED calculation for $L = 4, 6$ and 8 and the DMRG calculation for $L = 24$ and 48. The magnetization curves and spontaneous magnetization are calculated to obtain the ground-state phase diagram of Fig. 2. It should be remarked that the two ferrimagnetic phases with $m_{\rm sp} = 1$ are not a single phase, but are separated by the partial ferrimagnetic phase and nonmagnetic phase. The nonmagnetic phase continues to the TLL phase for large δ. Hence, the whole nonmagnetic phase is likely to be a TLL phase. However, since the sum of the spin magnitudes in a unit cell is an integer, the Lieb-Schultz-Mattis theorem does not exclude the gapped phase.

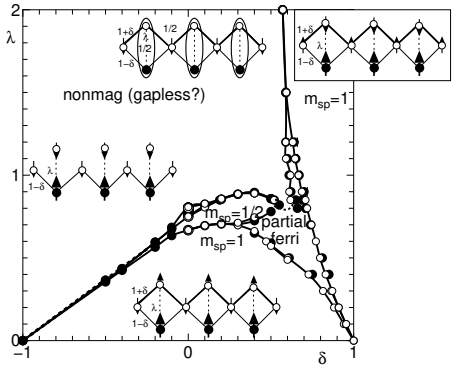

Figure 2: Ground-state phase diagram. The open circles are the phase boundaries estimated from the NED data extrapolated to the thermodynamic limit. The filled circles are the phase boundaries estimated from the DMRG data for $L = 24$ and 48. The curves are guides for the eye. The insets are schematical spin structures in different phases.

The fate of the infinite series of ferrimagnetic phases found for $\delta = 0$ in [1] is also investigated. The λ-dependence of the spontaneous magnetization for $\delta = 0.1$ is shown in Fig. 3. It seems that the width of the ferrimagnetic phase with $m_{\rm sp} = 1/2$ ($p = 2$) remains finite, while those with $p \geq 3$ are smeared out and the corresponding region turns into the partial ferrimagnetic phase suggesting the fragility of the ferrimagnetic phases with large p.

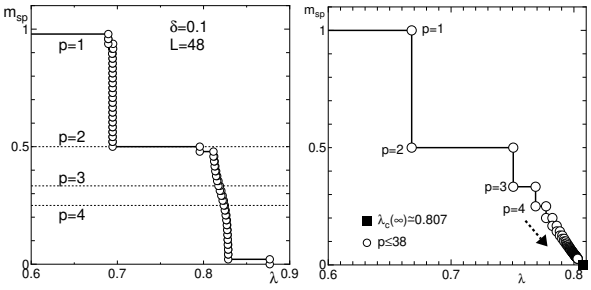

Figure 3: Left panel : λ-dependence of the spontaneous magnetization in the ground state for $\delta = 0.1$ calculated by the DMRG method for open chains with $L = 48$. Right panel: The corresponding figure for $\delta = 0$ taken from ref. [1].

References

[1] K. Hida, J. Phys. Soc. Jpn. **90**, 054701 (2021).

Novel phenomena in mismatched multilayer systems: Search for new candidate materials and analysis of electronic structures

Toshikaze KARIYADO

Research Center for Materials Nanoarchitectonics,

National Institute for Materials Science, Namiki, Tsukuba, Ibaraki 305-0044

Recently, artificially stacked 2D systems attract much attention as a playground for electronic structure manipulations. In particular, systems with nanoscale moiré pattern induced by slight mismatch between layers are interesting, since the nanoscale patterns tend to have striking effects on low energy band structures.

In this project, we propose twisted bilayer BC_3 as a system for realizing interesting valley related physics [1]. BC_3 is a graphene derivative with a honeycomb network of atoms [2]. The monolayer BC_3 is a three-valley semiconductor with its conduction minima at three M-points in the hexagonal Brillouin zone. Each of the valleys shows a 2D parabolic dispersion around the conduction minima, though there is anisotropy. It is found that upon making twisted bilayers, the 2D dispersion is squeezed into quasi-1D one. Interestingly, the quasi-1D directionality depends on the valley degrees of freedom. That is, twistronics applied on bilayer BC_3 leads to valley dependent band structure manipulation, which potentially paves a way to valleytronics applications.

In the analysis of monolayer and bilayer BC_3, we make full use of the ab initio method, using mainly Quantum Espresso and sometimes OpenMX. A characteristic feature of moiré bilayer systems is that the relation between two layers depends on position, and it is important to know the *local* crystalline and electronic structures to build a model to handle the nanoscale moiré pattern. This means that we need to work out computations on various local structures corresponding to the various positions in the nanoscale moiré unit cell. Then, large computational resources are required, and the numerical efficiency is important. For the numerical efficiency, the Quantum Espresso package offers an efficient parallelized version.

References

[1] T. Kariyado, Phys. Rev. B **107**, 085127 (2023).

[2] H. Tanaka *et al.*, Solid State Commun. **136**, 22 (2005).

Structure analysis of borophene by using 2DMAT

Akari TAKAYAMA

Department of Physics,

Waseda University, Ohkubo, Shinjuku-ku, Tokyo 169-8555

Introduction

Atomic-layer sheet composed of group XIV elements such as graphene and silicene have been actively studied. These atomic-layer sheets form a honeycomb structure and are expected to be applicable to various technologies because of their excellent electron mobility due to their peculiar band dispersion following the Dirac equation. Recently, an atomic-layer sheet material of boron (the group XIII element), called "borophene" is attracting attention, especially after the success of its fabrication on metal substrates. Unlike atomic-layer sheets of group XIV elements that form a honeycomb lattice, flat layers of boron are theoretically stable when composed of a triangular lattice and hexagonal hollows. Experimental observations of epitaxial borophene on Ag(111) have been consistent with the theoretical structural models [1, 2], but the atomic structure has not been examined directly. More interestingly, scanning tunneling microscopy (STM) observations of a honeycomb structure on an Al(111) substrate were reported [3], but the detailed atomic structure of this honeycomb lattice is unclear. Thus, there is a strong need to conduct structural analysis by an appropriate diffraction experiment on the surface.

In our research, we studied the atomic structure of borophene on Ag(111) and on Al(111) by means of total-reflection high-energy positron diffraction (TRHEPD). For structure analysis, calculations of the rocking curves for TRHEPD were performed by the structure-analysis program, "2DMAT" [4], which is included as standard software in ISSP's supercomputer. Using massive parallel computer simulations on supercomputer is very useful for structure analysis of large periodic structure and surface superstructure with lattice reconstruction because they require many variables for analysis.

Results and discussion

The TRHEPD experiment consists of measuring a series of the diffraction patterns for a fixed incident azimuthal direction at various glancing angles (θ). Here, the rocking curve is defined as the diffraction intensity of the (00) spot plotted as a function of θ. In the structural analysis, the experimental rocking curves are compared with those calculated for various structural models. Figure 1 shows the rocking curves of (a) a pristine Ag(111) surface and (b) the borophene grown on it, measured under the

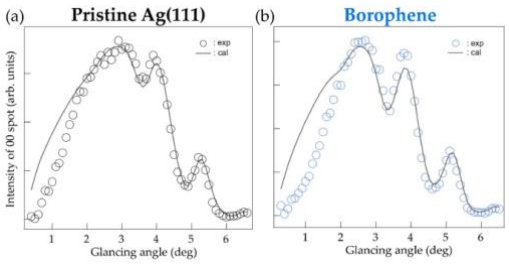

Fig. 1: Rocking curves under one-beam condition with calculated curves for (a) Ag(111) and (b) borophene on Ag(111).

one-beam condition. In the one-beam condition, the beam is incident along an off-symmetric direction, thus the rocking curve in the one-beam condition essentially gives the information on the atomic positions in the out-of-plane direction. The experimental profile was reproduced by the proposed model [2]; layer distance between Ag and borophene is 2.4 Å and the magnitude of bucking for borophene 0.04 Å. This indicates that there is no buckling, and we have directly confirmed that the borophene is a flat sheet [5].

Figure 2 shows the rocking curves of (a) a pristine Al(111) surface and (b) the borophene grown on it under the one-beam condition obtained from the experiment and from calculation of Al(111). After boron deposition, the peak position shifted slightly, but the whole shape of the rocking curve did not change much. According to angle-resolved photoemission spectroscopy (ARPES) measurements and band calculations for borophene on Al(111) substrates, it is predicted that the borophene forms AlB_2 at the top surface [6]. However, the rocking curve of the AlB_2 model differs significantly from our experimental results, which is inconsistent with the results of this study. One possible reason for the difference between our experiment and previous studies is the effect of ripple structure [3]. Since the ripple structure was not considered in this analysis, it is possible that the model used in the analysis did not correctly reproduce the experimental results. It has also been pointed out that borophene on Al substrate forms long-period moiré structures due to lattice mismatch with the substrate [7]. To determine the structure of honeycomb borophene on Al substrate, we will analyze the giant lattice system utilizing parallel computation on a supercomputer.

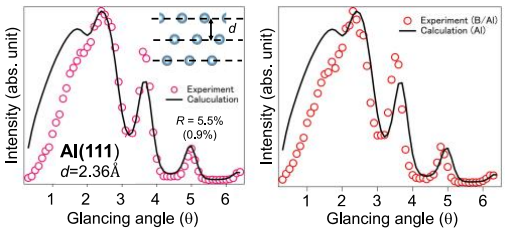

Fig. 2: Rocking curves under one-beam condition for (a) before and (b) after boron deposited on Al(111).

References

[1] R. Wu, *et al*., Nature Nanotechnology, **14** (2019) 44.

[2] G. P. Campbell, *et al.*, Nano Letters, **18** (2018) 2816.

[3] W. Li, *et al.*, Science, **63**, (2018) 282.

[4] Y. Motoyama, *et al*., Computer Physics Communications, **280** (2022) 108465.

[5] Y. Tsujikawa, AT *et al.*, Molecules. **27** (2022) 4219.

[6] D. Geng, *et al*., Physical Review B **101** (2020) 161407(R).

[7] A. B. Preobrajenski, *et al*., ACS Nano, **15**, (2021) 15153.

Magnetic structures of multiple-Q orders in inversion-symmetric Hubbard Models

Takashi UCHIDA
Hokkaido University of Science
4-1, 7-15, Maeda, Teine-ku, Sapporo 006-8585

In the last decade, multiple-Q orders in magnetic systems have attracted attention because they sometimes reveal topologically protected magnetic structures such as magnetic skyrmions. Typically, these structures are realized in the Dzyaloshinskii-Moriya (DM) interaction driven systems under magnetic field. The multiple-Q orders can also be realized in inversion-symmetric systems where the DM interaction is absent [1, 2].

In order to investigate the nature of the multiple-Q orders in inversion-symmetric itinerant systems, we have explored the magnetic structures of the triangular-lattice single-band Hubbard model by means of the molecular spin dynamics (MSD) method [3]. The present formulation of the MSD adopts the static approximation to the functional integral method and the isothermal molecular dynamics technique, and reduces to the generalized Hartree-Fock approximation at the ground state.

In the present work, we have performed the MSD calculation with use of the global charge neutrality condition instead of using the local charge neutrality condition [3]. This has the advantage that the charge transfer among the atoms is allowed in the magnetic structure formation. In the numerical calculations the most time-consuming process is the magnetic force calculation at each time step, where the local electronic structures are calculated in real space by means of the recursion method. We have adopted the MPI parallel calculation scheme and found it effective in saving both computing time and CPU resources.

We have performed magnetic structure calculations on a hexagonal supercell with 972 lattice points, which is embedded in a large cluster consisting of 6 such supercells, each of which are connected by the periodic boundary condition. Under zero magnetic field and the fixed value of the temperature $T/t = 0.0005$, we have explored the magnetic structures changing the Coulomb interaction strength U/t and the electron number n along the antiferromagnetic-ferromagnetic boundary. We have found that the stable states for $U/t < 4.0$ and $n = 1.45 \sim 1.53$ are the 3Q magnetic orders with the Q vectors pointing in the direction of three axes of the triangular lattice and that they are accompanied by 3Q charge density waves (CDW) with the same Q vectors as the magnetic ones. The present results with use of the global charge neutrality condition reveal the enhancement of the amplitude of the main 3Q magnetic order as compared to those with use of the local charge neutrality condition, showing that the CDW contributes to stabilize the magnetic 3Q order.

References

[1] T. Okubo, S. Chung, and H. Kawamura: Phys. Rev. Lett. **108** (2012) 017206

[2] Y. Kakehashi: J. Phys. Soc. Jpn. **89** (2020) 094710.

[3] Y. Kakehashi, S. Akbar, and N. Kimura: Phys. Rev. B**57** (1998) 8354.

Development of integrated interface of eigensolvers Rokko and application to quantum spin systems

Tatsuya Sakashita
Center for Quantum Information and Quantum Biology, Osaka University
1-2 Machikaneyamachō, Toyonaka, Osaka 560-0043

To establish universal exact diagonalization package for quantum lattice models including the Heisenberg-Kitaev model, we focused on developing integrated interfaces for eigensolvers, "Rokko"[1].

In Rokko, we implemented the integrated interfaces for the following types:

- Serial solvers for dense matrices (Eigen3, LAPACK)
- MPI parallelized solvers for dense matrices (EigenExa[2], ELPA[3], Elemental[4], ScaLAPACK)
- MPI parallelized solvers for sparse matrices (Anasazi in Trilinos[5], SLEPc[6]) to cover matrix representations below:
  - CRS (Compressed Row Storage)
  - Matrix-free method (the method to give matrix-vector product routines to solvers)

Rokko has the following features:

- Integrated interfaces for eigensolvers and matrices, independent of individual eigensolver libraries
- Rokko's interfaces are implemented by utilizing factory. It enables the user to dynamically select a solver.
- C, Fortran, and Python bindings of Rokko
- Automatically detecting libraries by using CMake in building Rokko
- Unit and integrated test programs by GoogleTest
- Install scripts of eigensolvers for various architectures

We prepare a paper to report design policy, software structure, and usage examples of Rokko.

References

[1] T. Sakashita, R. Igarashi, Y. Motoyama, T. Okubo, and S. Todo. Repository of Rokko. `https://github.com/t-sakashita/rokko.git`, 2012.

[2] T. Imamura, T. Hirota, and T. Fukaya. EigenExa web page. `https://www.r-ccs.riken.jp/labs/lpnctrt/projects/eigenexa/`, 2021.

[3] ELPA Consortium. ELPA (Eigenvalue soLvers for Petaflop Applications web page). `http://elpa.rzg.mpg.de`, 2013.

[4] J. Poulson. Distributed-memory dense linear algebra Elemental web page. `https://github.com/elemental/Elemental`, 2013.

[5] M. A. Heroux, R. A. Bartlett, and V. E. Howle. Trilinos Project web page. `https://trilinos.github.io`, 2003.

[6] V. Hernandez, J. E. Roman, and V. Vidal. SLEPc web page. `http://slepc.upv.es`, 2002.

Systematic understanding of the slip behaviors of slow and fast earthquakes and the effect of the upper value of porosity

Takehito SUZUKI
Department of Physical Sciences, Aoyama Gakuin University
5-10-1, Fuchinobe, Chuo-ku, Sagamihara, Kanagawa 252-5258

Two qualitatively different behaviors of earthquakes have been known. One is the fast earthquakes, which we feel naturally. The other one is slow earthquakes, which generate negligible seismic waves. Although the slow earthquakes are not disastrous, they are considered to sometimes change to the fast earthquakes after several repetitions. Whether this transition occurs or not is a fatal problem to the human society. Systematic understanding for the slip behaviors of the slow and fast earthquakes is aimed in this study.

The fault rocks can be considered as porous media, and the pores within the media are usually considered to be filled with water. If the dynamic earthquake slip (frictional slip) occurs, we can consider the interaction among heat, fluid pressure, and porosity [1, 2]. The slip is interpreted as the deformation around the contact area, called slip zone, which has a finite width w_h. During the dynamic slip, the generation of pores [frictional heating] reduces [raises] the fluid pressure in the slip zone, inducing the increase [reduction] in the friction stress and the reduction [increase] in the slip velocity [1, 2]. The fluid-pressure increase due to frictional heating will be called FH effect, whereas the fluid-pressure decrease due to the pore generation is referred to as PG effect. The slow and ordinary earthquakes are dominated by the PG and FH effects, respectively.

The spring-block model and the interaction between three quantities are employed to investigate both the slow and fast earthquakes. This system repeats the dynamic slip and cessation. The healing of pores in the cessation time is also taken into account.

With this system, we found an important function determining the system behavior [3]. For the derivation of the function, we employed three important assumptions: (i) we consider a single block, (ii) the diffusions of heat and fluid are neglected, and (iii) the change in the bulk modulus of the medium, M_0', due to porosity change is neglected; i.e., $M_0'(\phi) = M_0'(\phi_0)$, where ϕ_0 is the porosity at the onset of the slip. With these assumptions, we found a function of the slip u_f,

$$F(u_f) = \frac{1}{2}k_p u_f^2 + \mu_{\rm stat}(\sigma_n^0 + p_0)u_f - \mu_{\rm slid}\left[\frac{1}{\gamma}\left(\sigma_n^0 + p_0 - \frac{M_0'\alpha_0}{\frac{\alpha_0}{\phi_\infty} - \gamma}\right)(1 - e^{-\gamma u_f}) + \frac{M_0'\phi_\infty}{\frac{\alpha_0}{\phi_\infty} - \gamma}(1 - e^{-\alpha_0 u_f/\phi_\infty})\right], \quad (1)$$

where k_p is the spring constant, $\mu_{\rm slid}$ and $\mu_{\rm stat}$ are the sliding and maximum static friction coefficients, respectively, σ_n^0 is the normal stress acting on the interface, p_0 is the fluid pressure at the onset of the slip, γ is the positive constant, and α_0 and ϕ_∞ are the positive constants appearing in the porosity evolution law

$$\frac{\partial \phi}{\partial t} = \alpha_0 v\left(1 - \frac{\phi}{\phi_\infty}\right)[H(y + \frac{w_h}{2}) - H(y - \frac{w_h}{2})]. \quad (2)$$

Two solutions whose magnitudes are different in two orders emerge for the equation $F(u_f) = 0$, and the small and large ones correspond to the slow and fast earthquakes, respectively. Detailed analysis shows that this behavior of the solution can be interpreted as the phase transition of the first order [3].

We should now remove above-mentioned three assumptions to treat more realistic situation. We performed numerical calculations with ISSP supercomputer. The number of blocks is 40, and the diffusions of heat and fluid are included. Moreover, from Eq. (2), the assumption (iii) should be valid if the value of ϕ_∞ is negligibly small. We consider three values for ϕ_∞, and the condition where we can apply the analytical treatment will be clarified.

If we assume $\phi_\infty = 0.01$, only the fast earthquakes occur, and the slow earthquakes do not occur (Fig. 1a). This is because the porosity change is negligible, and the fluid pressure change due to the PG effect is negligibly small. If we assume $\phi_\infty = 0.1$, both the fast and slow earthquakes occur (Fig. 1b) because both the FH and PG effects work in this case. If we assume $\phi_\infty = 0.9$, the fast and slow earthquakes occur (Fig. 1c). The FH and PG effects work also in this case.

Additionally, the analytical treatment using $F(u_f)$ was found to be effective for $\phi_\infty = 0.01$ and 0.1, whereas it was not effective for the slow earthquake observed for $\phi_\infty = 0.9$. The value 0.9 may be too large to employ the above-mentioned assumption (iii). The function $F(u_f)$ is useful for predicting the dynamic slip behaviors of the natural fault zones if ϕ_∞ is much smaller than unity.

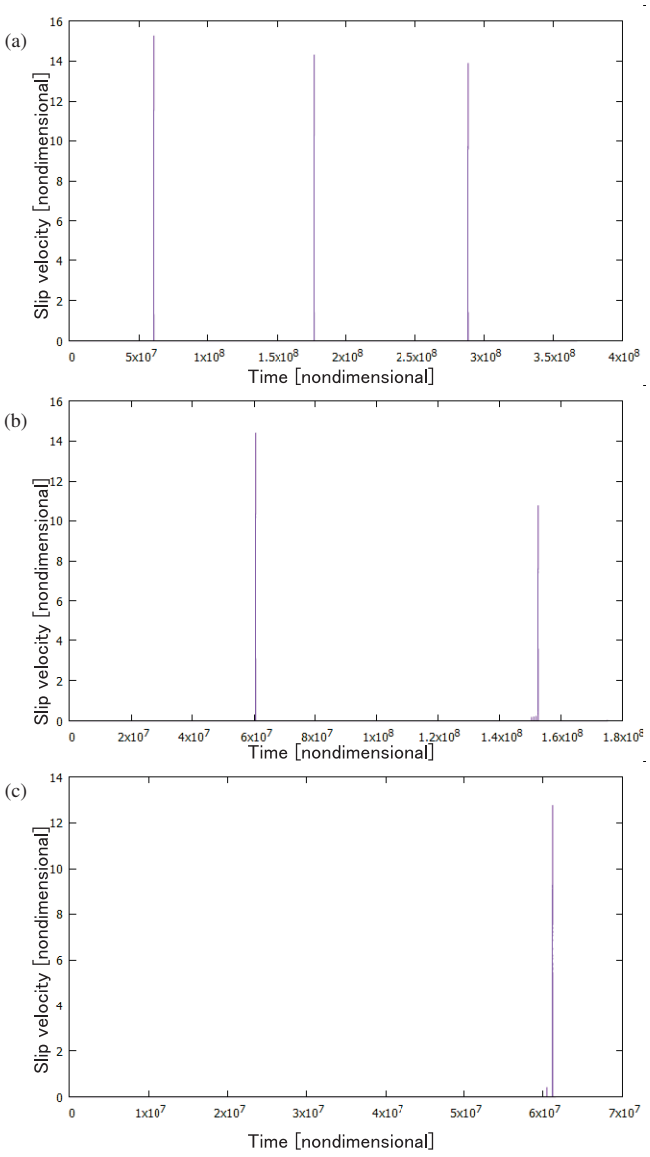

Figure 1: The slip velocity of the 20th block with (a) $\phi_\infty = 0.01$, (b) 0.1, and (c) 0.9.

References

[1] T. Suzuki, and T. Yamashita: J. Geophys. Res. **119** (2014)

[2] T. Suzuki: Phys. Rev. E **96** (2017)

[3] T. Suzuki, and H. Matsukawa, in prep.

Shape dependence of macroscopic friction between solids

Michio OTSUKI

Graduate School of Engineering Science,

Osaka University, Machikaneyama, Toyonaka, Osaka 560-8531

Amonton's law states that the static friction coefficient does not depend on the external pressure or the shape of the object. Recent studies have shown that Amonton's law systematically breaks down for macroscopic objects due to precursor slip before the onset of bulk sliding [1, 2]. However, it is unclear whether the results apply to more realistic 3D systems since the analysis in previous works is restricted to 2D systems.

First, we have numerically investigated the sliding motion of a 3D viscoelastic block on a rigid substrate using finite element simulation as shown in Fig. 1. The maximum computational size requires 500,000 nodes and 10 billion time steps, which takes 100 hours using our code compiled with the Intel Fortran compiler and a parallel computation of 2,000 MPI processes on the CPU server. The block exhibits stick-slip motion characterized by the static friction coefficient. The static friction coefficient decreases with increasing external pressure, length, or width of the block, which contradicts Amonton's law. The precursor slip occurs in the 2D interface between the block and substrate before bulk sliding. The instability analysis of a simplified model explains the decrease in the static friction coefficient and the behavior of precursor slip [3].

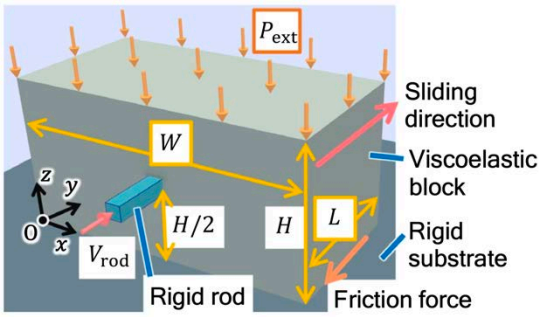

Fig. 1 Schematic of a 3D viscoelastic block on a fixed rigid substrate.

In addition, we have studied the effect of the shape of the frictional interface. Frictional interfaces of some industrial products, such as shoe soles and tires, are often grooved. However, there is a need to understand how grooves affect the frictional properties. Therefore, we have numerically investigated the slip of objects that are longitudinally grooved as shown in Fig. 2. The static friction coefficient is a decreasing function of groove width and depth. Furthermore, our theoretical analysis shows that the decrease is caused by a reduction in the effective viscosity due to the groove. These results provide new insight into the design of grooves for friction control.

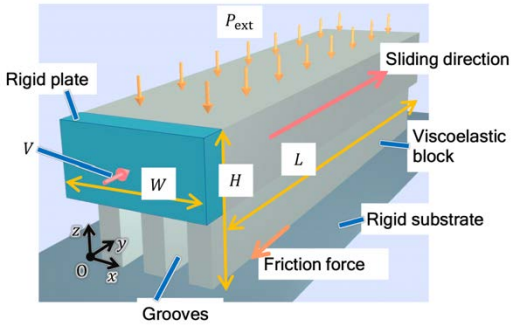

Fig. 2 Schematic of a 3D viscoelastic block with grooves block on a fixed rigid substrate.

References

[1] M. Otsuki and H. Matsukawa, Sci. Rep. **3**, 1586 (2013).

[2] Y. Katano, K. Nakano, M. Otsuki, and H. Matsukawa, Sci. Rep. **4**, 6324 (2014).

[3] W. Iwashita, H. Matsukawa, and M. Otsuki, Sci. Rep. **13**, 2511 (2023).